1992

Switching strategies for active power filters

Damrong Dejsakulrit
University of Wollongong

SWITCHING STRATEGIES FOR ACTIVE POWER FILTERS

A thesis submitted in fulfilment of the requirements for
the award of the degree of

MASTER OF ENGINEERING (HONOURS)

from

UNIVERSITY OF WOLLONGONG

by

DAMRONG DEJSAKULRIT, B.Eng (Hons.) KMIT., Thailand.

Department of Electrical and
Computer Engineering, 1992.

Dedicated to my *grandmother*

who first encouraged me to undertake postgraduate studies.

Errata

All graphs depicting harmonic spectra (including Figures 3.3, 4.2, 5.2, 5.7, 5.8, 6.14) should be shifted one harmonic number to the left on the x-axis.

CONTENTS

Acknowledgments

I would like to thank my supervisors, Dr J.F. Chicharo and Dr B.S.P. Perera for their guidance and support throughout this research. I am extremely grateful to my supervisors for helping me to understand some points that I was unable to work out for myself, I could not have done this thesis without them. Their contributions were not only of academic value but were also of the type which enhanced by personal life. I am greatly appreciated.

I would like to thank the many people in the Department of Electrical and Computer Engineering at the University of Wollongong for their suggestion and friendship, especially, Dr P Doulai, Dr D Platt, Peter J. Costigan, Vesna Gospic, Philip Secker, Geetha Sadagopan, Haihong Wang, Jiangtao Xi, Mehdi T. Kilani, Young K. Jang, too many to name, I am most grateful to all of them.

I wish to thank my brother, sisters and my girl friend for their support and understanding in me. Finally, I am deeply grateful to my grandmother who looked after me and always motivated me to undertake postgraduate studies. I hope she may rest in peace.

Abstract

This thesis is concerned with the development of simple and effective switching strategies for active power filtering applications. A switching strategy for active power filters which has been presented recently is based on an Equal-Sampling Technique (EST). This approach involves the solution of a set of non-linear equations. The main difficulty with the EST is its high computational burden and slow response when load current changes take place.

A Modified Equal Sampling Technique (MEST) and a Centroid Based Technique (CBT) are proposed in this thesis. The proposed strategies are computationally simpler to implement and in both cases provide equal or improved performance when compared to the EST. The common feature of the two new schemes is that the injected current pulsewidths are determined based on an equal area criteria. In addition, in case of CBT, the centroid of both the injected current pulses and corresponding harmonic current are constrained to occupy the same position in the time domain.

List of Symbols

$\boldsymbol{a_n}$, $\bar{\boldsymbol{a}}_{\boldsymbol{n}}$, a_n, a_0, a_1	Fourier coefficient
A_{hk}	area of harmonic current
A_{sk}	area of current pulse
$\boldsymbol{b_n}$, $\bar{\boldsymbol{b}}_{\boldsymbol{n}}$, b_n, b_0, b_1	Fourier coefficient
C_1,C_2	pulsewidth coefficient
DF	distortion factor
$\alpha(\theta)$	switching function
$\alpha_k(\theta)$	elementary switching function
e_h	harmonic voltage
δ	width of quasi-square wave
$f(\tau)$	matrix of non-linear equation
f_c	clock frequency
f_s	equal-sampling frequency
γ_k,γ_1,γ_2	switching angles
H_1,H_2,H_M	harmonic amplitude vector
H_k	per unit magnitude of harmonic current
i_C	compensating current
I_C	amplitude of compensating current
I_d	converter dc current
i_h	harmonic current
i_{hmax}	maximum amplitude of harmonic current
i_{hr}	residual harmonic current
i_L	converter line current
i_{L1}	fundamental converter line current

i_S	ac line current
φ	Fourier coefficient
L_k	converter line inductance
L_m	charged inductance
L	dc load inductance
M_i	modulation index
M	number of pulses per half cycle
n	harmonic order
n_c	number of samples per cycle
n_k'	number of samples per half pulsewidth
p	frequency ratio
PR	percentage reduction of harmonic current
r	injection ratio
ρ_k	Fourier coefficient
S_k,-S_k	sign vector of switching function
τ_k, τ_k'	half pulse width of switching function
T_c, T_S	equal sampling time
t_C	clock time
t_n	sample instant
w_f	width factor
$\bar{X}_k$	centroid co-ordinate
θ_k	sampling point, pulse position

CHAPTER 1

PRELIMINARIES

1.1 Introduction

Solid-state power converters which are widely used in industries can cause undesirable harmonic problems in the supply mains. Such harmonics can exist in the form of voltage and/or current harmonics. Harmonics increase transmission losses in power systems and reduce the efficiency of most connected loads. They can also deteriorate the proper functioning of various equipment, particularly, in electronic circuits.

In order to eliminate the harmonic currents and voltages, passive power filters or active power filters may be used. Passive power filters that are designed to filter the lower order harmonic components tend to be bulky, expensive and also lossy. To overcome some of the above problems of the passive power filters, active power filters have been studied and developed in recent years by Sasaki and Machida (1971), Gyugyi and Strycula (1976), Choe and Park (1988) and Akagi, Tsukamoto and Nabae (1990).

Active power filters fall into two major categories, viz. current fed and voltage fed (Gyugyi and Strycula, 1976). Switching strategies that are suitable for active power filters have received very little attention in the past. This thesis falls within the general area of active power filter applications. In particular this thesis deals with switching strategies that are suitable for current fed active power filters.

This chapter is organised as follows: Section 1.2 presents the phase controlled converter as a harmonic current source. Section 1.3 describes the effects of harmonics. The basic principles of passive and active power

filters are presented in Section 1.4. Section 1.5 discusses the approach and contribution of this thesis. Finally, Section 1.6 presents a brief summary of the contributions.

1.2 Harmonic Current Source (Phase Controlled Converter)

The typical three-phase controlled bridge converter shown in Figure 1.1 is assumed as the harmonic current source in this thesis as is the case for the majority of papers in literature.

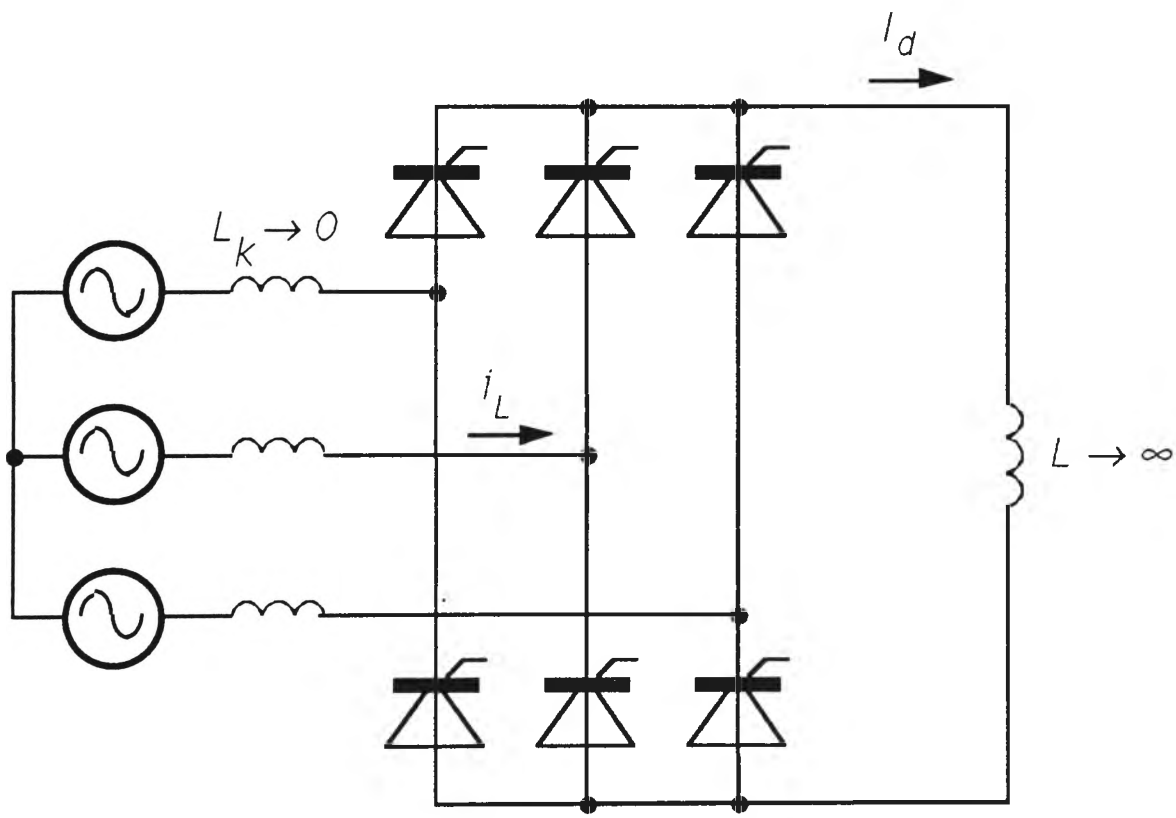

Figure 1.1 Three-Phase Bridge Converter

Figure 1.2 shows the waveform of line current and converter current based on the following assumptions:

1. The load inductance is very large (i.e. $L \rightarrow \infty$) hence a nonpulsating (constant) dc load current prevails;
2. There is no overlap angle as the commutation inductance L_k is neglected.

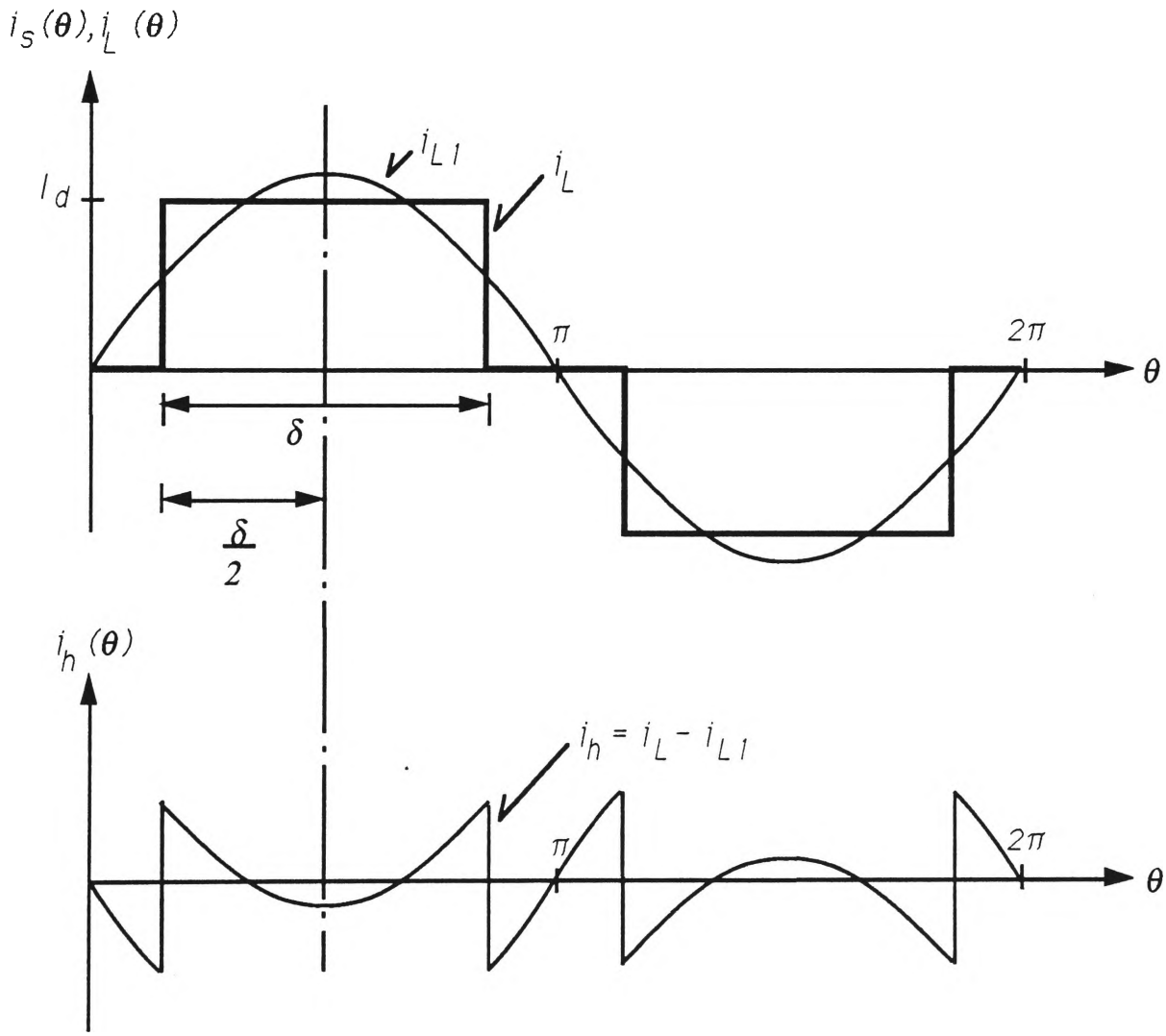

Figure 1.2 Line Current and Harmonic Current

Based on the above assumptions, converter line current i_L assumes quasi-square wave as shown in Figure 1.2 which may be expressed by Fourier series as follows:

$$i_L(\theta) = \frac{b_0}{2} + \sum_{n=1}^{\infty} [a_n \sin n\theta + b_n \cos n\theta] \qquad (1.1)$$

where

$$a_n = \frac{1}{\pi} \int_{-\pi}^{\pi} i_L(\theta) \sin n\theta \, d\theta \qquad n = 1, 2, \ldots \qquad (1.2)$$

$$b_n = \frac{1}{\pi} \int_{-\pi}^{\pi} i_L(\theta) \cos n\theta \, d\theta \qquad n = 0, 1, 2, \ldots \qquad (1.3)$$

The converter line current i_L is an odd function with half wave symmetry hence a_n and b_n can be solved to yield the following:

$$a_n = \frac{I_d}{\pi} \left[\int_{\frac{\pi-\delta}{2}}^{\frac{\pi+\delta}{2}} \sin n\theta \, d\theta - \int_{\frac{-\pi-\delta}{2}}^{\frac{-\pi+\delta}{2}} \sin n\theta \, d\theta \right]$$

$$= \frac{I_d}{n\pi} \left[-\cos n\theta \Big/_{\frac{\pi-\delta}{2}}^{\frac{\pi+\delta}{2}} + \cos n\theta \Big/_{\frac{-\pi-\delta}{2}}^{\frac{-\pi+\delta}{2}} \right]$$

Hence $$a_n = \frac{4I_d}{n\pi} \sin n \frac{\pi}{2} \sin n \frac{\delta}{2} \qquad (1.4)$$

and $$b_n = \frac{I_d}{\pi}\left[\int_{\frac{\pi-\delta}{2}}^{\frac{\pi+\delta}{2}} \cos n\theta \, d\theta - \int_{\frac{-\pi-\delta}{2}}^{\frac{-\pi+\delta}{2}} \cos n\theta \, d\theta\right] = 0$$

where I_d = amplitude of load current

δ = width of quasi-square current (converter line current)

Substituting Equation (1.4) into Equation (1.1) gives

$$i_L(\theta) = \sum_{n=1}^{\infty} \frac{4I_d}{n\pi} \sin\frac{n\pi}{2} \sin\frac{n\delta}{2} \sin n\theta \qquad (1.5)$$

Equation (1.5) describes the converter line current in terms of the Fourier series which comprises the fundamental term together with a number of harmonics.

The harmonic current i_h can be obtained by subtracting the fundamental current i_{L1} from the converter load current i_L given by Equation (1.1) as follows:

$$i_h(\theta) = i_L(\theta) - i_{L1}(\theta) \qquad (1.6)$$

$$i_h(\theta) = \sum_{n=3}^{\infty} a_n \sin n\theta \qquad (1.7)$$

where $$a_n = \frac{4I_d}{n\pi} \sin\frac{n\pi}{2} \sin\frac{n\delta}{2} \qquad n = 3, 5, 7, \ldots \qquad (1.8)$$

1.3 Effects of Harmonics

Harmonic currents and their magnitudes were given in the previous section for a particular converter environment. In this section the effects of harmonics on other systems are briefly described. The effects on the power system are illustrated with the aid of Figure 1.3.

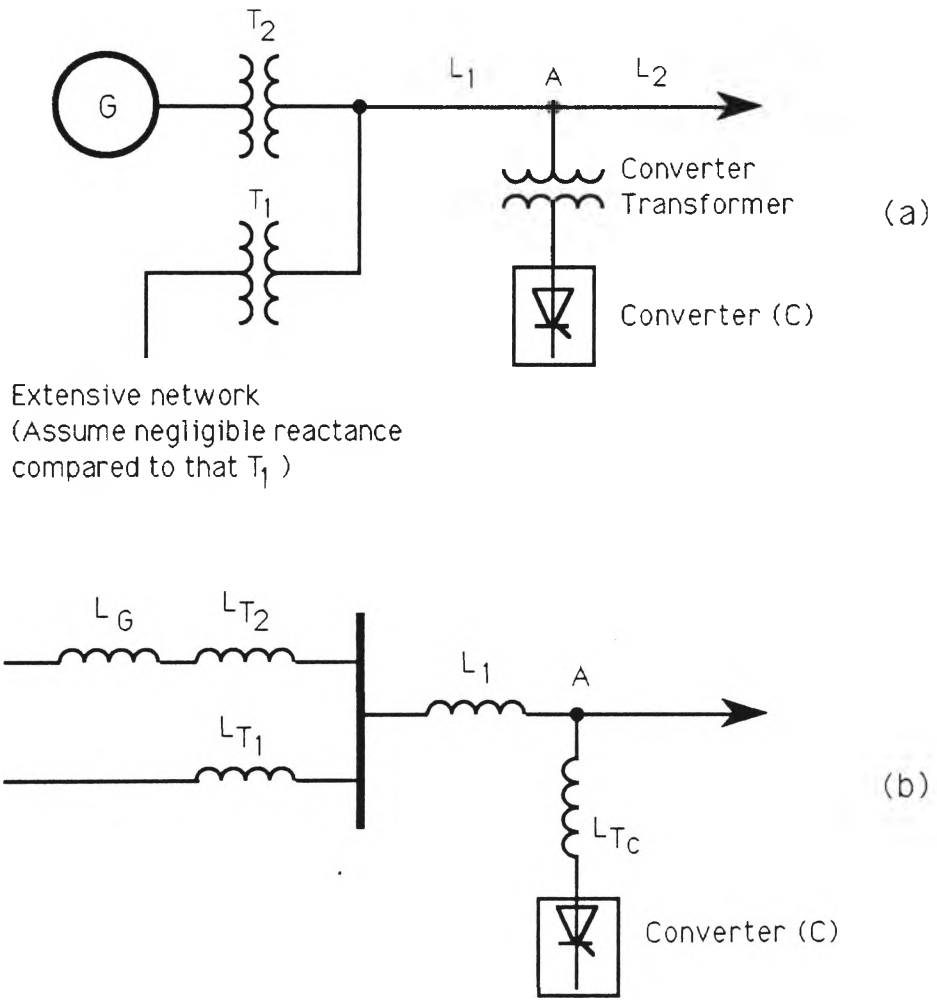

Figure 1.3 Typical Power System shows the Effect of Harmonics
(IEEE Std. 519, 1981)
(a) Schematic Diagram
(b) Impedance Diagram

The diagram of Figure 1.3 shows a converter (C) supplied from a power source (G) over a three-phase line L_1. The reactance of the source X_G+X_{T2} and the line X_{L1} are in series with the converter transformer reactance X_{TC}. If a harmonic current i_h flows between the converter and the source there will be harmonic voltage $e_h = i_h X_h$ at location A where X_h is the reactance between the converter and point A at the harmonic frequency. When there is an extension line, L_2, for supplying other loads, the harmonic voltage at A will cause a harmonic current to flow over that line as well, although the power to the rectifier is supplied only over line L_1. The higher the value of X_h, the greater will be the harmonic voltage at A and the higher the magnitude of the harmonic currents flowing over line L_2. Actually, the harmonic currents from a converter can flow into any part of an ac system to which it is connected, as determined by the impedances of the various branches of the system at the harmonic frequencies.

In communication systems, magnetic (or electrostatic) coupling (Miller, 1982) between electrical power circuits and communication circuits can cause what is known as communication interference. Current flowing in the power circuit produces a magnetic (or electrostatic) field that will induce a current (or voltage) in the nearby conductors of the communication circuit. The extent of interference will depend upon the magnitude of the induced current (or voltage), frequency and the efficiency of the magnetic (or electrostatic) coupling (Subjak and McQuilkin, 1990).

Harmonics can cause heating effects (Subjak and McQuilkin, 1990)

which are commonly identified as I^2R losses. By using superposition, the total losses can be expressed as the sum of the individual harmonic losses.

$$I^2R = I^2_{50Hz}R_{50Hz} + I^2_{250Hz}R_{250Hz} + I^2_{350Hz}R_{350Hz} + \ldots$$

Since most ac equipment ratings are based on 50Hz losses, the addition of the harmonic loss components requires derating the equipment (Miller, 1982). The total losses (50Hz plus harmonic losses) are to be within the specified equipment ratings. Regardless of actual quantities, it can be seen that they add to the total amount of heating.

On utility systems feeding domestic loads, interference with TV video signals by the harmonic currents generated by converters is usually the first indication of harmonic problems.

Ballasts for fluorescent or mercury lighting sometimes have capacitors which, together with the inductance of the ballast and circuit, have a resonant point. If this corresponds to one of the generated harmonics, excessive heating and failure can result.

Metering and instrumentation are affected by harmonic currents, particularly if resonant conditions occur which cause high harmonic voltage on the circuits. Induction disk devices such as watt-hour meters and overcurrent relays normally see only fundamental current, but phase unbalances caused by harmonic distortion can cause erroneous operation of these devices (IEEE Std. 519, 1981).

1.4 Basic Principles of Power Filters

The primary objective of power filters is to remove the unwanted harmonic currents or voltages from power systems. Harmonic voltages may be produced partially by the power generator itself (source harmonics) and partially by non-sinusoidal load currents (load harmonics). The filters can be inserted between the power supply and the load (series filters) to remove the harmonic voltage at the load (this series filter is usually used to reduce source harmonics), or can be connected across the load (shunt filters) to remove the harmonic current (this shunt filter is often used to filter the load harmonics). Both the series and shunt filters may employ passive tuned LC networks (Gyugyi and Strycula, 1976) or active power filters employing controllable electronic devices. This Section briefly outlines both types of power filters.

1.4.1 Passive Power Filter

Passive filters are usually formed in power systems by connecting a number of separate shunt branches across the terminals of ac source as shown in Figure 1.4.

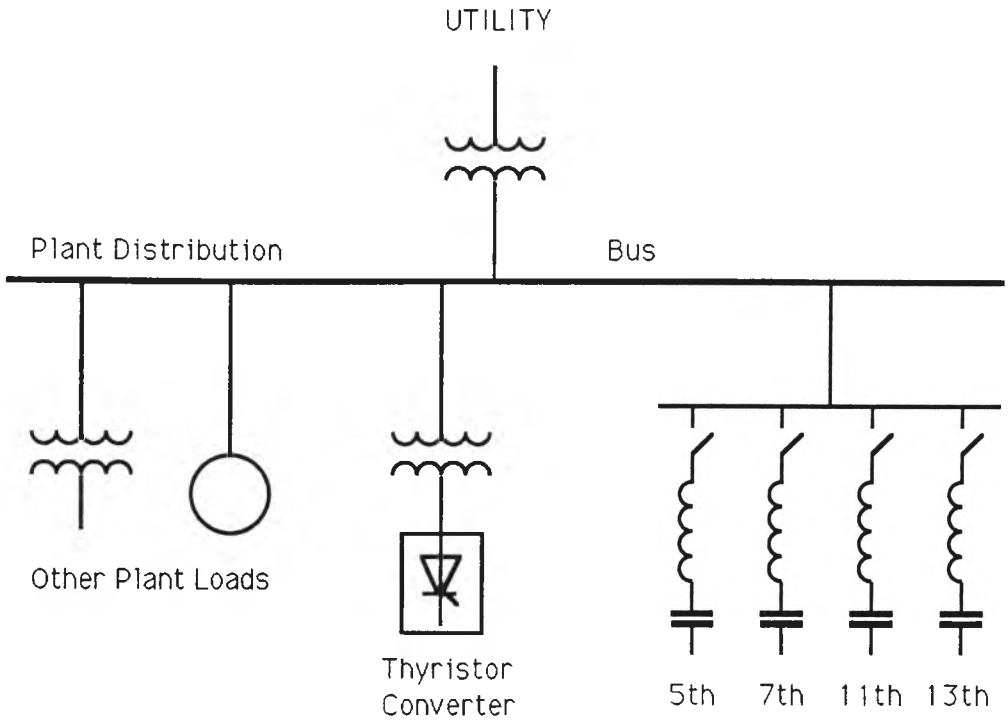

Figure 1.4 Power System with Shunt Filters (IEEE Std. 519, 1981)

Each of these branches is designed so that its impedance is very small at a specific harmonic frequency as compared to the rest of the power system impedances. Because the filters will absorb almost all of the harmonic currents generated by the converter, the filters must be sized to absorb these currents, as well as any other currents not isolated from the filter with impedance (i.e. transformer).

The capacitors in the filter must be of such a rating as to enable it to withstand the arithmetic sum of the fundamental and tuned harmonic voltage in the filter. As shown in Figure 1.5 the voltage and current rating of the capacitor and reactor are expressed as follows:

$$I_F = \sqrt{I_1^2 + I_h^2} \qquad (1.9)$$

$$I_1 = \frac{V_S}{X_C - X_L} \tag{1.10}$$

where V_S = system nominal voltage (fundamental)

X_C = reactance of capacitor

X_L = reactance of inductor

h = harmonic to which the filter is tuned

I_h = harmonic current

I_F = filter current

X_{Ch} = harmonic reactance of capacitor

X_{Lh} = harmonic reactance of inductor

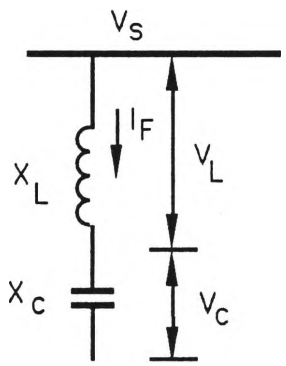

Figure 1.5 Shunt Power Filter

$$V_C = \sqrt{(I_1 X_C)^2 + (I_h X_{Ch})^2} \tag{1.11}$$

$$V_L = \sqrt{(I_1 X_{L1})^2 + (I_h X_{Lh})^2} \tag{1.12}$$

The volt-ampere rating of the capacitor is then $I_F V_C$

Table 1 lists the configuration of filters for power systems of different size. Other factors to be considered are capacitor size for reactive compensation, number of capacitor equipment, local factors influencing choices and the total converter load on the power system (IEEE Std. 519, 1981).

System Short-Circuit Capacity	Tuned Filter
0-250 MVA	5th
251-750 MVA	5th,7th
751-1500 MVA	5th,7th,11th
1500- MVA	5th,7th,11th,13th

Table 1 Typical Filter Configuration versus System Size

However, passive power filters have many problems in power systems. As shown in Figure 1.6, the shunt power filter exhibits lower impedance at a tuned harmonic frequency than the source impedance to reduce the harmonic currents flowing into the source.

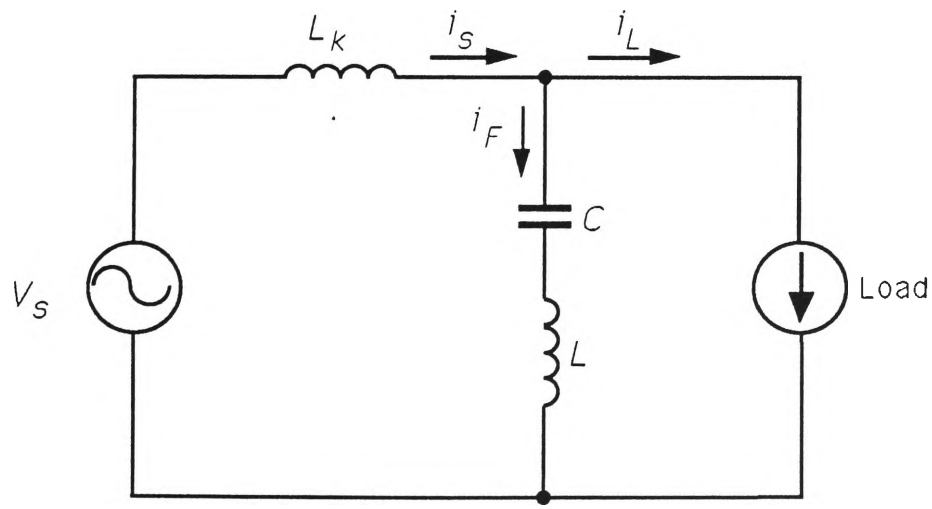

Figure 1.6 Equivalent Circuit of Shunt Power Filter System

Therefore the shunt power filters have the following problems (Akagi, Nabae and Atoh, 1986) :

1. The source impedance, which is not accurately known varies with the system configuration and thus strongly influences filtering characteristics of the shunt power filters.

2. The shunt power filters act as a current sink to the harmonic voltage included in the source voltage. In the worst case, the shunt power filters fall in series resonance with the source impedance.

3. At the specific frequency ($f_o = \frac{1}{2\pi\sqrt{(L_k+L)C}}$), resonance occurs between the source impedance and the shunt power filter, which is the so called harmonic amplifying phenomenon.

1.4.2 Active Power Filter

Because of the above problems associated with passive power filters, active power filters have been studied and developed in recent years. The active power filter was originally presented by Sasaki and Machida in 1971. The configuration of this system is shown in Figure 1.7. This method of eliminating the harmonic current is based on the principle of magnetic flux compensation in a transformer core. This is accomplished by controlling the amplifier injecting the compensating current into the tertiary winding of the transformer supplying the converter.

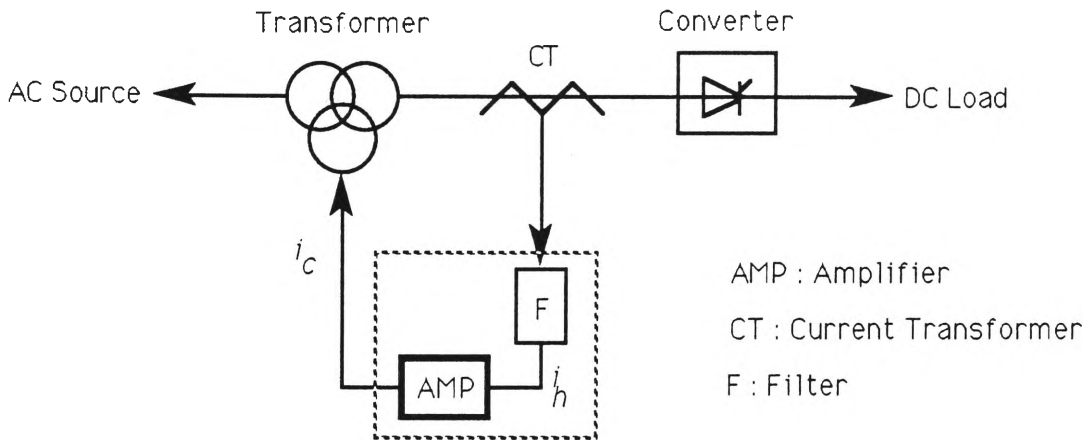

Figure 1.7 Configuration of Active Power Filter by Magnetic Flux Compensation

In Figure 1.7, F denotes the filter which removes the fundamental component in the sensed transformer secondary current. After filtering the fundamental frequency component, the detected signal is amplified so as to induce the same ampere-turns as that by secondary current. When the output current of the amplifier is made to flow into the tertiary winding differentially against the secondary current, harmonic components in the magnetic flux are theoretically cancelled by perfect compensation. However, this method is impractical in high power applications because the size, cost and losses in the linear amplifier rapidly become prohibitive (Gyugyi and Strycula, 1976).

In 1976, Gyugyi and Strycula presented a family of shunt and series active power filters and established the concept of the active power filter based on switched current injection consisting of voltage/current source inverters using power transistors. The basic setup of the active power filter based on switched current injection is shown in Figure 1.8 where

the active power filter comprises a constant current source and a modulation controller.

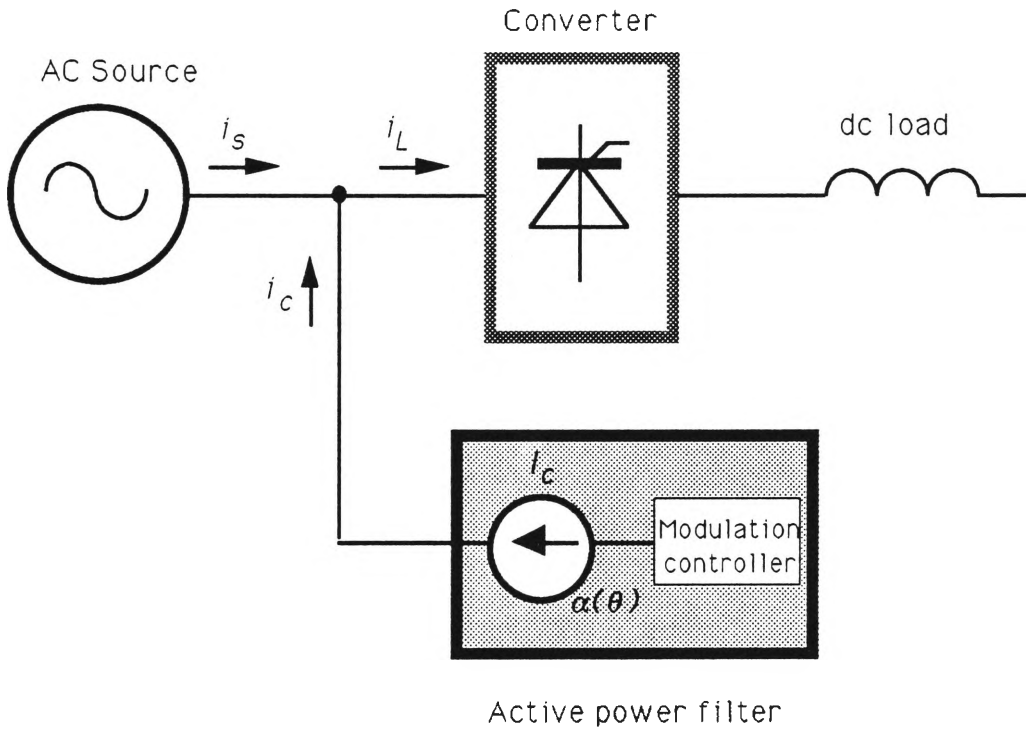

Figure 1.8 Basic Setup of Active Power Filter using Switched Current Injection

The basic operation is to inject the switched compensating current i_C that represents the harmonic current i_h into the ac line. The modulation controller generates a switching function using established modulation strategies. After injecting the compensating current i_C into the ac line, the line current i_S can be given as:

$$i_S(\theta) = i_L(\theta) - i_C(\theta) \tag{1.13}$$

A single-phase implementation of the active power filter is shown in

Figure 1.9 where a charged inductor L_m acts as the dc current source. In this arrangement, a smooth dc current I_C is maintained in the inductor. The output terminals of this circuit are connected between a line and the neatral of the 3-phase ac supply. Therefore in total of three such circuits are required tocompensate for the three line currents in a 3-phase situation. The solid state switches (transistor or gate controlled switches) are operated according to the command of a switching function $\alpha(\theta)$ which is generated by the modulation controller that converts I_C into the compensating current $i_C(\theta)$.

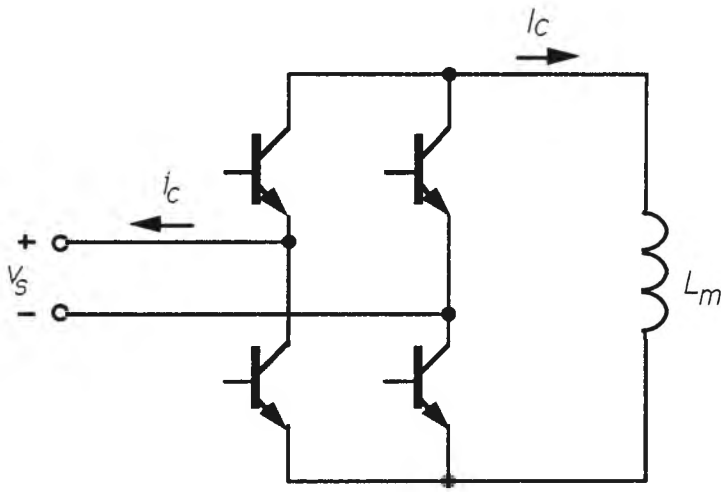

Figure 1.9 Practical Circuit of the Active Power Filter using Charged Inductor

1.5 Approach and Contribution of this Thesis

This thesis deals with active power filter applications, particularly the switching strategies that are suitable for current fed active power filters. The main contribution of this thesis is made by development of alternative switching strategies which are simple to implement while at

the same time are characterised by comparable and/or improved performance.

An important issue associated with active power filter performance is the choice of switching strategy. Historically, switching strategies have been developed for applications such as the conventional inverter (Bowes and Midoun, 1985) where the reference waveform is a continuous sinusoid. These techniques are not entirely suitable for power filtering applications where the reference waveform is discontinuous and is made up of infinite order harmonic components. Recently, an optimised switching strategy based on an Equal-Sampling Technique (EST) has been proposed for active power filter applications (Choe and Park, 1988). This switching strategy is presented in Chapter 2. However, the EST requires considerable memory capacity and intensive computing power to obtain the desired switching angles for the current pulses. Computationally less demanding and simple techniques are more favourable for active power filter applications especially in situations where load changes occur.

This thesis proposes two new switching strategies for active power filters based on equal current-time area criteria by matching the area of the current pulses of switching function and the area of the harmonic current waveform. The proposed techniques are computationally simple to implement and in both cases provide equal or better performance in terms of improved distortion factor characteristics when compared to EST.

The first of the two new switching strategies presented in Chapter 3 is called a Modified Equal-Sampling Technique (MEST). The MEST determines the width of the current pulses, which in this case is also equally spaced, by rectangular approximation of the relevant section of

the harmonic current waveform.

The second scheme presented in Chapter 4 is a Centroid Based Technique (CBT) which is essentially a non-equal sampling method. In this case the exact current-time area is determined and the current pulse to be injected is constrained to have the same area. Further, the centroids of both areas are established and aligned.

The performance of each switching strategy is evaluated based on the harmonic distortion factor and computational burden. This performance evaluation is presented in Chapter 5.

Finally, the implementation of switching strategies including MEST and CBT is presented in Chapter 6. The switching strategies are implemented based on Digital Signal Processor (DSP). The DSP being used in this thesis is Motorola DSP56001 which provides high speed, accuracy and flexibility. Finally, an analog circuit is used to simulate the line current of converter after compensating. This is used to prove the feasibility of the proposed techniques.

1.6 Summary of Contributions

- Investigation of existing switching strategies including switching strategies for inverter applications as well as active power filter applications.

- Development of a Modified-Equal Sampling Technique (MEST) which has a much reduced computational burden when

compared the EST proposed by Choe and Park, 1988. The effectiveness of the MEST in terms of reducing the harmonics is comparable to the EST approach.

- Development of a Centroid Based Technique which provides near optimal performance in terms of the harmonic distortion factor as well as requiring a relatively low computational burden.

- Performance evaluation and comparison of the proposed switching strategies and the EST.

- Implementation and verification of the proposed switching strategies on a stand alone digital signal processing card.

CHAPTER 2

SURVEY OF PULSE-WIDTH MODULATION (PWM) SWITCHING STRATEGIES

2.1 Introduction

Several switching strategies suitable for inverter applications have been developed in the last two decades. The majority of such switching strategies have been developed based on pulse width modulation (PWM) by switching an output waveform at a rate higher than the required fundamental frequency.

It is interesting to survey the literature, to trace the historical development of PWM inverter control techniques and relate these developments to the changes in technology. To clarify the current situation, it is helpful to recognise three distinct approaches currently being used to generate PWM switching strategies. The first, and the one which has been most widely used because it can be implemented easily using analogue techniques is the strategy based on 'natural sampled PWM' (Bowes and Bird, 1975). More recently, a new switching strategy referred to as 'regular sampled PWM' has been proposed which is considered to have a number of advantages when implemented using digital technique (Bowes and Clement, 1982). The third approach uses the so-called 'programmed PWM' switching strategy which is based on minimisation of certain performance criteria e.g. elimination of particular harmonics or the minimisation of harmonic current distortion (Buja, 1980).

This chapter provides a literature review of PWM switching strategies of interest and is organised as follows: Section 2.2 examines the existing PWM switching strategies for inverter applications. The Equal-sampling switching strategy for active power filter applications is discussed in Section 2.3. Finally, Section 2.4 concludes the Chapter.

2.2 Review of Existing Switching Strategies

2.2.1 Natural Sampled PWM

Natural sampled PWM is based on a well-defined modulation process, involving a direct comparison of a sinusoidal modulating wave with a triangular carrier (sampling) wave (Bowes, 1985). The general feature of this mode of PWM is shown in Figure 2.1.

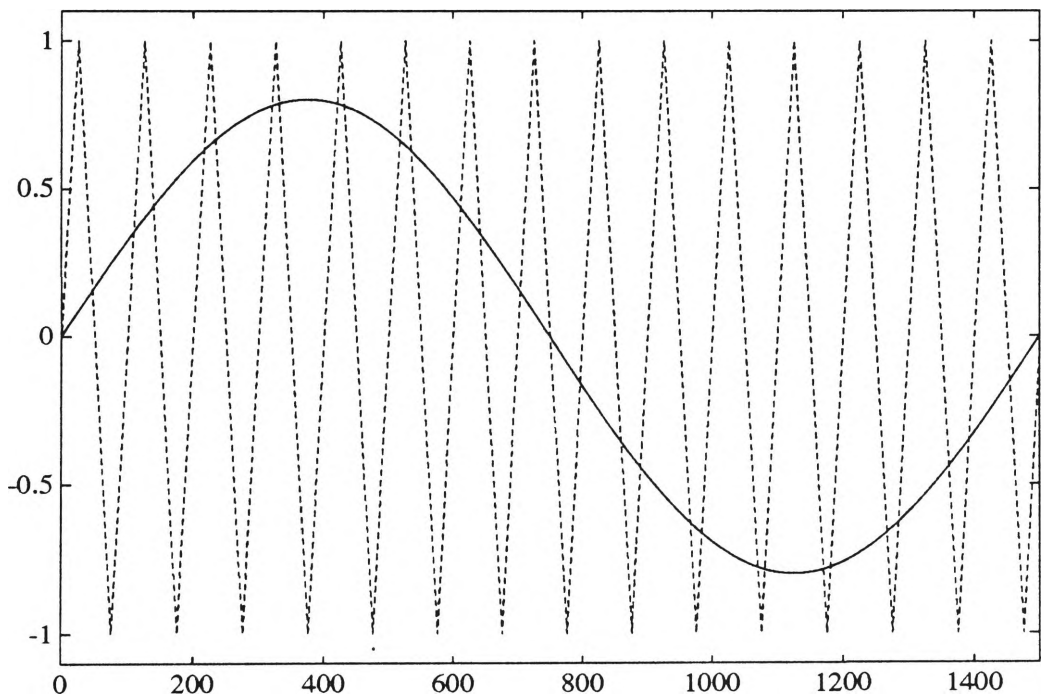

Figure 2.1 Natural Sampled PWM Process

The triangular carrier has a fixed amplitude and the ratio of sine wave amplitude to carrier amplitude is termed the modulation index (M_i) which is defined as follows:

$$M_i = \frac{amplitude\ of\ sine\ wave}{amplitude\ of\ triangular\ wave} \qquad (2.1)$$

The switching edge of the width-modulated pulse is determined by the instantaneous intersection between sinusoidal reference waveform and triangular waveform as shown in Figure 2.2. The sinusoidal reference waveform $d(t)$ has a frequency f. The triangular waveform has an amplitude of 1 and frequency equal to pf.

where $$p = \frac{frequency\ of\ triangular\ wave}{frequency\ of\ sinusoidal\ wave}$$

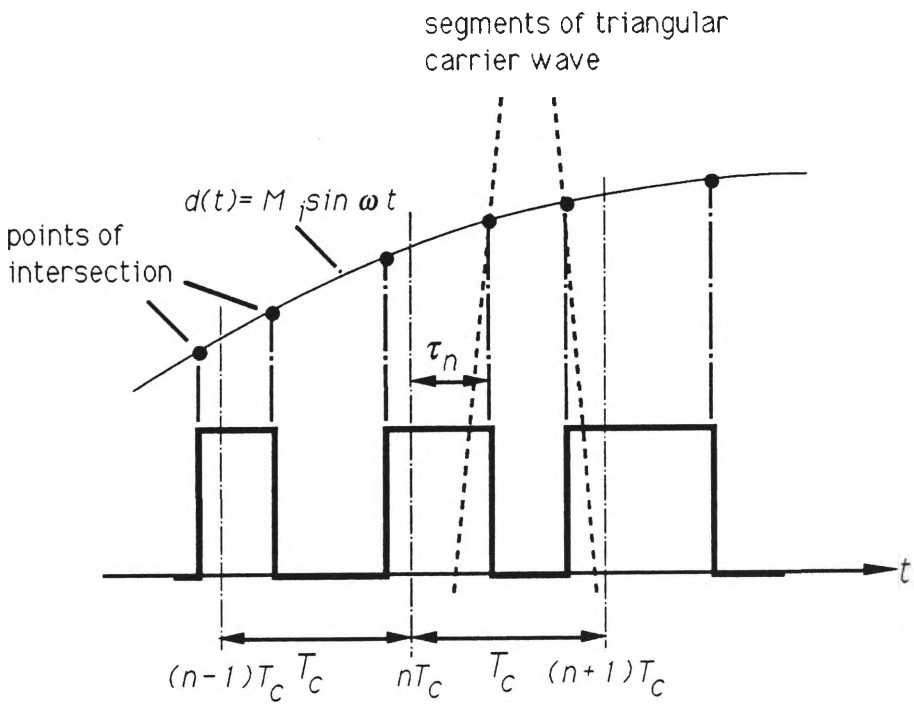

T_C = period of triangular wave

Figure 2.2 PWM Based on Natural Sampling

Note that because the switching edge of the width-modulated pulse is

determined by the instantaneous intersection of the two waves, the resultant pulse width is proportional to the amplitude of the modulating wave at the instant the switching occurs. This has two important consequences: first, the centres of the pulses in the resultant PWM wave are not equidistant or uniformly spaced; and, secondly, it is not possible to define the widths of the pulses using analytical expressions (Bowes and Clements, 1982).

In recent years, there has been increasing emphasis on the use of digital and microprocessor based techniques for the generation of PWM waveforms. Sinusoidal PWM, as described in this section, has been widely adopted because of its ease of implementation using analog control circuitry. In digital hardware implementation, the sine wave reference may be stored as a look-up table in Read Only Memory (ROM), and the sine values are counted at a rate corresponding to the required fundamental frequency. A triangular carrier wave is generated by using an up/down counter, and the two waveforms are compared using a digital comparator.

2.2.2 Regular Sampled PWM

An alternative approach which is essentially digital in nature and more appropriate for digital hardware or microprocessor implementation is illustrated in Figure 2.3 (Bowes, 1985).

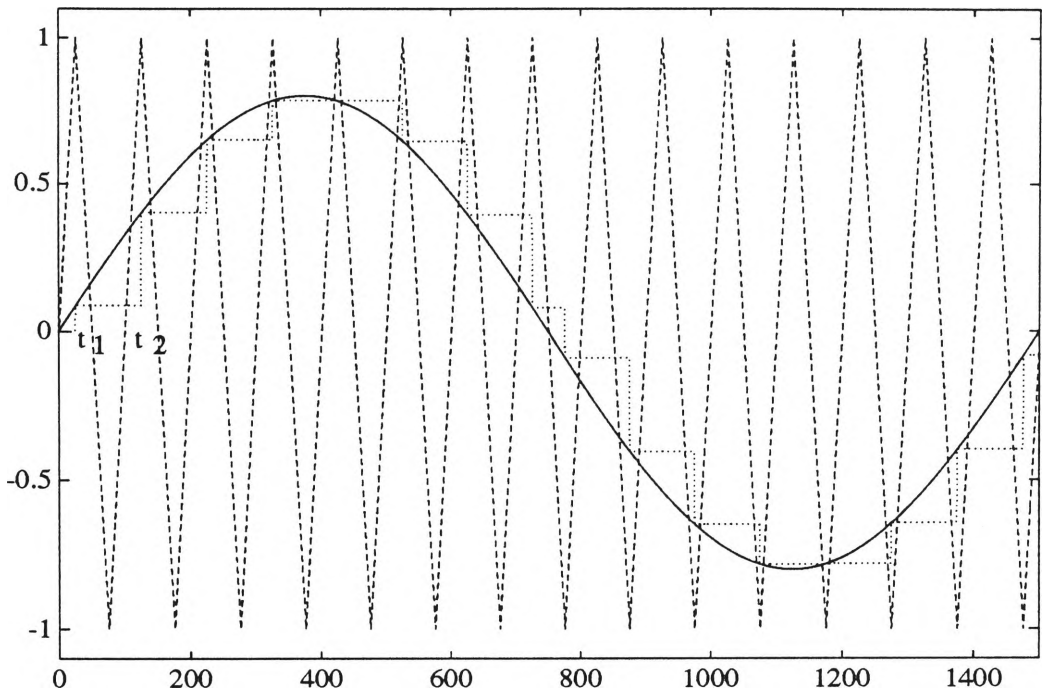

Figure 2.3 Regular Sampled PWM

The sinusoidal modulating wave is now sampled at sample instant t_1, and a first order sample and hold circuit maintains the above constant level of the sinusoidal modulating wave during the intersample period t_1 and t_2 until the next sample is taken at t_2. This process results in a stepped waveform. This stepped waveform is then compared with the triangular carrier wave and the points of intersection determine the switching instants of the width modulated pulses. Consequently the widths of the pulses are proportional to the amplitude of the modulating wave and the centre of the pulses occurs at uniformly spaced sampling times equal to the period (T_C) of the triangular wave as illustrated in Figure 2.4. This technique is known as uniform sampled or regular sampled PWM.

An important characteristic of regular sampling is that the sampling positions and sampled values can be defined unambiguously, such that

the pulses produced are predictable both in width and position. It should be noted that this was not the case in the natural sampled process as discussed in the previous section.

Because of this ability to define the pulse configuration precisely, it is now possible to derive a simple trigonometric function to calculate the pulse widths.

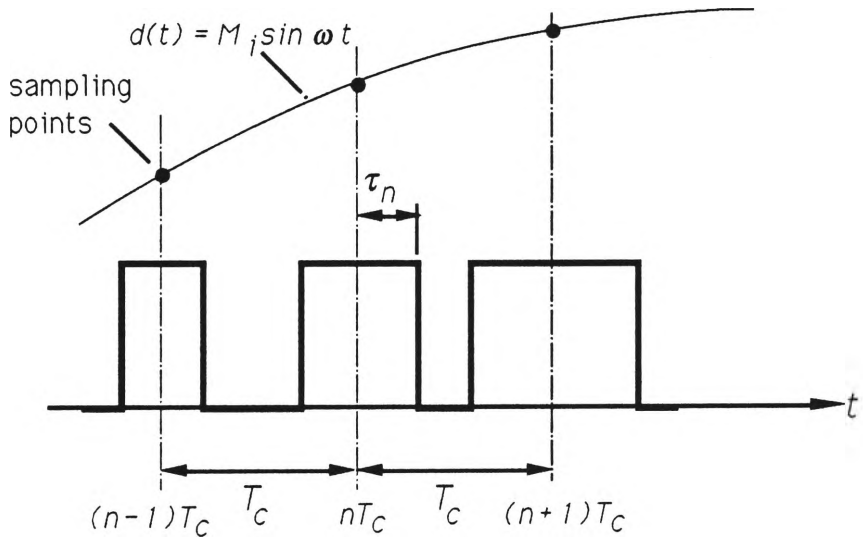

T_C = period of triangular wave

Figure 2.4 PWM Based on Regular Sampling

With reference to Figure 2.4 the half width of a pulse τ_n may be defined in terms of the sampled value of the modulating wave taken at time t_n ($t_n = nT_C$) as follows (Bowes, 1985):

$$\tau_n = \frac{T_C}{4}\left[1+M_i \sin(\omega t_n)\right] \qquad (2.2)$$

where T_C is the sampling time, t_n is the sampling instant and $M_i \sin(\omega t)$

is the modulating signal of Figure 2.4. The first term in this equation corresponds to the unmodulated carrier frequency pulse width, and the second term corresponds to the sinusoidal modulation required at time t_n. The significance of the simple analytical expression is that it has the potential to be used directly as the basis for a microprocessor software algorithm to calculate the pulse width in real time (Bowes, 1985).

2.2.3 Programmed PWM (Patel and Hoft, 1973)

The advantage of this strategy is that it offers the benefits of reduced low order harmonics and a reduction in the effective switching frequency for the same level of harmonics when compared to other conventional switching strategies (i.e. natural sampled and regular sampled PWM schemes). As discussed in the previous section, both natural and regular sampled PWM are generated with the intersection of a carrier wave and a modulating wave processes. By contrast, it is usual to generate programmed PWM by defining a general PWM waveform in terms of a set of switching angles and then solving for these switching angles by selecting the harmonics which are desired to be eliminated using a numerical technique.

The general features of programmed PWM waveform are illustrated in Figure 2.5 where it is assumed to be the output waveform of a PWM inverter. This waveform possesses periodic and quarter wave symmetry with the unit amplitude of ± 1 and M pulses per half cycle. Therefore, the switching function must obey the relationship:

$$\alpha(\theta) = -\alpha(\theta+\pi) \tag{2.3}$$

where $\alpha(\theta)$ is a switching function of the PWM periodic wave

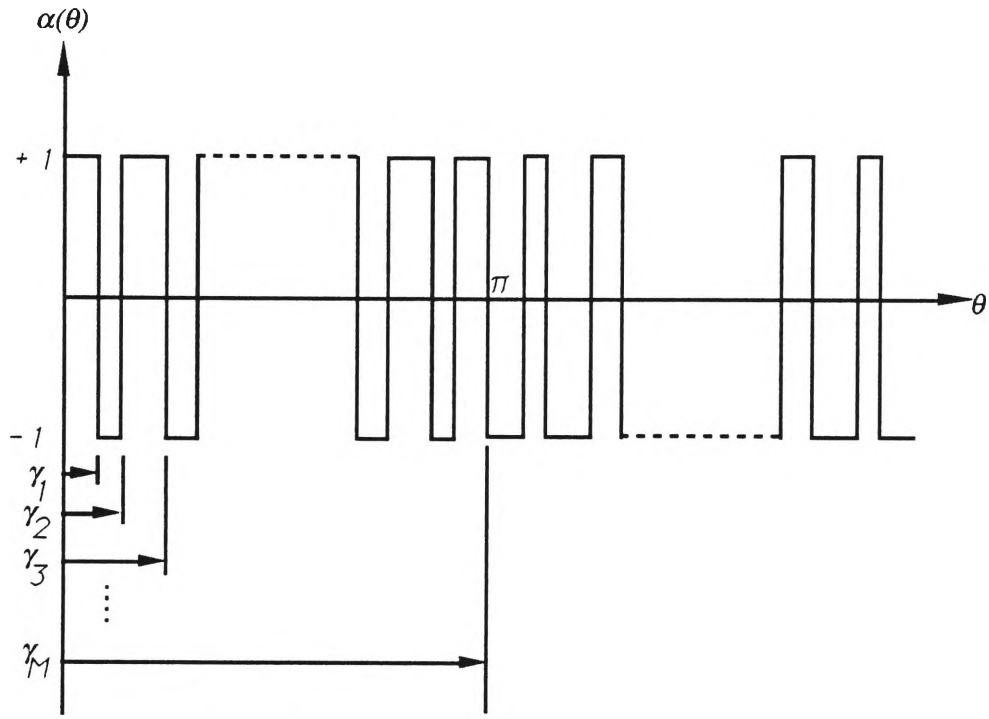

Figure 2.5 Programmed PWM

Let $\gamma_1, \gamma_2, \ldots, \gamma_M$ define the switching angles as shown in Figure 2.5. The Fourier series of this switching function can be given as follows (Enjeti, Ziogas and Lindsay, 1990):

$$\alpha(\theta) = \sum_{n=1}^{\infty} \left[a_n \sin n\theta + b_n \cos n\theta \right] \tag{2.4}$$

where

$$a_n = \frac{4}{n\pi} \left[1 + 2 \sum_{k=1}^{M} (-1)^k \cos n\gamma_k \right] \tag{2.5}$$

$$b_n = 0 \tag{2.6}$$

Equation (2.5) has M variables (γ_1 to γ_M) and a set of solutions can be obtained by setting it equal to zero and assigning a specific value to the amplitude of the fundamental a_1. These equations are non-linear in terms of the unknown switching angles and can be solved using a computer and numerical techniques to determine the switching angles. In the next section, further details of this switching strategy will be described as applied to active power filters.

2.3 Equal-Sampling Switching Strategy for Active Power Filter Applications

This section considers the programmed PWM switching strategy as applied to the active power filters (Park and Choe, 1988). The aim of this technique is to eliminate the selected harmonics using the filter circuit shown in Figure 1.9 of Chapter 1 that required no supply other than the main supply. The PWM control scheme of this active power filter is based on an Equal-Sampling Technique (EST) where the reference waveform is discontinuous (i.e. harmonic series). In contrast, for inverter applications the reference waveform is continuous and sinusoidal in shape. Following section discusses the above switching strategy in detail.

2.3.1 General Aspects

The general features of this strategy are shown in Figure 2.6 where the reference harmonic current $i_h(\theta)$ is represented by the switching function $\alpha(\theta)$.

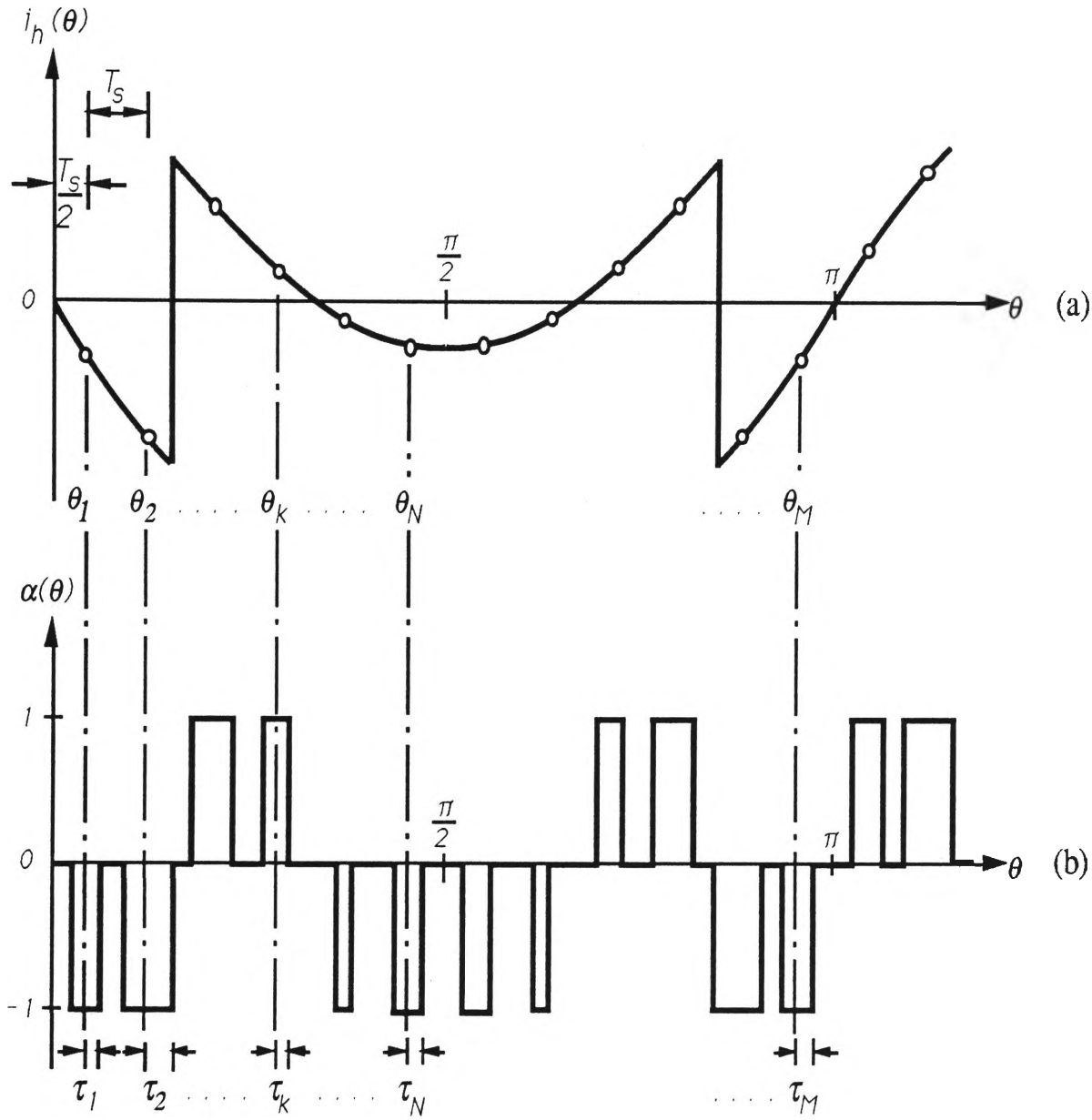

Figure 2.6 (a) Harmonic Current based on Equal-Sampling Technique
(b) Typical Switching Function

Suppose the reference harmonic current is sampled M times per half cycle of the ac supply waveform with pulse positions θ_1, θ_2, ... , θ_M. At each sampling point, absolute values and signs of the harmonic current are

collected in vector variables $H=(H_1, H_2,..., H_M)$ and $S=(S_1, S_2,..., S_M)$ respectively and subsequently used to calculate vector variables of the half pulse widths $\tau=(\tau_1,\tau_2,...,\tau_M)$. A typical switching function of this strategy is shown in Figure 2.6(b). The subscript k is introduced to identify the *kth* pulse width $2\tau_k$ at the pulse position θ_k where τ_k is defined as the half pulse width.

2.3.2 Theoretical Synthesis of EST

Let α_k, an elementary switching function, be defined as given in Figure 2.7 to facilitate the analysis. Assuming half-wave symmetry, the elementary switching function must obey the relationship:

$$\alpha_k(\theta) = -\alpha_k(\pi+\theta) \qquad (2.7)$$

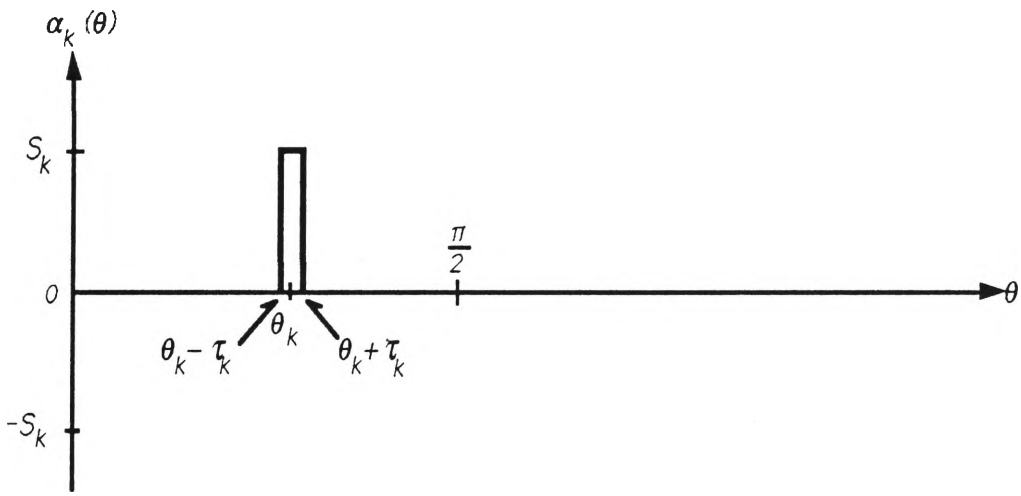

Figure 2.7 Elementary Switching Function

The elementary switching function can be represented by the Fourier expansion as follows:

$$\alpha_k(\theta) = \sum_{n=1}^{\infty}(a_n \sin n\theta + b_n \cos n\theta) \qquad (2.8)$$

where
$$a_n = \frac{2}{\pi}\int_{\theta_k-\tau_k}^{\theta_k\tau_k} \alpha_k(\theta) \sin n\theta \, d\theta \qquad n= 1, 2, \ldots \qquad (2.9)$$

and
$$b_n = \frac{2}{\pi}\int_{\theta_k-\tau_k}^{\theta_k+\tau_k} \alpha_k(\theta) \cos n\theta \, d\theta \qquad n= 1, 2, \ldots \qquad (2.10)$$

Solving for a_n and b_n gives

$$a_n = \frac{4}{n\pi} S_k \sin n\theta_k \sin n\tau_k \qquad \text{n=1,3,5..} \qquad (2.11)$$

$$b_n = \frac{4}{n\pi} S_k \cos n\theta_k \sin n\tau_k \qquad \text{n=1,3,5..} \qquad (2.12)$$

The switching function can be obtained by summing the M elementary switching functions. As the switching function also possesses half-wave symmetry, the number of its pulsewidth variables reduces to the sampling number M.

$$\alpha(\theta) = \sum_{k=1}^{M} \alpha_k(\theta) \qquad (2.13)$$

$$\alpha(\theta) = \sum_{n=1}^{\infty}(\bar{a}_n \sin n\theta + \bar{b}_n \cos n\theta) \qquad (2.14)$$

where
$$\bar{a}_n = \sum_{k=1}^{M} a_n \tag{2.15}$$

$$\bar{b}_n = \sum_{k=1}^{M} b_n = 0 \quad \text{for any odd } n \tag{2.16}$$

Furthermore, the switching function here also possesses quarter-wave symmetry. This reduces the number of pulse width variables to N (refer to Figure 2.5) and the relationship between N and M can be given as:

$$N = \frac{M}{2} \qquad \text{for } M = \text{even}$$
$$N = \frac{(M+1)}{2} \qquad \text{for } M = \text{odd} \tag{2.17}$$

Therefore, applying Equation (2.17), Equation (2.15) reduces to a simpler form as follows:

$$\bar{a}_n = \frac{4}{n\pi} \sum_{k=1}^{N} \rho_k \sin n\tau_k \tag{2.18}$$

where
$$\rho_k = 2S_k \sin n\theta_k \quad \text{for } k = 1, 2, \ldots, (N-1) \tag{2.19}$$

$$\rho_k = 2S_k \sin n\theta_k \quad \text{for } k = N \text{ and } M = \text{odd}$$
$$\rho_k = S_k \sin n\theta_k \quad \text{for } k = N \text{ and } M = \text{even} \tag{2.20}$$

Consequently, the Fourier series of the switching function $\alpha(\theta)$ with quarter-wave symmetry can be expressed as:

$$\alpha(\theta) = \sum_{n=1}^{\infty} \bar{a}_n \sin n\theta \qquad (2.21)$$

where $\bar{a}_n$ is given by Equation (2.18) which is expressed in terms of the pulse position θ_k and the half pulse width τ_k.

According to Figure 1.8, the current-fed inverter generates the compensating current $i_C(\theta)$ with constant amplitude I_C. Thus instantaneous compensating current i_C can be expressed as:

$$i_C(\theta) = I_C \cdot \alpha(\theta) \qquad (2.22)$$

When the compensating current i_C is injected into the ac lines, the compensated line current i_S can be expressed in Fourier series form using Equation (1.13) as follows:

$$i_S(\theta) = \sum_{n=1}^{\infty} \varphi \sin n\theta \qquad (2.23)$$

where for any order of n, the coefficient φ is

$$\varphi = a_n - I_C \cdot \bar{a}_n \qquad (2.24)$$

Substituting Equation (1.8) and Equation (2.18) into Equation (2.24) gives

$$\varphi = \frac{4}{n\pi}\left(I_d \sin\frac{n\pi}{2}\sin\frac{n\delta}{2} - I_c \sum_{k=1}^{N} \rho_k \sin n\tau_k\right) \qquad (2.25)$$

The difference between the harmonic current i_h and the compensating current i_c can cause the residual harmonic current i_{hr} to remain in the ac line current i_s. The residual harmonic current can be defined as:

$$i_{hr} = i_h - i_c \qquad (2.26)$$

The residual current may contain infinite order of the harmonic magnitudes. The coefficient φ of Equation (2.25) denotes the residual harmonic magnitude for any order n. To eliminate the undesirable harmonics, Equation (2.24) can be used to establish the following criteria:

$$I_c.\bar{a_1} = 0 \qquad \text{for } n = 1 \qquad (2.27)$$

$$a_n - I_c.\bar{a_n} = 0 \qquad \text{for } n = 3, 5, \ldots, N \qquad (2.28)$$

As the Fourier coefficient $\bar{a_n}$ of Equation (2.18) is a function of N pulsewidth variables $(\tau_1, \tau_2, \ldots, \tau_N)$, to determine various pulsewidths, N equations are required. These N equations can be set up using Equations (2.27) and (2.28) as follows:

for $n = 1$,

$$\sum_{k=1}^{N} \rho_k \sin \tau_k = 0 \qquad (2.29)$$

for $n = 3, 5, \ldots, N$,

$$\frac{4}{n\pi}\left(I_d \sin\frac{n\pi}{2}\sin\frac{n\delta}{2} - I_c \sum_{k=1}^{N} \rho_k \sin n\tau_k\right) = 0 \qquad (2.30)$$

Let us now define an injection ratio r as the ratio of compensating current amplitude to dc load current amplitude given by

$$r = \frac{I_c}{I_d} = \text{injection ratio} \qquad (2.31)$$

Now Equation (2.30) can be simplified as follows:

$$\left(I_d \sin\frac{n\pi}{2}\sin\frac{n\delta}{2} - r \sum_{k=1}^{N} \rho_k \sin n\tau_k\right) = 0 \qquad (2.32)$$

Once r is specified, the N pulsewidths are established using Equation (2.32) which corresponds to $(N-1)$ unknowns and the remaining unknown corresponds to the Equations (2.29). These N equations can be represented in vector form as:

$$f(\tau) = 0 \qquad (2.33)$$

where $f = [f_1, f_2, \ldots, f_N]^T$, an $N \times 1$ matrix

$\tau = [\tau_1, \tau_2, \ldots, \tau_N]^T$, an $N \times 1$ matrix

Equation (2.33) is a set of non-linear equations which is transcendental in nature. These non-linear equations can be solved by a digital computer using a numerical technique (e.g. Newton-Rapson method). However, in

solving a set of non-linear equations numerically, the primary concern is the convergence of the technique used. It is usually a trial and error process, and no general method exists that can guarantee convergence to a solution (Enjeti, Ziogas and Lindsay, 1990).

Figure 2.8 shows the trajectory of each switching instant versus the injection ratio obtained by numerical solution. This trajectory is based on a number of pules per half cycle $M=12$.

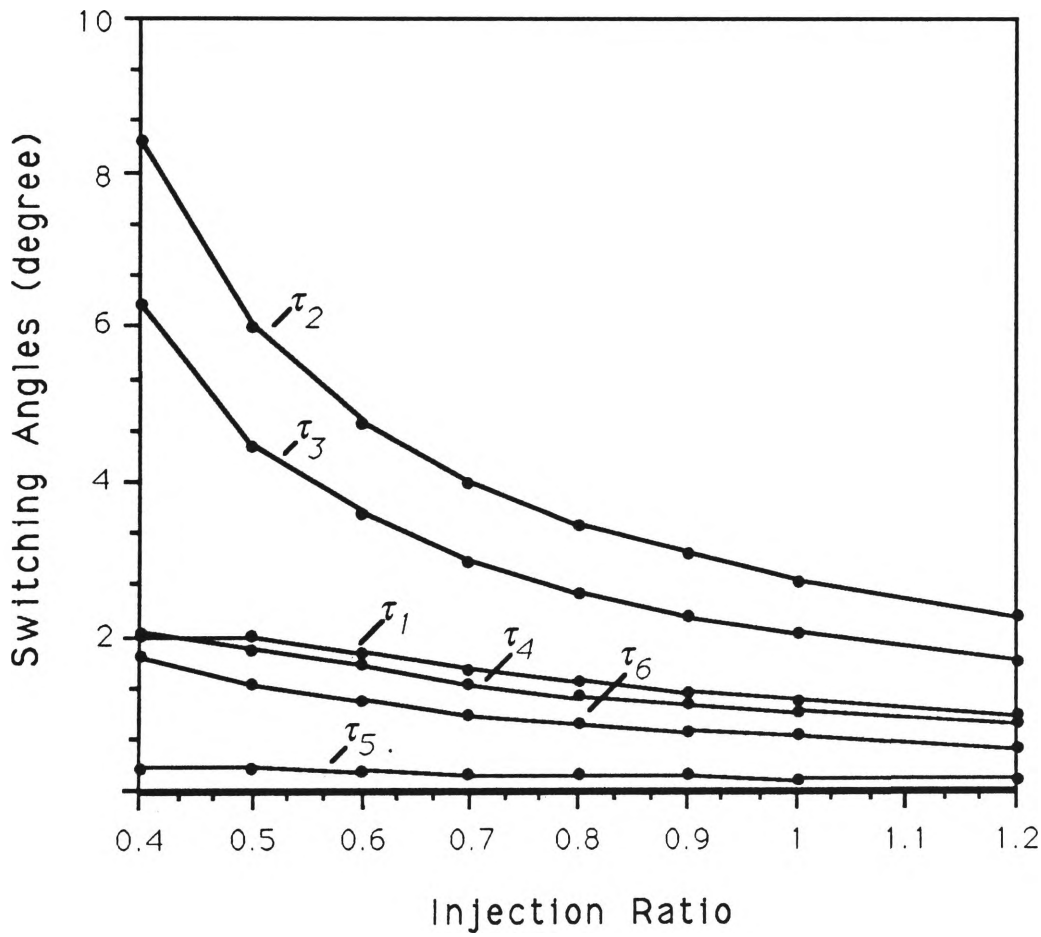

Figure 2.8 The Variation of the Switching Angles with the Injection Ratio.

2.4 Conclusion

A survey of the pulse-width modulation switching strategies of interest to this project has been presented in this chapter. A Literature review revealed that the switching strategies were initially developed for analogue implementation based on the natural sampled PWM. The increasing availability of digital circuits and Large Scale Integrated (LSI) technology offered the possibility of realising digital PWM techniques. New switching strategies were then developed including the regular sampled PWM and the programmed PWM.

The programmed PWM which is essentially an Equal-Sampling Technique was applied to active power filter. It was shown that to obtain the pulsewidth, a set of non-linear equations has to be solved. This implies that the computational burden is high as well as implementation in real-time is difficult.

CHAPTER 3

MODIFIED EQUAL-SAMPLING SWITCHING STRATEGY

3.1 Introduction

This chapter presents a novel switching strategy which is essentially a Modified Equal-Sampling Technique that is suitable for active power filter applications. In current fed active power filters, the compensating current has to be able to remove or cancel the energy of the unwanted harmonic current. This implies that the energy of the compensating current should be equal to the energy of the unwanted harmonic current.

Kim and Ehsani (1990) showed that a PWM waveform can be generated by using a simple algorithm where the area of the reference waveform is matched to the area of the output PWM waveform. However, this technique was developed based on the reference waveform being a single sinusoid. In the case of active power filter where the reference waveform is a harmonic series, this technique cannot be applied easily.

This chapter is organised as follows: Section 3.2 presents general aspects and theoretical synthesis of MEST. Section 3.3 describes the boundary conditions applicable to MEST. Fourier series of the switching function of MEST is derived in Section 3.4. Simulation results are included in Section 3.5 and, finally, Section 3.6 concludes the chapter.

3.2 General Aspects and Theoretical Synthesis of MEST

The general features of the proposed modified equal-sampling technique are shown in Figure 3.1. The reference harmonic waveform is sampled

using a high frequency clock with a period of t_C. At M number of equal-sampling points per half cycle which are separated by a period T_S (i.e. θ_{k-1}, θ_k,..., θ_M), the absolute values and signs of the harmonic current are gathered in vector variables $H=(H_1, H_2,..., H_M)$ and $S=(S_1, S_2,..., S_M)$ respectively.

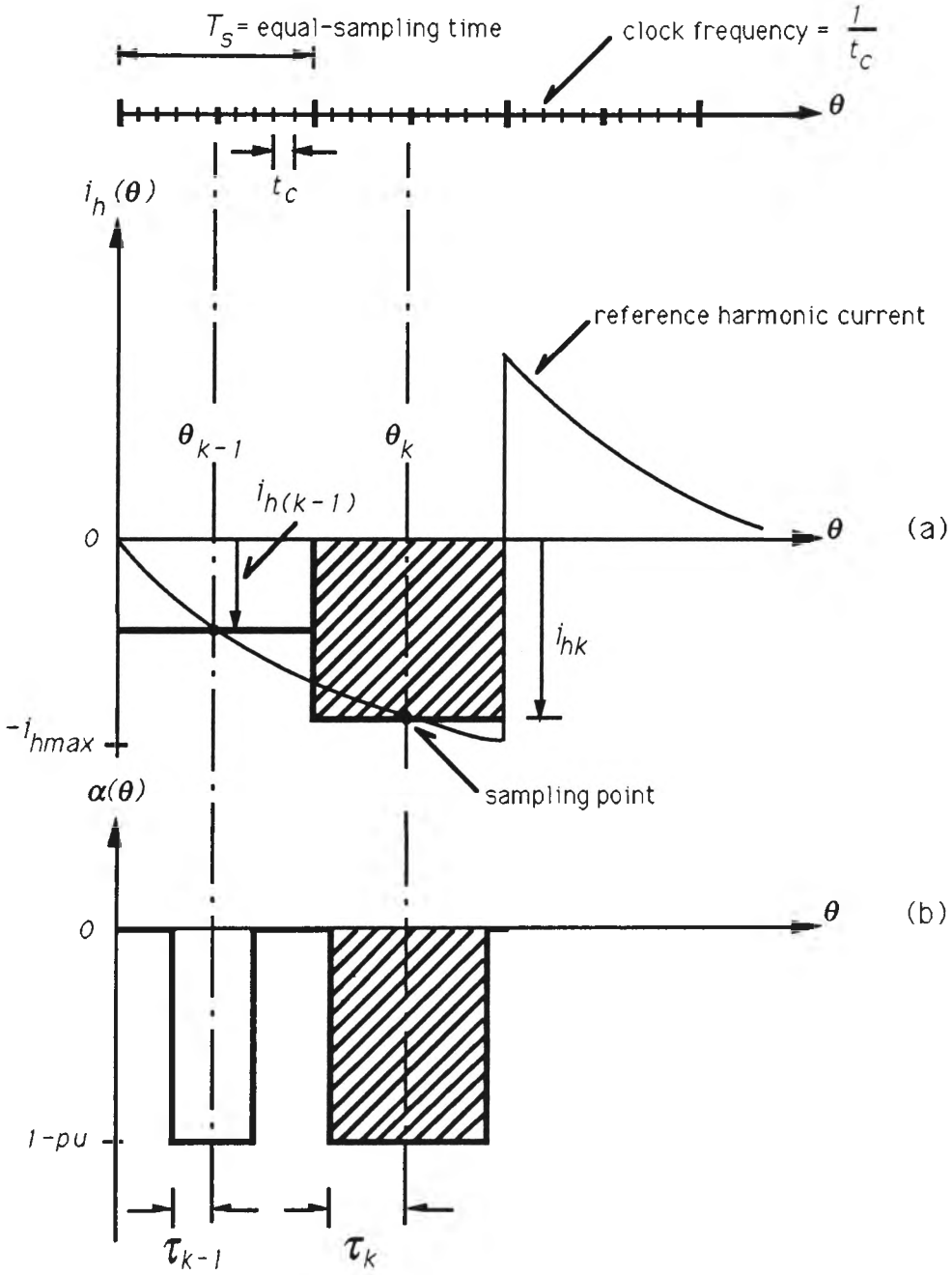

Figure 3.1 Pulse Details of the Switching Function based on the Modified Equal-Sampling Technique

At the sampling point θ_k the area under the reference harmonic current is approximated by the hatched rectangular area as shown in Figure 3.1(a). This approximation becomes increasingly valid if the number of sampling points per half cycle is large.

Thus, the hatched area A_{hk} is given by

$$A_{hk} = i_{hk} \cdot T_S \tag{3.1}$$

Referring to Figure 3.1(b) the hatched area under the actual injected current pulse with a width of $2\tau_k$ is given by

$$A_{sk} = I_C \cdot 2\tau_k \tag{3.2}$$

Equating A_{hk} and A_{sk} from the Equations (3.1) and (3.2), the half pulsewidth τ_k is obtained as follows:

$$\tau_k = \frac{i_{hk} \cdot T_S}{2I_C} \tag{3.3}$$

Consider the clock frequency f_C at which the reference harmonic current is sampled. As the clock frequency is a multiple of the equal-sampling frequency f_S, the relationship between the clock frequency f_C and the equal-sampling time T_S can be given as:

$$T_S = n_C \cdot t_C = \frac{n_C}{f_C} \tag{3.4}$$

where n_C = number of samples per cycle of the equal-sampling frequency

Substituting Equation (3.4) in Equation (3.3) gives

$$\tau_k = \frac{i_{hk} \cdot n_c \cdot t_c}{2I_c} \tag{3.5}$$

Let us define the 'width factor' as a ratio of the pulsewidth τ_k and the time per half pulsewidth as:

$$wf = \frac{\tau_k}{n_k' \tau_c} \tag{3.6}$$

where n_k' = number of samples for the half pulsewidth τ_k

Applying Equation (3.6) in Equation (3.5) gives

$$n_k' = \frac{i_{hk} \cdot n_c}{2I_c \cdot wf} \tag{3.7}$$

Considering the reference harmonic current waveform in Figure 3.1, at each equal-sampling point the amplitude of the current waveform can be normalised to 1 pu using i_{hmax}. Therefore Equation (3.7) can be rewritten as:

$$n_k' = \frac{H_k \cdot i_{hmax} \cdot n_c}{2I_c \cdot wf} \tag{3.8}$$

where $H_k = \frac{i_{hk}}{i_{hmax}}$ = per unit magnitude of the reference harmonic current at the *kth* equal-sampling point

i_{hmax} = peak amplitude of the reference harmonic current

As the peak amplitude i_{hmax} of the harmonic current is equal to the fundamental current of the converter supply line at $\theta = \frac{\pi-\delta}{2}$ (see Figure 1.2), Equation (3.8) can be expressed as:

$$n_k' = \frac{H_k n_c \frac{4Id}{\pi} \sin\frac{\pi}{2} \sin\frac{\delta}{2} \sin\frac{\pi-\delta}{2}}{2I_c \cdot w_f} \qquad (3.9)$$

which can be simplified as follows:

$$n_k' = \frac{H_k n_c \sin\delta}{\pi r w_f} \qquad (3.10)$$

where r = injection ratio

Equation (3.10) is a linear equation and it defines the *kth* pulsewidth of the switching function which is linearly proportional to the amplitude of the reference harmonic current at each equal-sampling point and inversely proportional to the injection ratio. This implies that the pulsewidth of the switching function can be obtained simply when the injection ratio is given.

3.2 Boundary Conditions applicable to MEST

The number of samples n_k' per half pulsewidth must be an integer number and proportional to the number of samples n_c per cycle of the equal-sampling frequency. Naturally as n_c increases, the accuracy of the

injected current pulsewidth also increases. As expected the variation of the injection ratio also affects the pulsewidths at the various equal-sampling points. For this reason the boundary conditions must be defined.

Clearly from Figure 3.1, the smallest pulsewidth that can be generated has a width t_c. This can be expressed as:

$$n_k' \geq 1 \tag{3.11}$$

Next consider the maximum pulsewidth that is possible to be generated as illustrated in Figure 3.2.

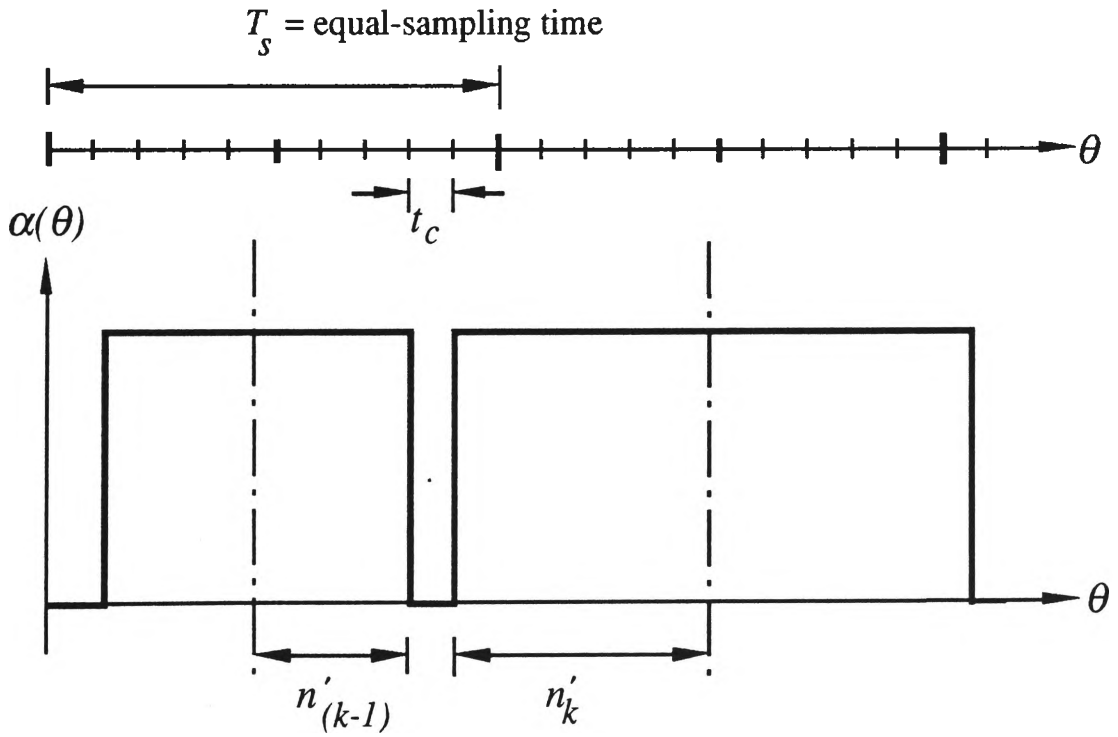

Figure 3.2 Pulsewidth detail showing the Maximum Width of Pulses

From Figure 3.2 we can see that a summation of *kth* pulsewidth (n'_k) and *(k-1)th* pulsewidth ($n'_{(k-1)}$) must be equal to or less than the ratio of equal-sampling time T_S and clock time t_C which can be expressed as follows:

$$n'_k + n'_{(k-1)} \leq \frac{T_S}{t_C} \tag{3.12}$$

The pulsewidth which is obtained using Equation (3.10) must satisfy both Equations (3.11) and (3.12).

3.3 Fourier Series Analysis

Fourier series of the switching function of the modified equal-sampling technique can be expressed in a form similar to the equal-sampling technique (Park and Choe, 1988). The Fourier series of the switching function is given as follows:

$$\alpha(\theta) = \sum_{n=1}^{\infty} \bar{a}_n \sin n\theta \tag{3.13}$$

where

$$\bar{a}_n = \frac{4}{n\pi} \sum_{k=1}^{N} \rho_k \sin n\tau'_k \tag{3.14}$$

and

$$\rho_k = 2S_k \sin n\theta_k \quad \text{for } k=1, 2,..., (N-1) \tag{3.15}$$

$$\begin{aligned} \rho_k &= 2S_k \sin n\theta_k \quad \text{for } k=N \text{ and } M= \text{odd} \\ \rho_k &= S_k \sin n\theta_k \quad \text{for } k=N \text{ and } M= \text{even} \end{aligned} \tag{3.16}$$

The compensating current which has to be injected into the ac supply line can be expressed using Equation (2.22) of Chapter 2 as follows:

$$i_C(\theta) = I_C \cdot \sum_{n=1}^{\infty} \bar{a}_n \sin n\theta \qquad (3.17)$$

Following the injection of the compensating current, the line current can be expressed as:

$$i_S(\theta) = \frac{4}{n\pi} \sum_{n=1}^{\infty} \left[I_d \sin\frac{n\pi}{2} \sin\frac{n\delta}{2} - I_c \sum_{k=1}^{N} \rho_k \sin n\tau_k' \right] si\, n\, n\theta \qquad (3.18)$$

which can be simplified to the following:

$$i_S(\theta) = \frac{4I_d}{n\pi} \sum_{n=1}^{\infty} \left[\sin\frac{n\pi}{2} \sin\frac{n\delta}{2} - r \sum_{k=1}^{N} \rho_k \sin n\tau_k' \right] \sin n\theta \qquad (3.19)$$

3.4 Simulation Results

In this section the simulation results are presented. The switching function of this strategy can be generated using Equation (3.10) if the injection ratio and width-factor are given. The simulation program was written using MATLAB (software package). This simulation program is

given in Appendix 1.

Figure 3.3(a) shows the switching function and reference harmonic current per half cycle for an injection ratio r equal to 0.5. The number of pulses per half cycle M is equal to 12 and width-factor w_f is equal to 1. Since the number of pulses per half cycle is equal to 12, this implies that if the line frequency is 50 Hz, the switching frequency would be 1,200 Hz. This is an ideal case based on switching devices having zero turn on/off times and the charged inductor as shown in Figure 1.8 where a constant current without ripple is assumed. The harmonic spectrum of reference harmonic current and switching function are shown in Figure 3.3 (b) and (c) respectively.

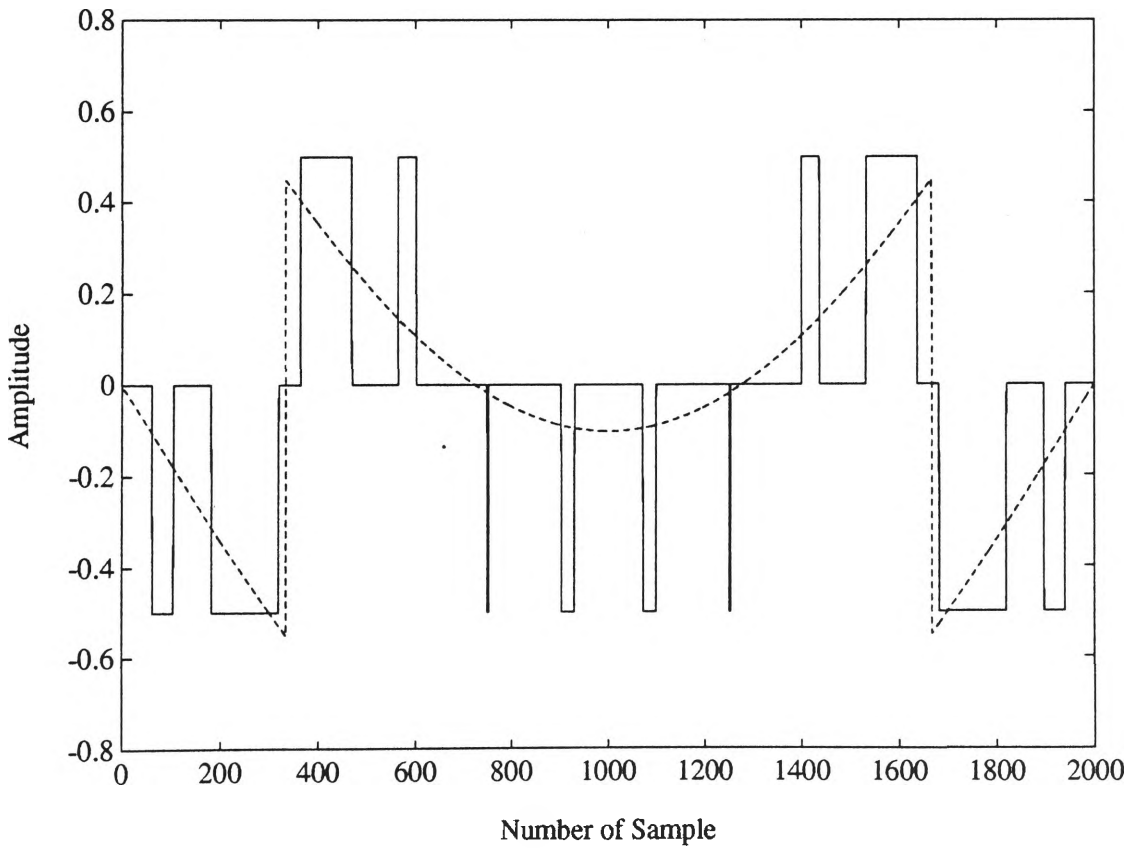

(a)

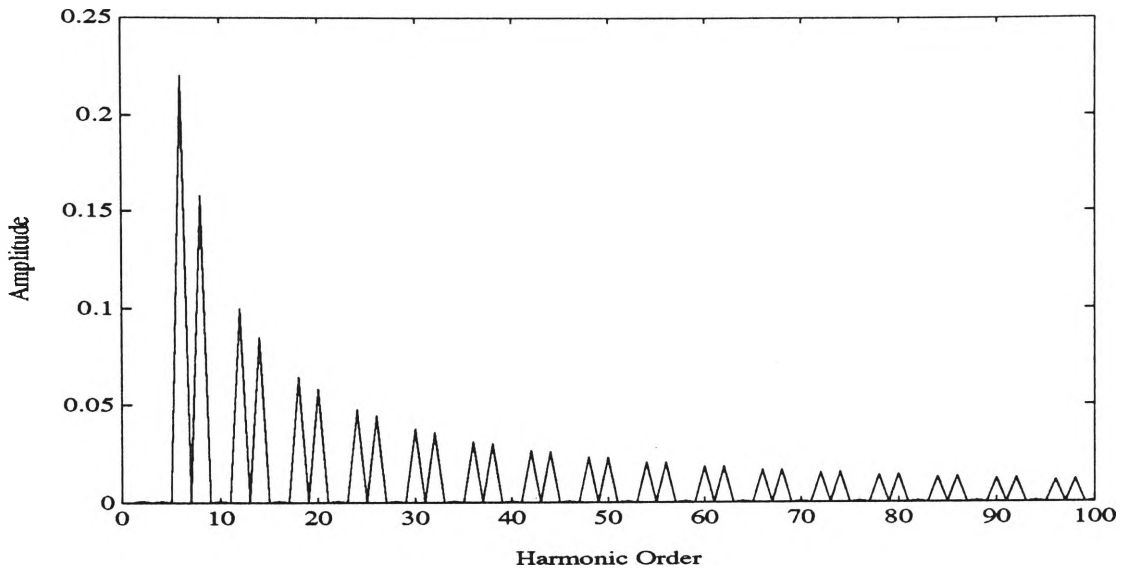

(b)

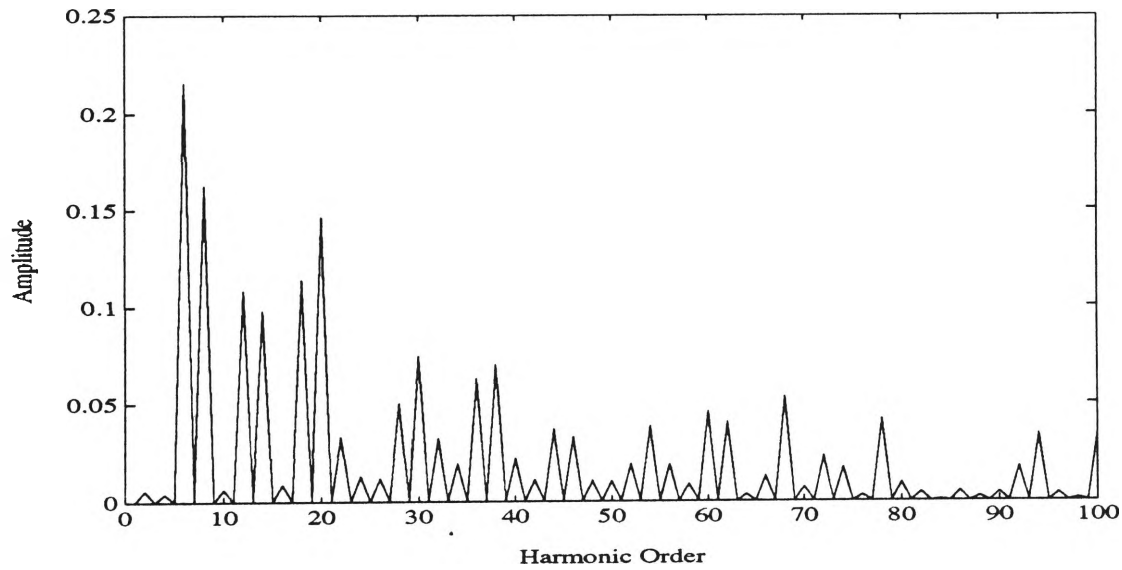

(c)

Figure 3.3 (a) Reference Harmonic Current and Switching Function per Half Cycle, M=12, r=0.5, w_f=1

(b) Harmonic Spectrum of Reference Harmonic Current Waveform

(c) Harmonic Spectrum of Switching Function

Theoretical waveform of line current i_S following the injection of the compensating current is shown in Figure 3.4.

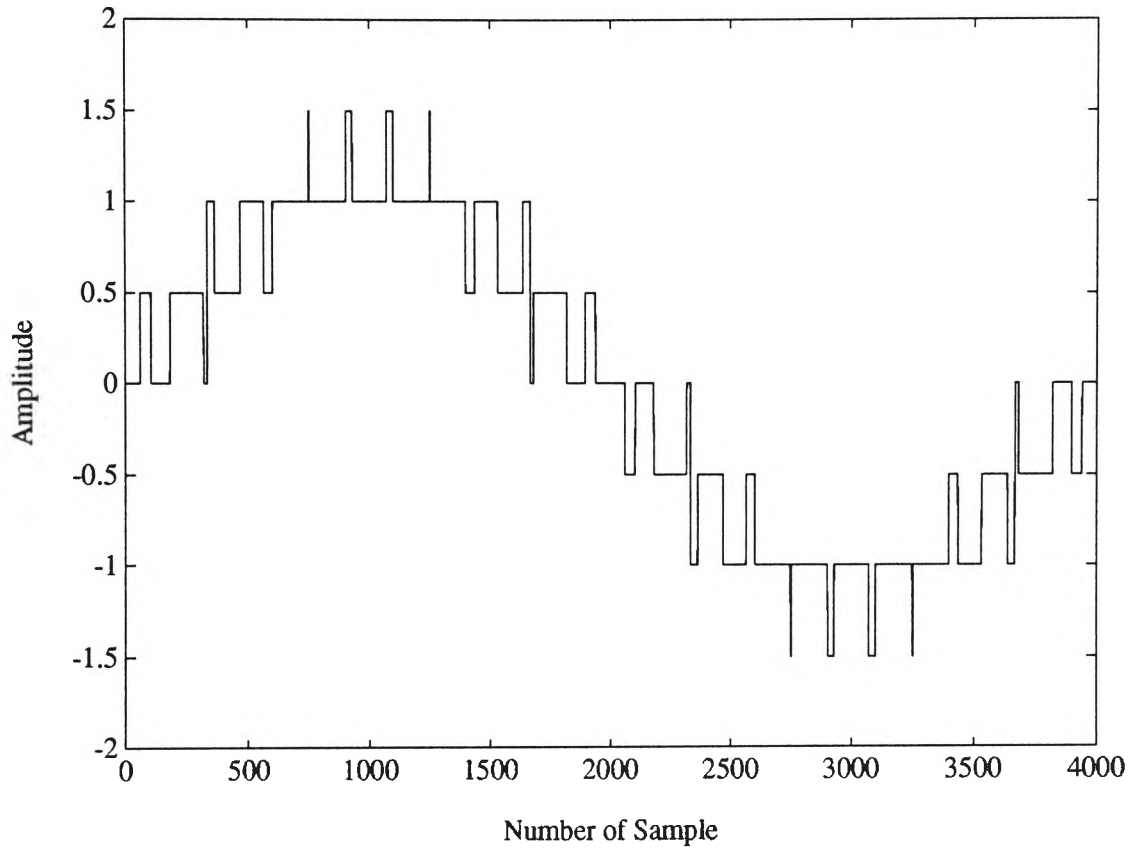

Figure 3.4 Waveform of the Compensated Line Current

3.5 Conclusion

In this chapter the modified equal-sampling switching strategy was presented. The proposed technique is based on an equal-current time area criteria, whereby the area of the reference harmonic current waveform is matched with that of the switching function waveform. The primary objective of this proposed technique is to generate a switching function employing a simple algorithm. To avoid the complexity involved in

computing exact areas under the reference harmonic current wave, the areas are approximated by rectangular pulses.

Performance evaluation of the MEST together with other switching strategies will be made in Chapter 5.

CHAPTER 4

CENTROID BASED SWITCHING STRATEGY

4.1 Introduction

This chapter presents a new centroid based switching strategy which is effectively a non equal-sampling technique. The aim of this centroid based technique (CBT) is not only to generate a more effective switching function than the modified equal-sampling technique but also to maintain simplicity.

It appears logical that any switching strategy based on either uniform or non-uniform sampling technique should lead to current pulses which have equivalent current-time areas as the harmonic current waveform being sampled. In general it expected that a non-uniform sampling approach should lead to superior harmonic cancellation. This is because the compensating current can be placed at appropriate positions of choice so that their areas are better matched with the areas under the harmonic current waveform being sampled. On the basis of this intuitive notion it is logical to align the time-axis centroid co-ordinate of both the compensating current pulse and a corresponding area of the harmonic current waveform.

For the CBT, we require a higher level of accuracy and need to ensure that current pulses have the same current-time area as the corresponding reference area. Thus the area of compensating current pulse may be obtained by employing the integral $\int i_h dt$ over the sampling period of specific harmonic waveform.

This chapter is organised as follows: Section 4.2 presents characteristics of the proposed switching strategy. Fourier series analysis of CBT is

derived in Section 4.3, the simulation results are included in Section 4.4, and finally, Section 4.5 concludes the chapter.

4.2 Characteristics of the Proposed Switching Strategy

The general features of this switching strategy are shown in Figure 4.1 where the reference harmonic current waveform is subdivided into time intervals. The equation of the reference harmonic current waveform can be given as:

$$i_h(\theta) = \begin{cases} \frac{-4}{\pi} I_d \sin\frac{\delta}{2} \sin \omega t & 0 \le \omega t < \frac{\pi-\delta}{2} \\ I_d \left(1-\frac{4}{\pi}\sin\frac{\delta}{2}\sin \omega t\right) & \frac{\pi-\delta}{2} < \omega t \le \frac{\pi}{2} \end{cases} \qquad (4.1)$$

In each sub-division there are two requirements for obtaining the switching pulses. Firstly, the width of the switching pulse can be obtained by integrating the reference waveform over each sub-division and then matching the area of obtained reference waveform area with the area of switching pulse. Secondly, the position of switching pulse can be obtained by calculating the centroid of the reference waveform over each sub-division and aligning the centre of switching pulse with the centroid of the area of the reference waveform over the same sub-division. It is expected that by doing this, the harmonic elimination will be more effective.

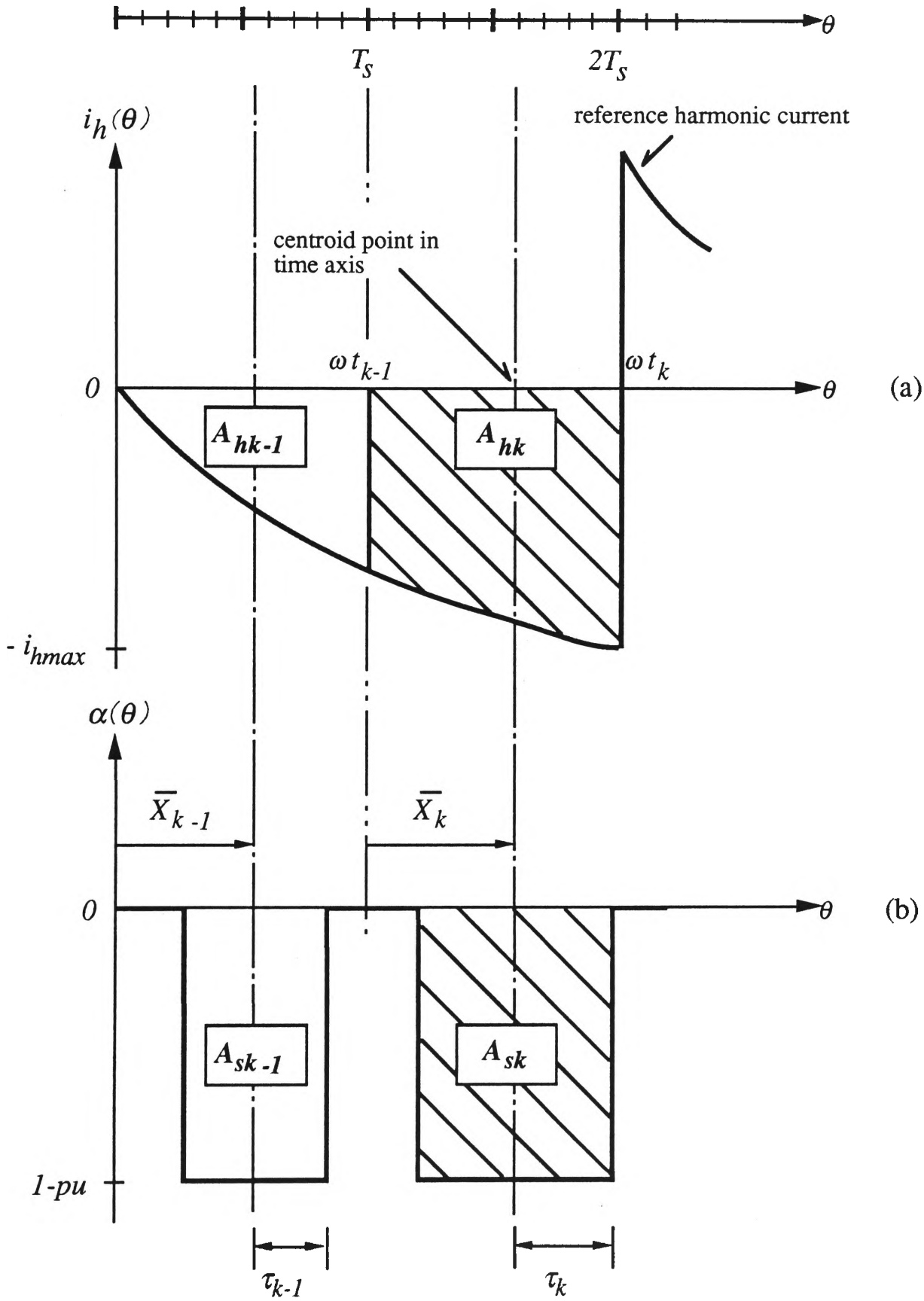

Figure 4.1 Pulse Details of Centroid Based Switching Strategy

4.2.1 Equal Current-Time Area Criteria

The exact area of the reference harmonic current waveform can be obtained by employing a simple integral. Referring to Figure 4.1(a), the hatched area A_{hk} under the reference harmonic current waveform between ωt_{k-1} to ωt_k can be established by integrating Equation (4.1) as follows:

$$A_{hk} = \int_{\omega t_{k-1}}^{\omega t_k} i_h(\theta)\, d\theta \tag{4.2}$$

$$A_{hk} = \begin{cases} \dfrac{4I_d}{\pi} \sin\dfrac{\delta}{2} \cos \omega t \Big/_{\omega t_{k-1}}^{\omega t_k} & 0 \le \omega t < \dfrac{\pi-\delta}{2} \\ I_d \left(\omega t + \dfrac{4}{\pi} \sin\dfrac{\delta}{2} \cos \omega t\right) \Big/_{\omega t_{k-1}}^{\omega t_k} & \dfrac{\pi-\delta}{2} < \omega t \le \dfrac{\pi}{2} \end{cases} \tag{4.3}$$

The hatched area A_{sk} of Figure 4.1(b) of the actual injected current pulse having a width $2\tau_k$ and an amplitude I_c is given by:

$$A_{sk} = I_c \cdot 2\tau_k \tag{4.4}$$

Equating areas A_{hk} and A_{sk} using Equations (4.3) and (4.4), and solving for τ_k leads to the following:

$$\tau_k = \begin{cases} \frac{2}{\pi r} \sin\frac{\delta}{2} \cos\omega t \Big/ \begin{matrix}\omega t_k \\ \omega t_{k-1}\end{matrix} & 0 \le \omega t < \frac{\pi-\delta}{2} \\ \frac{1}{2r}(\omega t + \frac{4}{\pi}\sin\frac{\delta}{2}\cos\omega t) \Big/ \begin{matrix}\omega t_k \\ \omega t_{k-1}\end{matrix} & \frac{\pi-\delta}{2} < \omega t \le \frac{\delta}{2} \end{cases} \qquad (4.5)$$

where r = injection ratio

If the number of pulses per cycle of the switching function is fixed and the shape of the reference harmonic current is also fixed (i.e. δ is constant), Equation (4.5) can be further simplified to yield:

$$\tau_k = \begin{cases} \frac{C_1}{r} & 0 \le \omega t < \frac{\pi-\delta}{2} \\ \frac{C_2}{r} & \frac{\pi-\delta}{2} < \omega t \le \frac{\pi}{2} \end{cases} \qquad (4.6)$$

where $$C_1 = \frac{2}{\pi}\sin\frac{\delta}{2}\cos\omega t \Big/ \begin{matrix}\omega t_k \\ \omega t_{k-1}\end{matrix}$$

$$C_2 = \frac{1}{2}(\omega t + \frac{4}{\pi}\sin\frac{\delta}{2}\cos\omega t) \Big/ \begin{matrix}\omega t_k \\ \omega t_{k-1}\end{matrix} \qquad (4.7)$$

Equation (4.6) defines the *kth* pulsewidth of the desired switching function. Clearly the *kth* pulsewidth is linear and inversely proportional to the injection ratio if the number of pulses per cycle is fixed. Therefore the pulsewidth τ_k of the switching function can be easily obtained by precalculating Equation (4.7) (C_1 and C_2) and storing the results in memory as a look-up table.

4.2.2 Centroid Co-ordinate

Now, consider the position of pulse within an equal-sampling period. In effect the position of the pulse is constrained such that the centroid of both areas (switching pulses and reference harmonic current) must be aligned. The equation for calculating the time axis co-ordinate of the centroid of area A_{hk} shown in Figure 4.1 is given by:

$$\bar{X}_k = \frac{\int_{\omega t_{k-1}}^{\omega t_k} \omega t \, i_h(\theta)\, d\omega t}{\int_{\omega t_{k-1}}^{\omega t_k} i_h(\theta)\, d\omega t} \tag{4.8}$$

The centroid of the reference harmonic current can be calculated by substituting Equation (4.1) into Equation (4.8) which gives:

$$\bar{X}_k = \begin{cases} \left. \dfrac{\omega t \cos \omega t - \sin \omega t}{\cos \omega t} \right/ \begin{matrix} \omega t_k \\ \omega t_{k-1} \end{matrix} & 0 \le \omega t < \dfrac{\pi - \delta}{2} \\ \left. \dfrac{\dfrac{(\omega t)^2}{2} + \dfrac{4}{\pi} \sin \dfrac{\delta}{2} (\omega t \cos \omega t - \sin \omega t)}{\omega t + \dfrac{4}{\pi} \sin \dfrac{\delta}{2} \cos \omega t} \right/ \begin{matrix} \omega t_k \\ \omega t_{k-1} \end{matrix} & \dfrac{\pi - \delta}{2} < \omega t \le \dfrac{\delta}{2} \end{cases} \tag{4.9}$$

Equation (4.9) describes the position of the *kth* pulse in terms of the time limit of the sampling interval. For the case where the harmonic current waveform remains unchanged (i.e. the width δ of quasi-square wave unchanged) and the number of pulses per cycle of the switching function

is fixed, the time interval of integration is also fixed. Clearly, under these circumstances the time axis co-ordinates of the different centroids are fixed and independent of the amplitude of the load current or harmonic current. Consequently the task of updating the centroid everytime is eliminated which means that these centroid co-ordinates can be held in memory as a look-up table.

4.3 Fourier Series Analysis

The Fourier series of the switching function and line current can be derived based on the equal-sampling technique. The Fourier series of the switching function can be expressed as follows:

$$\alpha(\theta) = \sum_{n=1}^{\infty} \bar{a}_n \sin n\theta \qquad (4.10)$$

where

$$\bar{a}_n = \frac{4}{n\pi} \sum_{k=1}^{N} \rho_k \sin n\tau_k \qquad (4.11)$$

and

$$\rho_k = 2S_k \sin n(\omega t_{k-1} + \bar{X}_k) \qquad \text{for } k=1,2,\ldots,(N-1) \qquad (4.12)$$

$$\rho_k = 2S_k \sin n(\omega t_{k-1} + \bar{X}_k) \qquad \text{for } k=N \text{ and } M= \text{odd}$$

$$\rho_k = S_k \sin n(\omega t_{k-1} + \bar{X}_k) \qquad \text{for } k=N \text{ and } M= \text{even} \qquad (4.13)$$

The compensating current which has to be injected into the ac supply line has the same waveform as the switching function except for the

magnitude which is equal to I_C. Thus the compensating current can be expressed as follows:

$$i_C(\theta) = I_C \cdot \sum_{n=1}^{\infty} \bar{a}_n \sin n\theta \qquad (4.14)$$

Following Equation (1.13) the line current after injecting the compensating current is expressed as follows:

$$i_S = \frac{4I_d}{n\pi} \sum_{n=1}^{\infty} \varphi \sin n\theta \qquad (4.15)$$

where

$$\varphi = \sin\frac{n\pi}{2} \sin\frac{n\delta}{2} - r \sum_{k=1}^{N} \rho_k \sin n\tau_k \qquad (4.16)$$

and ρ_k is as same as in Equations (4.12) and (4.13).

4.4 Simulation Results

In this section simulation results of the centroid based switching strategy are presented. The switching function can be obtained by employing Equation (4.6) to calculate the width of pulses, and Equation (4.9) to calculate the centroid time axis co-ordinate. The simulation program of this strategy was written using MATLAB (software package). The simulation program is given in Appendix 2.

The number of pulses per half cycle M of this simulation is assumed to be 12 (i.e. the sampling frequency is 1,200 Hz when compared to the fundamental frequency 50 Hz) and the injection ratio r is 0.5. If we assume that the shape of reference harmonic current is unchanged, the values of the centroid co-ordinate can be pre-calculated using Equation (4.9). Furthermore, the pulsewidth coefficient (C_1 and C_2) can also be pre-calculated using Equation (4.7) which is subsequently used to evaluate the pulsewidth τ_k from Equation (4.6). The resulting switching function and reference harmonic waveform are illustrated in Figure 4.2(a) where the injection ratio is 0.5. As stated earlier, this is an ideal case where switching devices have zero turn on/off times and the charged inductor in Figure 1.8 has a constant current without ripple. Figure 4.2(b) and (c) shows the harmonic spectrum of reference harmonic current waveform and switching function respectively.

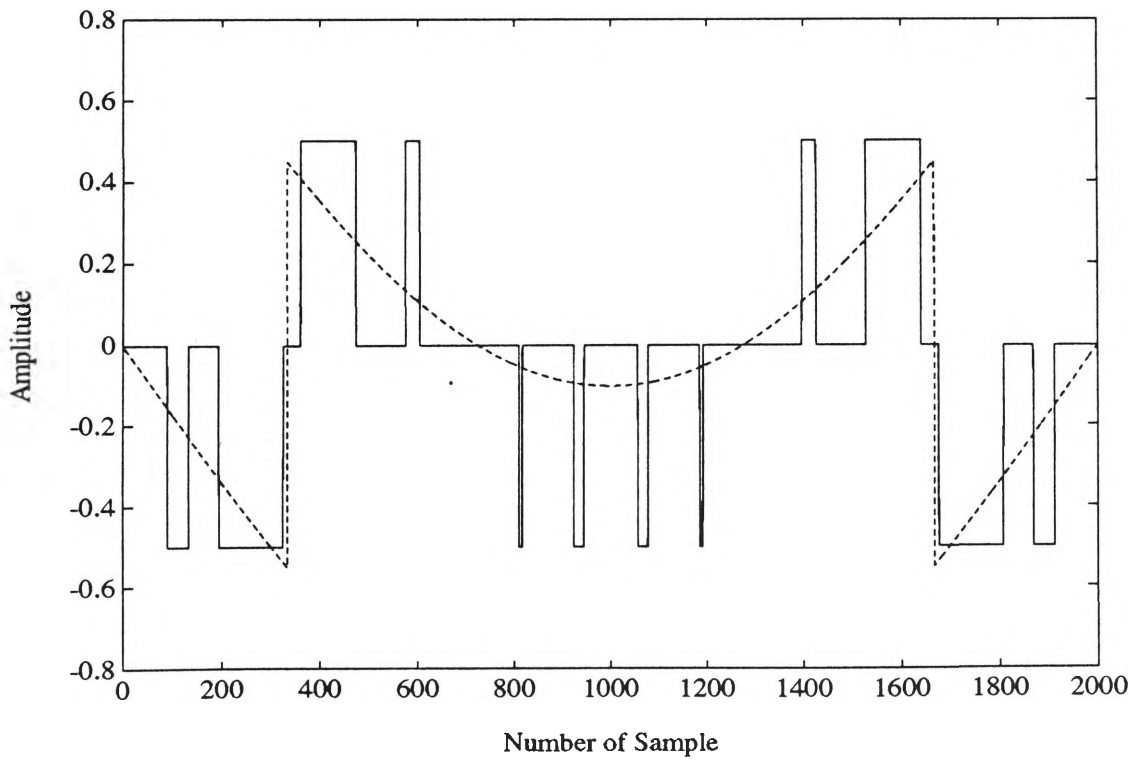

(a)

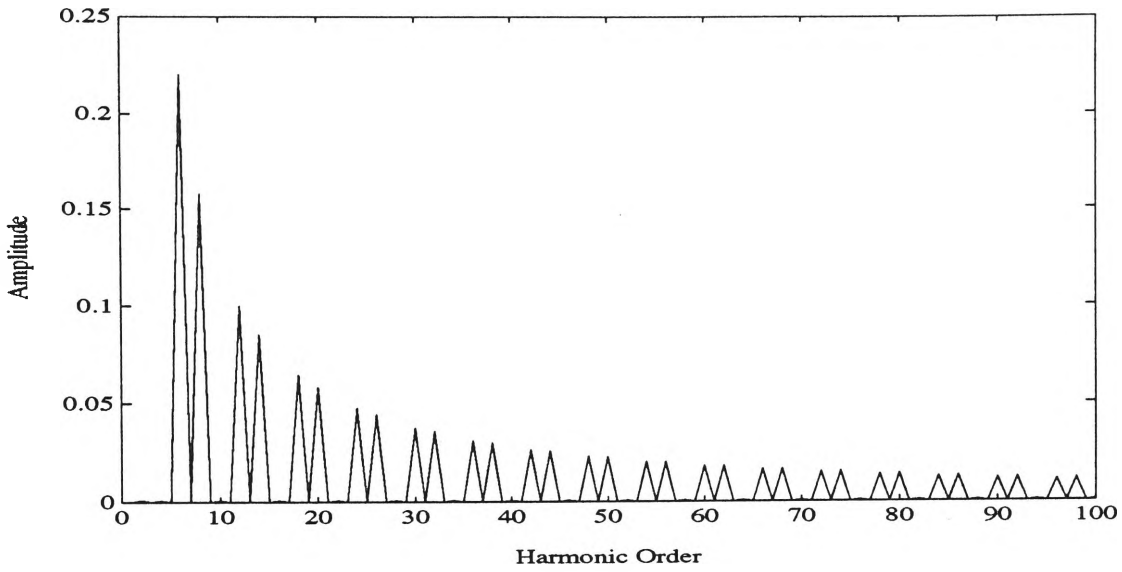

(b)

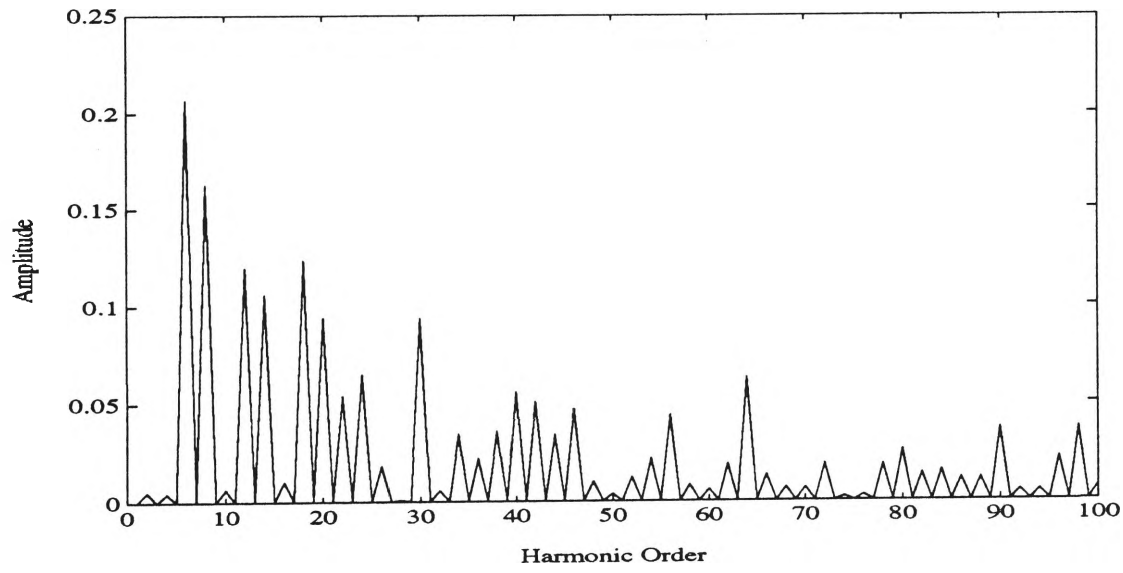

(c)

Figure 4.2 (a) Reference Harmonic Current and Switching Function per half Cycle, $M=12$, $r=0.5$

(b) Harmonic Spectrum of Reference harmonic Current Waveform

(c) Harmonic Spectrum of Switching Function

Theoretical waveform of the line current i_S following the injection of the compensating current is shown in Figure 4.3.

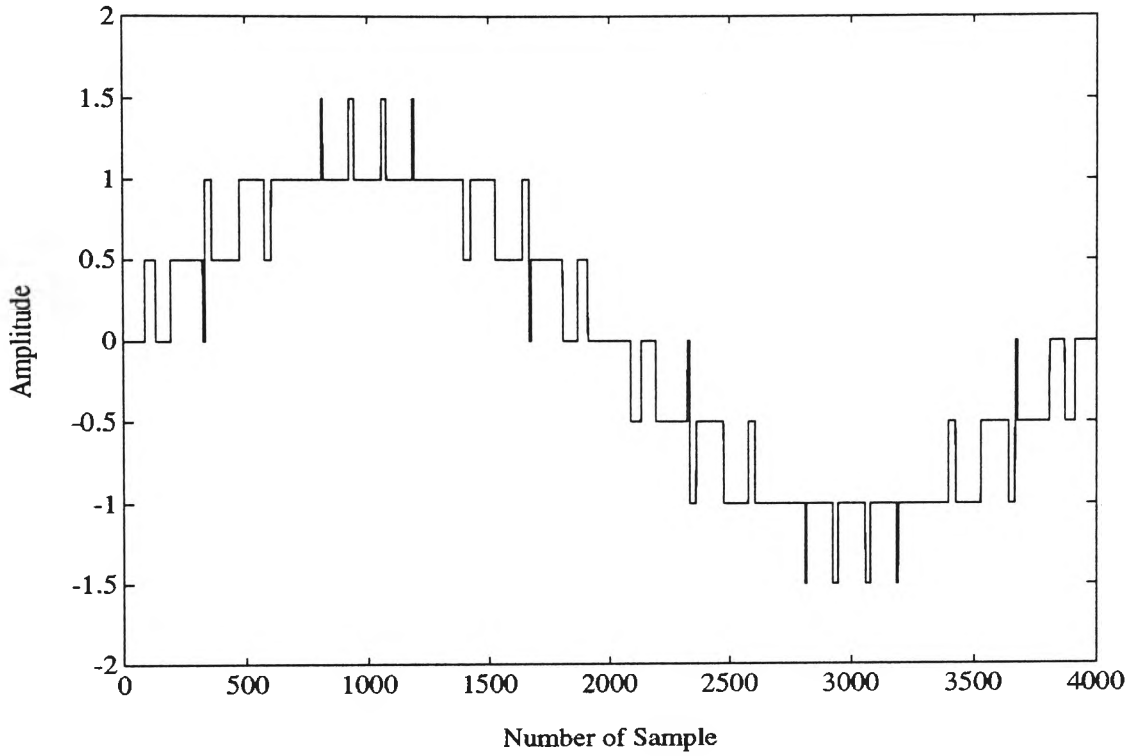

Figure 4.3 Waveform of the Compensated Line Current

4.5 Conclusion

A novel switching strategy for active power filters based on a centroid based technique has been presented. The algorithm for calculating the switching function has been clearly defined. The general feature of this switching strategy is that the position of each pulse corresponds to the centroid of the various areas of reference harmonic waveform. In addition, the pulsewidths of the compensated current are based on the equal current-time area criteria. In this case, the accurate numerical

integration is used to ensure that the areas of the switching function and harmonic current waveform are exactly the same. Furthermore, from theoretical analysis it was shown that the switching function can be established by a simple linear equation provided the reference harmonic current waveform remains unchanged. Comparison of the results from CBT with those from EST and MEST will be made in next Chapter.

CHAPTER 5

PERFORMANCE EVALUATION

5.1 Introduction

The performance evaluation of different switching strategies is presented in this Chapter. Various switching strategies can be evaluated based on their ability to eliminate the unwanted harmonic components. The primary quality factor which is used in measuring the harmonic performance is the harmonic distortion factor. The harmonic distortion factor is defined as:

$$DF = \frac{100}{I_{s1}} \sqrt{\sum_{n=2}^{\infty} \left[\frac{I_{sn}}{n}\right]^2} \qquad (5.1)$$

where I_{sn} = amplitude of the *nth* harmonic current in ac supply line

I_{s1} = amplitude of the fundamental component of the current in ac supply line

To compare the effectiveness of each switching strategy more clearly, let us define a percentage reduction of distortion factor as follows:

$$PR = \frac{DF_{uncomp} - DF_{comp}}{DF_{uncomp}} \times 100\% \qquad (5.2)$$

where PR = Percentage Reduction of harmonic distortion factor

DF_{uncomp} = distortion factor for the uncompensated case

DF_{comp} = distortion factor for the compensated case

Another performance index is used to evaluate the computational burden of each strategy on microprocessor implementation. The computational burden can be evaluated by employing the FLOP (Floating Point Operations) count which is available in MATLAB software package. The flop count represents the cumulative number of floating point operations which have been used to obtain a set of results. Although the MATLAB flop count may not be strickly speaking an accurate measure of the computational burden since algorithms have not been optimised for this particular application, it is nevertheless a good approximate indicator of performance.

The organisation of this chapter is as follows. Section 5.2 discusses the performance of the Equal-Sampling Technique (EST). In Section 5.3 the performance of the Modified Equal-Sampling Technique (MEST) is presented. The performance of the Centroid Based Technique (CBT) is discussed in Section 5.4. Section 5.5 presents a comparison of performance while Section 5.6 concludes the chapter.

5.2 Performance of Equal-Sampling Technique (EST) (Choe and Park, 1988)

Table 5.1 shows the various switching pulsewidths τ_k for M =12 for different values of the injection ratio. These results were obtained by solving the set of non-linear equations (i.e. Equations (2.29) and (2.30)) using MATLAB software. Note that low injection ratios result in an increase of the pulsewidth which may cause overlap between the adjacent pulses. Therefore the injection ratios have to be chosen by taking the boundary conditions into account so that resulting pulsewidths are valid

from an implementation point of view.

τ_k (degree)	τ_1	τ_2	τ_3	τ_4	τ_5	τ_6
Injection Ratio	S_1 -1	S_2 -1	S_3 1	S_4 1	S_5 -1	S_6 -1
0.4	1.99	8.40	6.33	2.07	0.29	1.76
0.5	2.02	5.98	4.47	1.87	0.29	1.40
0.6	1.81	4.78	3.57	1.62	0.26	1.16
0.7	1.60	4.02	2.98	1.41	0.23	1.00
0.8	1.43	3.46	2.57	1.25	0.20	0.86
0.9	1.28	3.06	2.27	1.12	0.18	0.77
1.0	1.16	2.74	2.03	1.00	0.16	0.69
1.2	0.98	2.26	1.67	0.85	0.14	0.58

Table 5.1 Pulsewidths of the Switching Function for Different Values of Injection Ratio

The pulsewidths obtained from Table 5.1 can be used to establish the switching function as shown in Figure 5.1(a) for an injection ratio $r=0.5$. After injecting the switching function with amplitude I_C into the ac supply lines, the line current i_S obtained is shown in Figure 5.1(b).

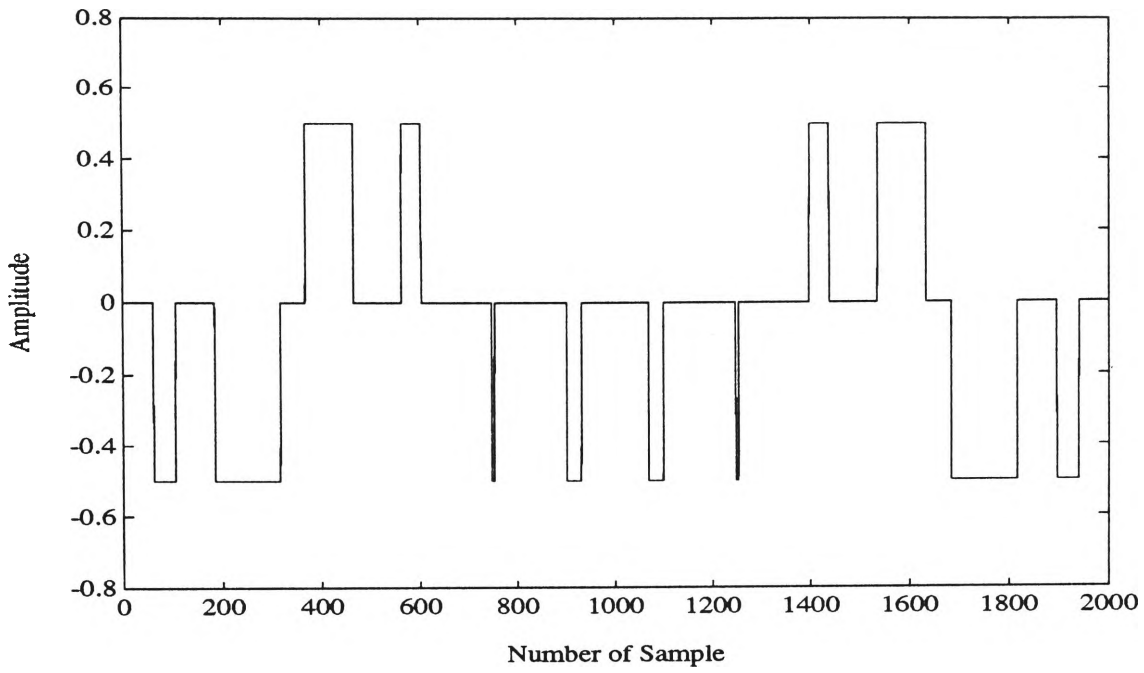

(a)

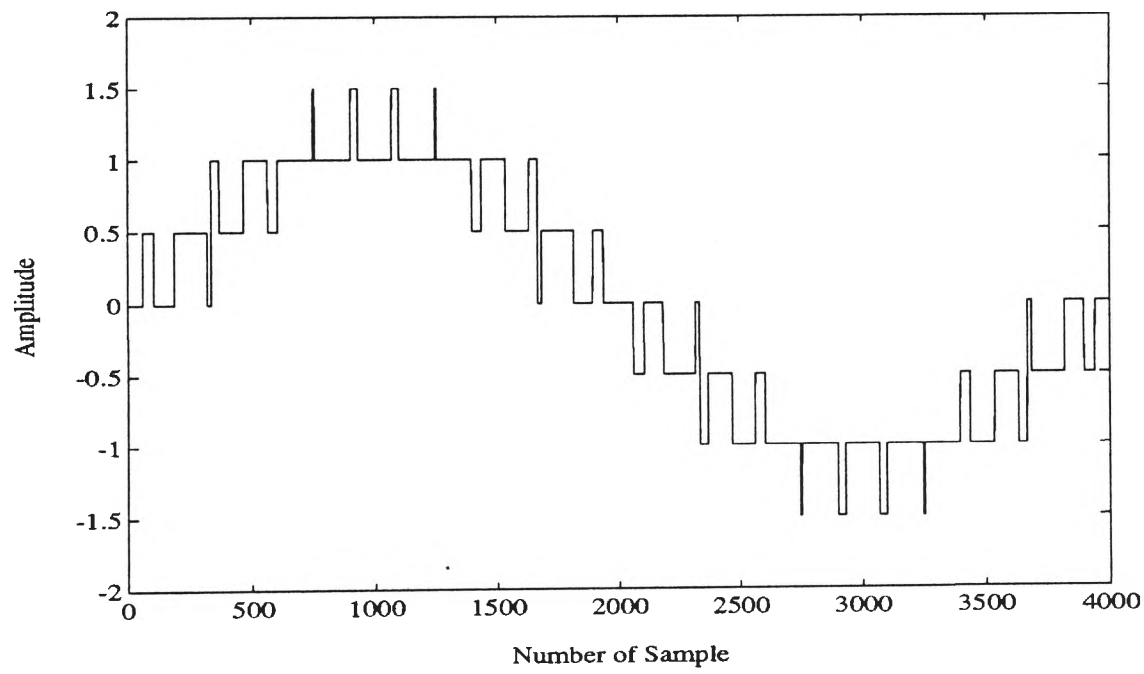

(b)

Figure 5.1 (a) Switching Function
(b) Line Current after Injecting the Compensating Current, $r=0.5$

The comparison of harmonic spectrum of the line current before and after compensation are shown in Figures 5.2(a) and (b) respectively. From Figure 5.2 (b), it is seen that as the compensating current generated is based on a constant sampling frequency. The two side-band harmonics exist around the sampling frequency (i.e. 24th harmonic order) and at integer multiples of the sampling frequency.

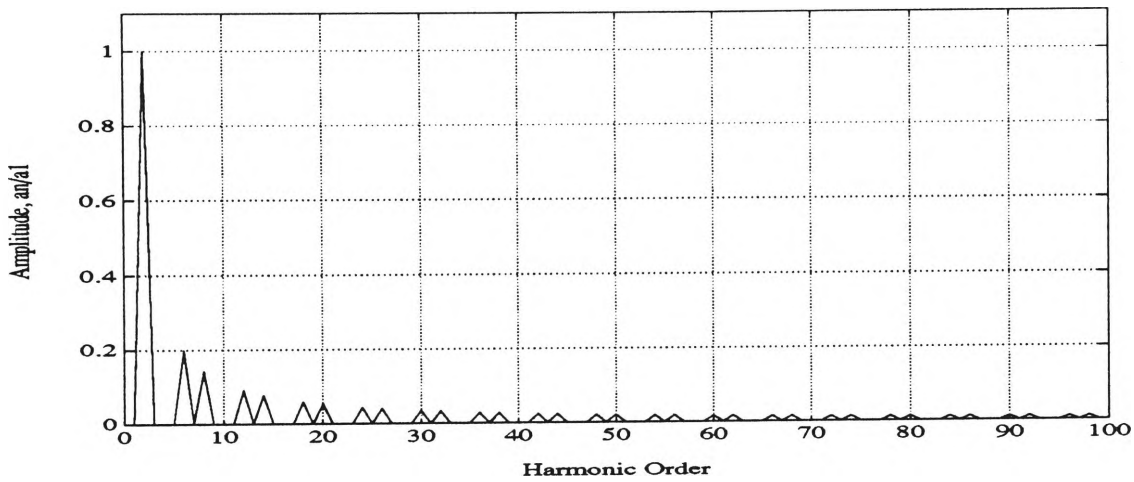

(a)

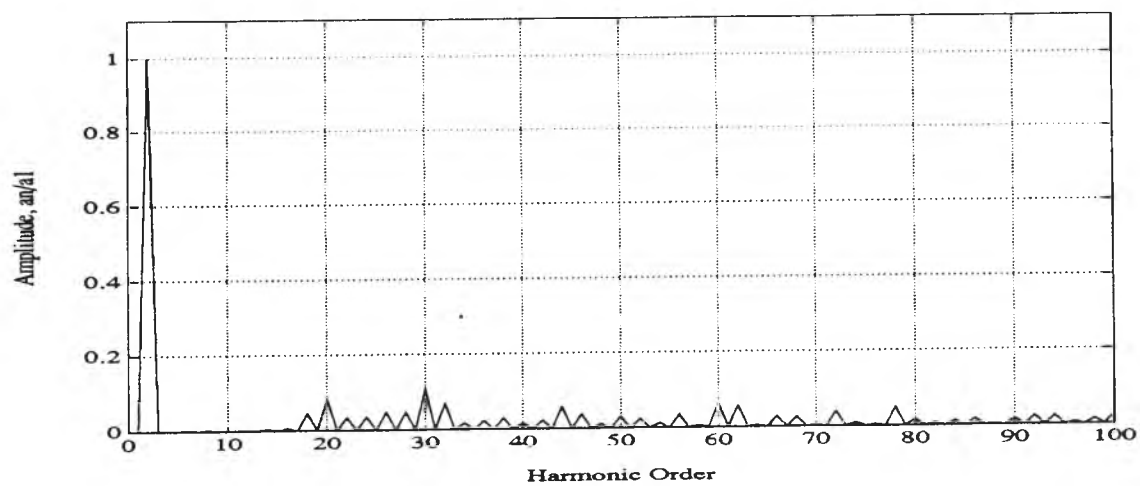

(b)

Figure 5.2 (a) Harmonic Spectrum before Compensation

(b) Harmonic Spectrum after Compensation

The ability to eliminate harmonics can be seen more precisely from Table 5.2 which compares the harmonic content in the ac supply line before and after compensation for various injection ratios. In the case where the line current is compensated, it was found that the harmonics of order less than M are eliminated as expected.

Harmonic Order	Uncom-pensated Case, i_L	a_n/a_1 for i_S							
n	a_n/a_1	r=0.4	r=0.5	r=0.6	r=0.7	r=0.8	r=0.9	r=1.0	r=1.2
1	100	100	100	100	100	100	100	100	100
3	0.00	0.06	0.03	0.01	0.00	0.14	0.13	0.09	0.12
5	20.00	0.08	0.08	0.07	6.06	0.20	0.14	0.16	0.16
7	14.28	0.04	0.07	0.05	4.39	0.17	0.11	0.22	0.31
9	0.00	0.06	0.03	0.02	0.02	0.03	0.09	0.02	0.01
11	9.09	0.05	0.05	0.02	2.74	0.00	0.04	0.08	0.02
13	7.69	0.71	0.36	0.73	1.67	1.04	1.16	1.26	1.22
15	0.00	0.99	0.55	0.35	0.19	0.21	0.05	0.13	0.07
17	5.88	1.26	4.62	5.94	2.82	6.97	7.30	7.38	7.55
19	5.26	3.61	8.38	10.47	6.57	12.26	12.78	13.11	13.58
21	0.00	5.33	3.51	2.45	1.27	1.27	1.02	0.83	0.52
23	4.34	3.62	3.56	3.69	4.01	3.91	4.03	4.12	4.13
25	4.00	4.53	4.81	4.71	4.38	4.50	4.36	4.25	4.24
27	0.00	5.30	4.65	3.55	1.92	2.06	1.68	1.38	0.92
29	3.44	6.92	11.37	14.61	12.78	18.14	19.16	19.92	20.95

Table 5.2 a_n/a_1 [percent] of the ac Line Current

Now let us consider the harmonic distortion factor. Using the data of Table 5.2 the calculated harmonic distortion factors for each injection ratio are tabulated in Table 5.3. Clearly, the harmonic distortion factor increases with increasing injection ratio. This implies that if the load current of the converter decreases, the distortion factor increases and vice-versa.

Injection Ratio $r = \frac{I_c}{I_d}$	**Distortion Factor** (DF), %
0.4	0.596 %
0.5	0.827 %
0.6	1.006 %
0.7	1.133 %
0.8	1.223 %
0.9	1.298 %
1.0	1.354 %
1.2	1.442 %

Table 5.3 Harmonic Distortion Factor for each Injection Ratio

Next let us consider the flop count used in obtaining the switching function of this switching strategy. To obtain the switching instants of EST, the set of non-linear equations have to be solved. Obviously, the flop count increases with the number of non-linear equations. In addition, the flop count also varies depending on the applied initial values to the numerical algorithm used to solve the equations. If the set of initial

values is poor and the solutions diverge, it is necessary to make a new initial guess.

In the simulation program, the flop count obtained is based on the following conditions:

1. The number of pulses per half cycle $M = 12$. This means the set of non-linear equations which have to be solved has 6 equations.
2. The injection ratio used is $r = 0.5$.
3. The algorithm for solving non-linear equations is based on the standard built-in routines of the MATLAB software package.

Under the above conditions the flop count obtained varies between 5,689-11,746. Experience showed that the flop count varied primarily due to the effect of initial values applied to the set of non-linear equations.

5.3 Performance of Modified Equal-Sampling Technique (MEST)

The simulation program which was used to generate the switching function of the modified equal-sampling technique is given in Appendix 1. In order to establish the switching function based on Equation (3.10), the width-factor is required. The appropriate width-factor can be found by observing the minimal values of the harmonic distortion factor while the width-factor is being applied. Figure 5.3 shows the variation of the harmonic distortion factor with the width-

factor for different injection ratios.

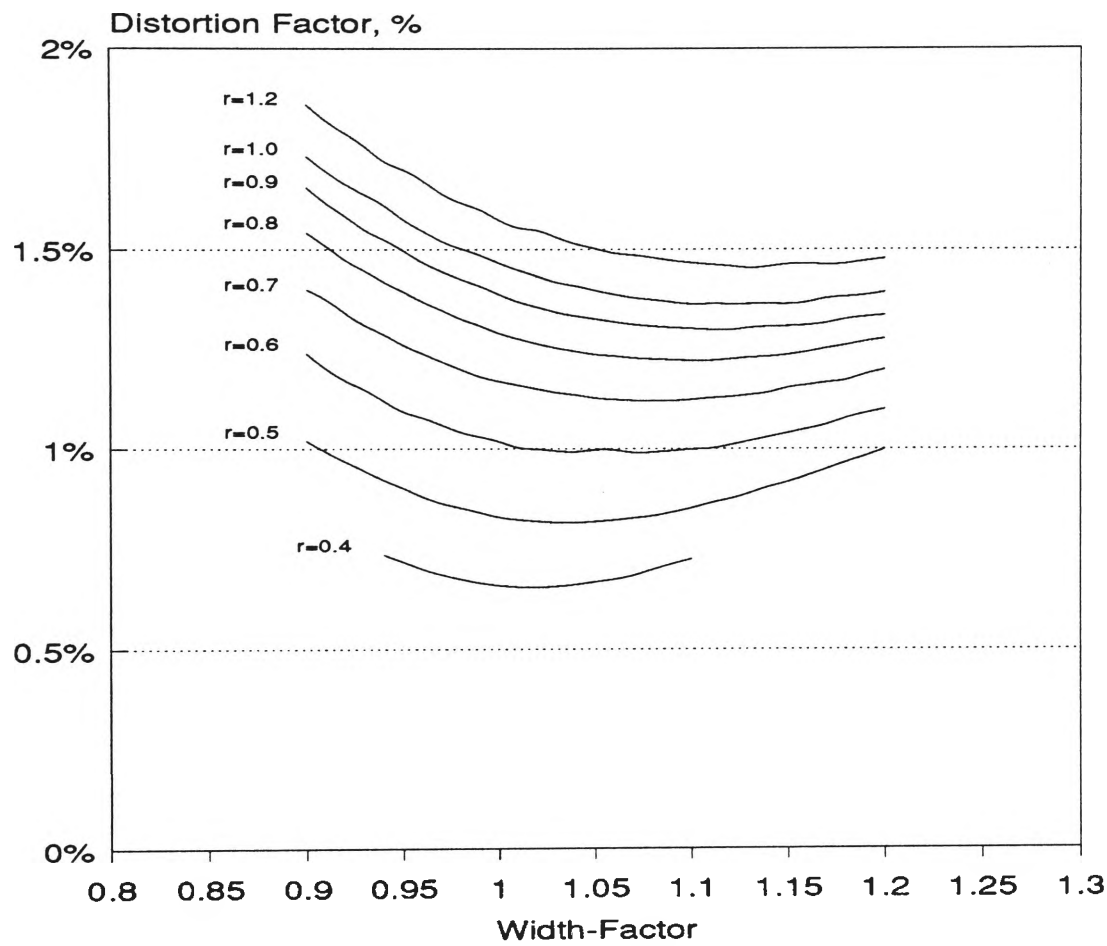

Figure 5.3 Variation of Harmonic Distortion Factor of EST with width factor

As shown in Figure 5.3 for each injection ratio an optimal point in terms of the harmonic distortion factor can be obtained together with an appropriate width-factor. The trajectory followed by the optimal harmonic distortion factor as a function of the injection ratio, is shown in Figure 5.4.

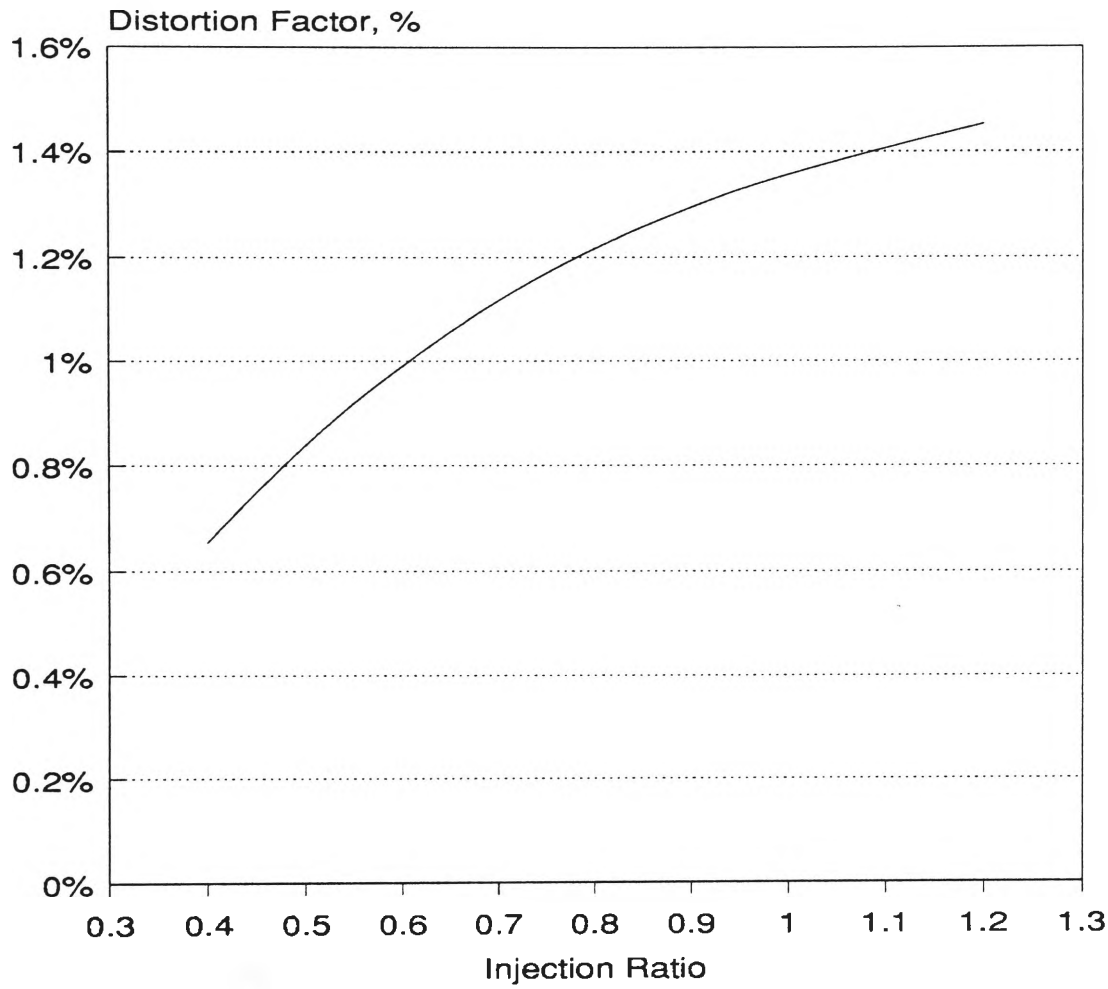

Figure 5.4 Trajectory of Minimum Distortion Factor with Injection Ratio

The summary of the optimal harmonic distortion factors for each injection ratio with appropriate width-factor is shown in Table 5.5.

Injection Ratio r	Distortion Factor (DF),%	Width-Factor W_f
0.4	0.653 %	1.02
0.5	0.815 %	1.04
0.6	0.991 %	1.04
0.7	1.120 %	1.09
0.8	1.222 %	1.11
0.9	1.298 %	1.12
1.0	1.363 %	1.12
1.2	1.452 %	1.13

Table 5.5 Harmonic Distortion Factor for each Injection Ratio

This modified equal-sampling switching strategy can be implemented effectively using a microprocessor by pre-programming the calculated trajectory of the width-factors in memory as a look-up table. This look-up table is subsequently used to determine the pulsewidth of the switching function as defined by Equation (3.10). Furthermore, as the width-factor is completely independent of the number of pulses per cycle or the load current level, the look-up table only requires a fixed amount of memory.

Figure 5.5 shows the simulated switching function for the modified equal-sampling technique with the injection ratio r = 0.5, width-factor w_f = 1.04 and number of pulses per half cycle M = 12.

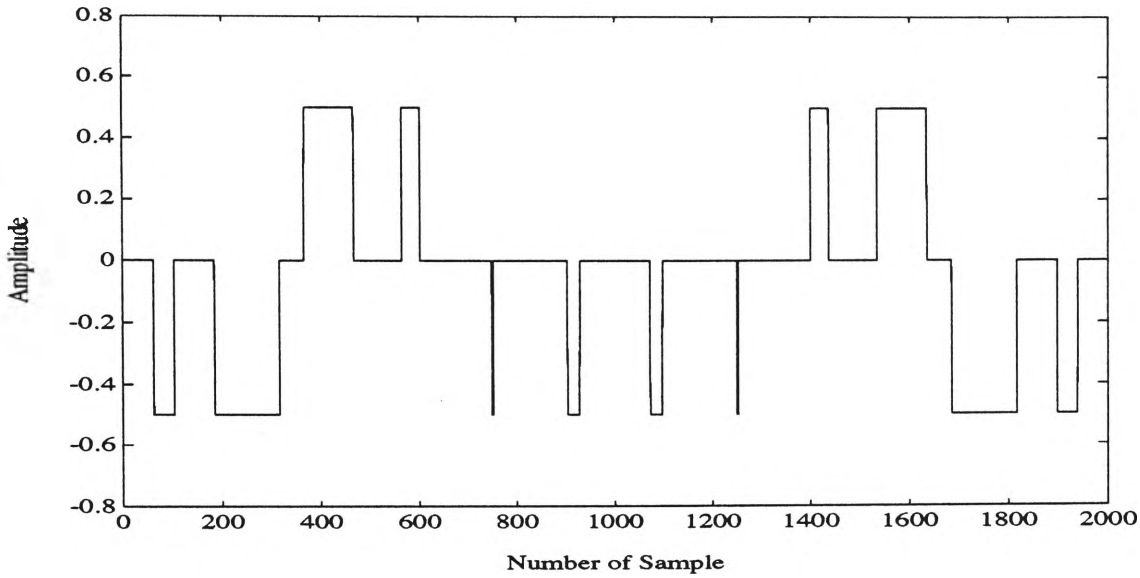

Figure 5.5 Switching Function based on MEST

r=0.5, M=12, w_f=1.04

Following the injection of the compensating current with amplitude I_c into ac supply line, the compensated line current obtained is as shown in Figure 5.6.

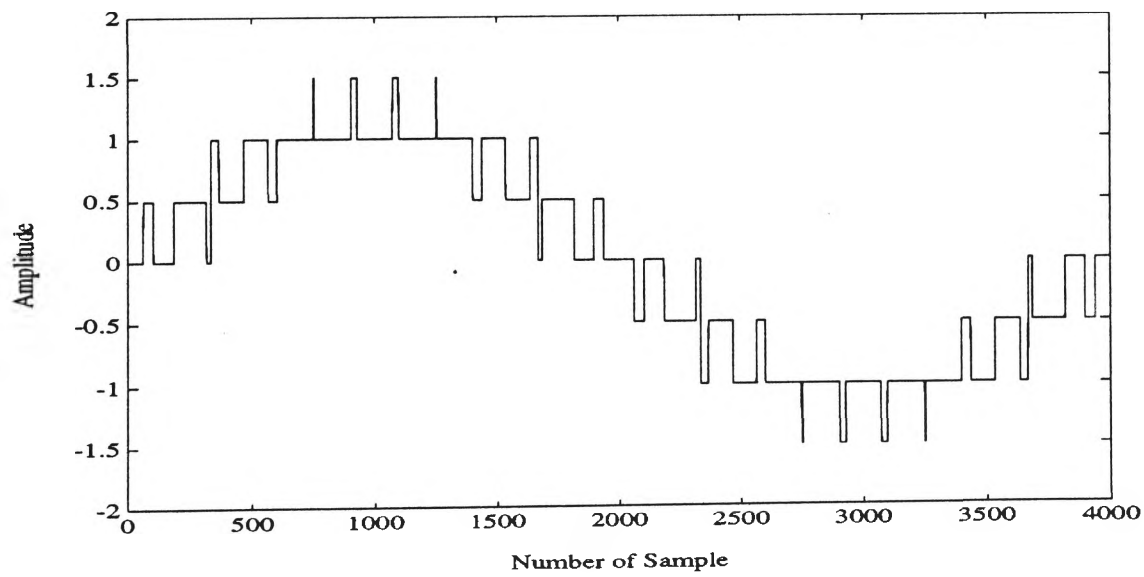

Figure 5.6 Compensated Line Current

The harmonic spectrum of the compensated line current is shown in Figure 5.7. Once again the two side-band harmonics exist around the sampling frequency and integer multiples of the sampling frequency as in the case of EST.

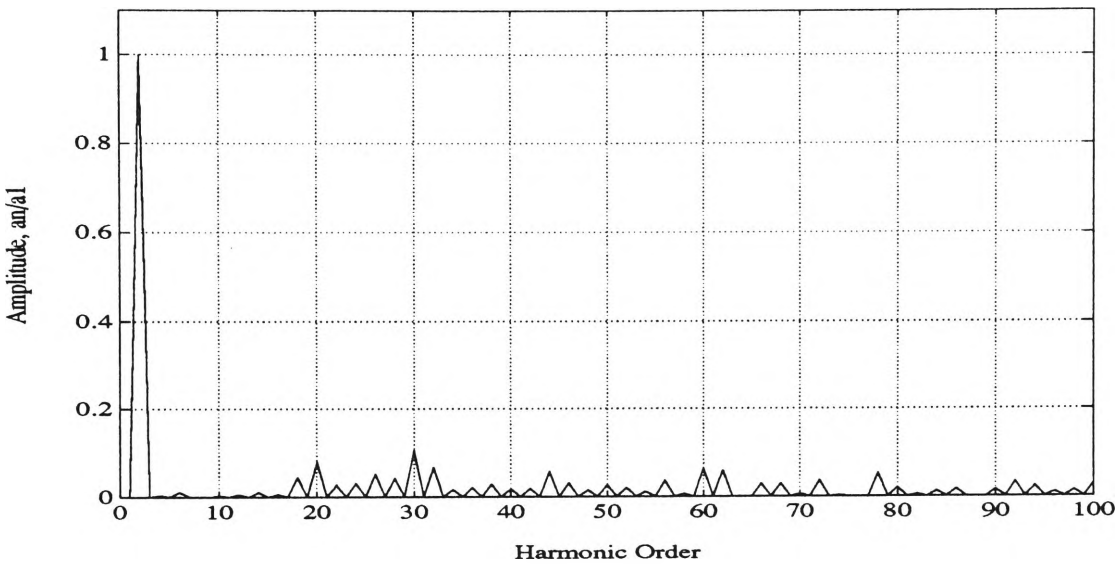

Figure 5.7 Harmonic Spectrum of Compensated Line Current (MEST)

Next consider the flop count of the MEST. The flop count obtained for this switching strategy is based on the same conditions which have been defined previously in Section 5.2. Equation (3.10) leads to the flop count for one pulse. Thus to obtain the flop count in one cycle of the reference harmonic current wave, the flop count has to be multiplied by the number of pulses per cycle. Here the number of pulses per cycle is 24. The flop count obtained for the MEST was 125.

5.4 Performance of Centroid Based Technique (CBT)

In this section the performance aspects of the centroid based technique

(CBT) are presented. The simulated switching function was shown in Figure 4.2 (a). Figure 5.8 shows the harmonic spectrum of the ac supply line current after injection has taken place for the injection ratio $r = 0.5$.

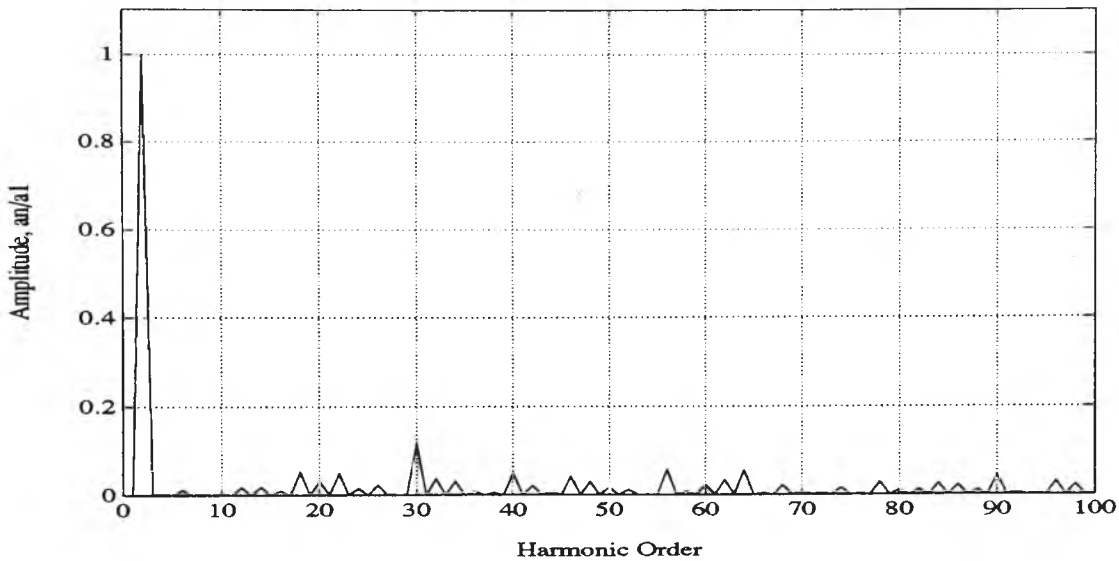

Figure 5.8 Harmonic spectrum of Line Current, $r = 0.5, M = 12$

From the harmonic spectrum of this technique we can see that as the switching function is essentially non equal-sampling in nature, the harmonic components do not exist uniformly around the sampling frequency as in the case of constant equal-sampling (i.e. EST and MEST).

The harmonic distortion factor of CBT can be obtained by applying Equation (4.16) to Equation (5.16). The harmonic distortion factor with the various injection ratio is shown in Table 5.6. It was observed that for a switching function with an injection ratio $r = 0.4$, the resulting adjacent pulses were overlapping and therefore the switching function was invalid.

Injection Ratio *r*	**Distortion Factor** DF, %
0.5	0.739 %
0.6	0.937 %
0.7	1.087 %
0.8	1.203 %
0.9	1.287 %
1.0	1.348 %
1.2	1.442 %

Table 5.6 Harmonic Distortion Factor for Different Injection Ratios

Next consider the flop count for this switching strategy. Under the case that the reference harmonic current waveform is unchanged. The centroid co-ordinates of the various subdivisions are fixed and therefore can be pre-calculated. Thus, the flop count required for calculating the centroids is neglected. Moreover, as discussed previously, the equation for the pulsewidth (Equation (4.6)) can be simplified if the number of pulses per cycle is fixed, the area of the reference harmonic current can also be pre-calculated. Consequently, the flop count in such a situation is only dependent on the equation of the pulsewidth (Equation 4.6). Note that the flop count obtained from this strategy is still based on the same conditions that have been defined previously for EST in Section 5.2 as well. The flop count of the CBT in this case is 24.

However, for case where the waveform of reference harmonic current is changing, both the area and centroid need to be calculated. Hence the flop count in this case is equal to 1,124.

5.5 Comparison of Performance

In this section the performance of the EST, MEST and CBT will be compared. As discussed previously, there are two types of performance indexes to be evaluated. Firstly, the harmonic distortion factor is used to evaluate the capability of each switching strategy in eliminating the unwanted harmonics. The second performance evaluation is the flop count which is an approximate measure of the computational burden in implementation of the particular strategy. The details of each performance evaluation will be discussed in the following sub-section.

5.5.1 Comparison based on Harmonic Distortion Factor

The harmonic distortion factor of each switching strategy is illustrated graphically in Figure 5.9.

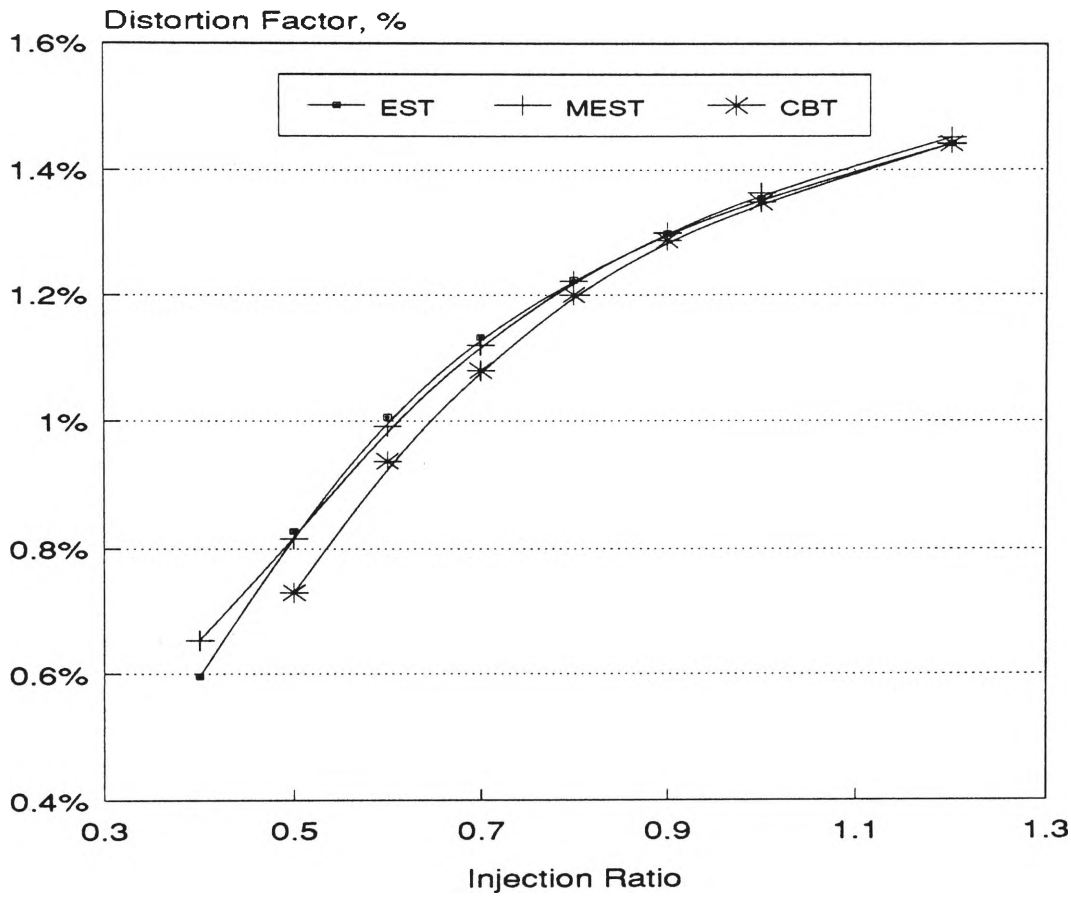

Figure 5.9 Variation of Distortion Factor with Injection Ratio

From Figure 5.9 it can be seen that the harmonic distortion factors are approximately the same for both EST and MEST, while the CBT gives a distortion factor which is superior to both EST and MEST, particularly for low injection ratios.

Figure 5.10 illustrates the comparison of the percentage reduction of distortion factor obtained using Equation (5.2) versus injection ratio for all switching strategies. Note that the harmonic distortion factor before compensation is equal to 4.638 %. From Figure 5.10 we can see that, the highest percentage reduction is provided by CBT.

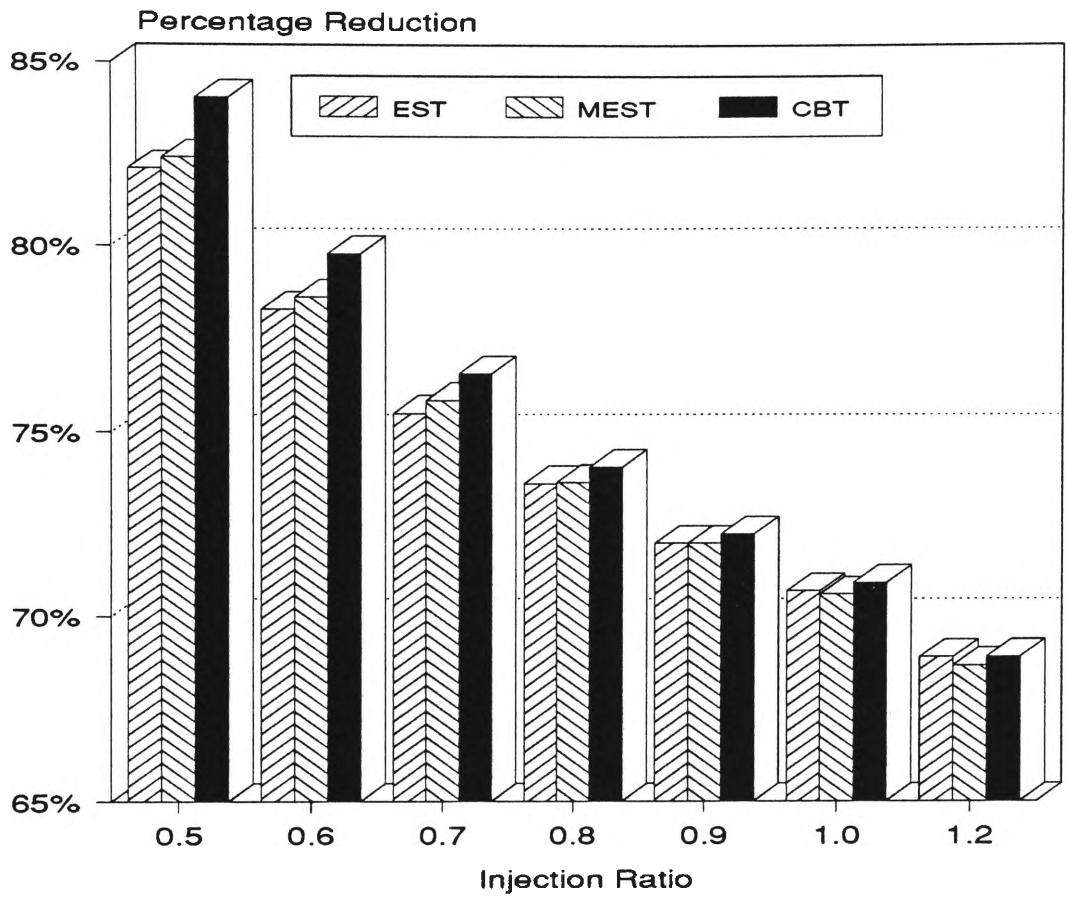

Figure 5.10 Percentage Reduction of Distortion Factor for each Switching Strategy

5.5.2 Comparison based on Computational Burden

The flop count for the EST varies between 5,689 and 11,746 while the MEST is 125 and for the CBT it varies between 24 and 1,124. Considering the worse case of the flop count, the percentage flop of each switching strategy can be given in Table 5.7 where the flop count of MEST is taken as the reference (i.e. 100%).

Switching Strategy	Flop Count as a Percentage
EST	100 %
MEST	1-2 %
CBT	9-20 %

Table 5.7 Percentage Flop Count

5.6 Conclusion

This chapter presented a performance evaluation of the switching strategies including the EST, MEST and CBT. The same conditions were assumed for methods considered. The factors used to evaluate the performance are the harmonic distortion factor, percentage reduction of distortion factor and the flop count.

The overall results clearly show that, the CBT performs better than the MEST and EST. This is particularly at low injection ratios. In terms of distortion factor the performance of the MEST was similar to the EST. As far as the computational burden is concerned, the EST was found to have a rather intensive computational burden when compared to both the MEST and CBT.

CHAPTER 6

IMPLEMENTATION OF THE MEST AND CBT ON A DIGITAL SIGNAL PROCESSING ENVIRONMENT

6.1 Introduction

This chapter is concerned with the implementation of the proposed switching strategies (MEST and CBT) on a Digital Signal Processing (DSP) chip. Advances in very-large-scale integration (VLSI) technology have made possible the expanding use of digital processors in many new real-time application areas. A DSP implementation has been decided upon since it is envisaged that the final active power filter system will require the available computing power. As expected, there are many DSP chips available today which are characterised by different levels of performance. For example, the processor speed, memory space (both on-chip and off-chip), arithmetic precision, multiprocessor interface capability and development tools must be considered. The DSP chip selected for this project is the Motorola DSP56001 which is considered to be a good compromise between performance and cost.

The DSP56001 is used to generate the switching functions for the MEST and CBT respectively. This will enable at a latter stage the proper real time evaluation of both methods on a complete active power filter system. In the system developed the DSP performs not only the calculation of pulsewidths but also the necessary input/output processing such as converter load current sensing, amplitude of current source sensing and switching function output.

The organisation of this chapter is as follows. Section 6.2 presents the architectural overview of DSP56001. Section 6.3 describes the DSP based system. Section 6.4 discusses the DSP software development. Section 6.5 presents the experimental results. Finally, Section 6.6 concludes the chapter.

6.2 Architectural Overview of DSP56001

The DSP56001 is a member of Motorola's family of general purpose digital signal processors. The DSP56001 features 512 words of full speed on-chip program RAM (PRAM) memory, two pre-programmed data ROMs, and special on-chip bootstrap hardware to permit convenient loading of user programs into the program RAM. The core of the processor consists of three execution units operating in parallel : the data arithmetic logic unit (ALU), the address generation unit (AGU) and the program controller (Motorola DSP56001 Technical data). The DSP56001 block diagram is depicted in Figure 6.1.

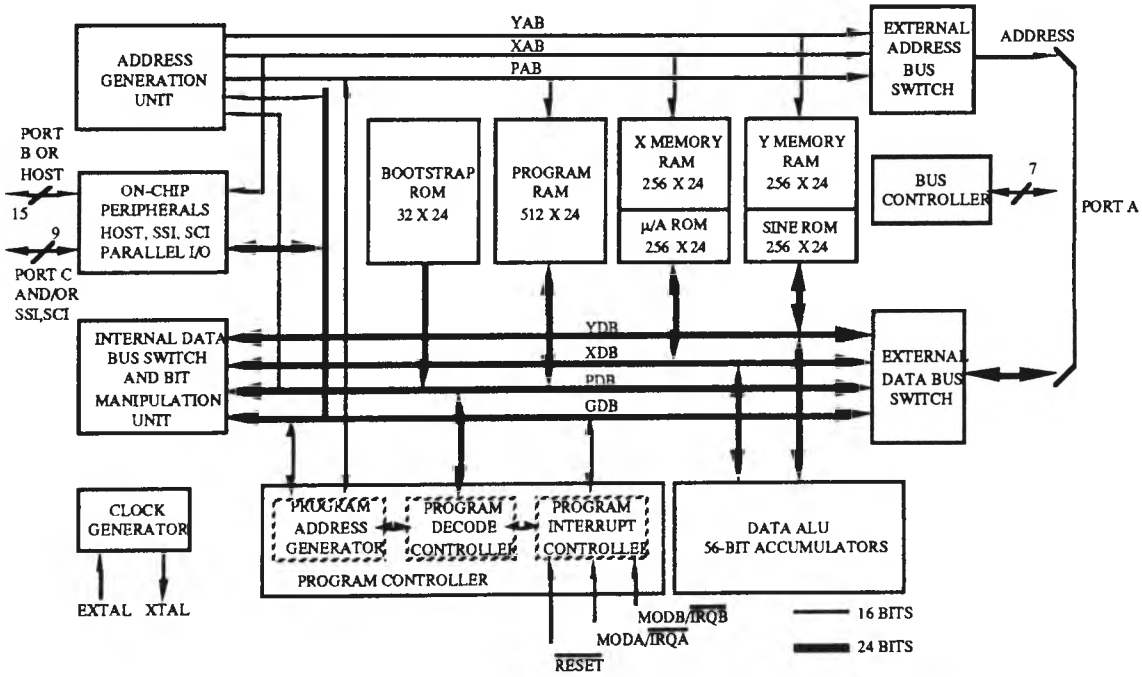

Figure 6.1 DSP56001 Block Diagram (DSP56000/56001 User's Manual)

The DSP56001 architecture has been designed to maximise throughput in

data intensive digital signal processing applications. This objective has resulted in a dual natured, expandable architecture with sophisticated on chip peripherals and general purpose I/O. It is dual-natured in that there are two independent expandable data memory spaces, two address arithmetic units and a data ALU which has two accumulators and two shifter/limiters. The duality of the architecture makes it easier to write software for DSP applications (Motorola DSP56001 Technical data).

The memory spaces of the DSP56001 are shown in Figure 6.2. Note that the program and data memory are separate, and the data memory is, in turn, divided into two separate memory spaces, X and Y.

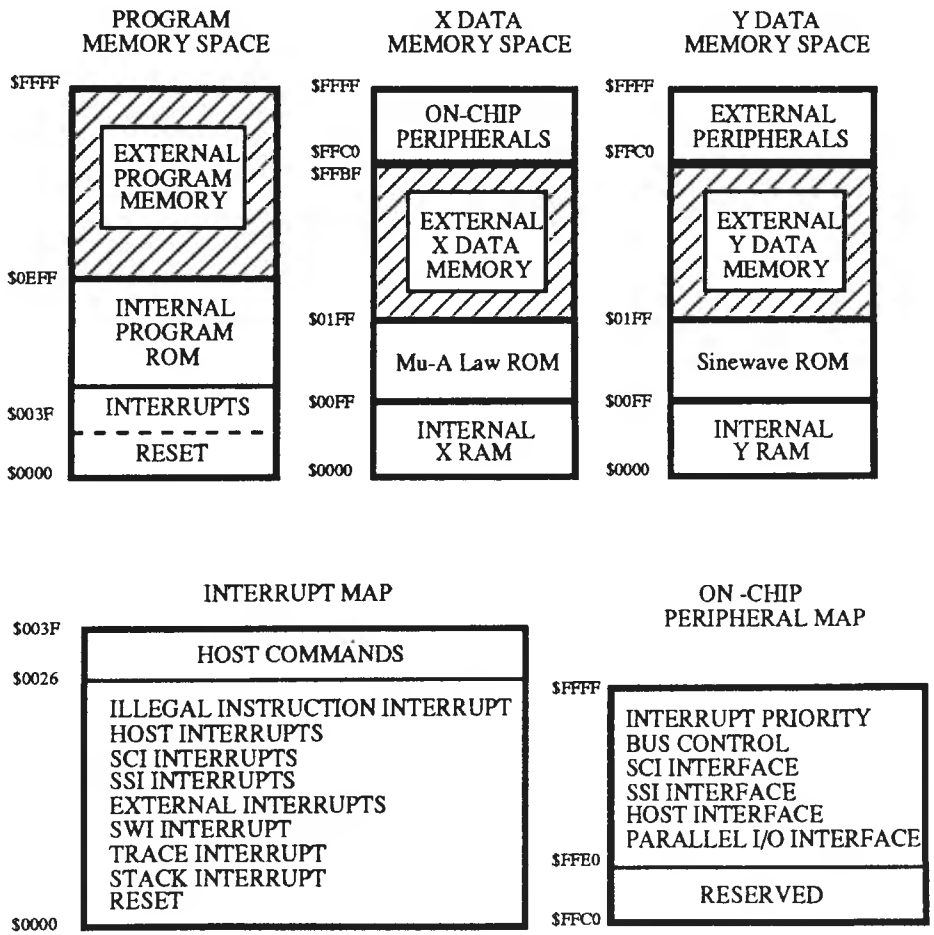

Figure 6.2 DSP56001 Memory Map (DSP56000/56001 User's Manual)

A summary of general features of DSP56001 is as follows:

- 512 × 24 bits of data RAM
- 512 × 24 bits of program RAM
- 24 programmable I/O port pins
- one 8 bits of parallel host MPU interface
- one serial communication port with baud-rate generator
- one synchronous serial port
- 16 bits address bus and 24 bits data bus
- capacity of 13.5 million instructions per second (MIPS) with a 27 MHz clock

6.3 DSP Based System

The DSP based system being used in implementation is shown in Figure 6.3. The central computing unit (a 56SB DSP development system) is provided by Precision Design Services Company in the form of a Printed Circuit Board (PCB). The 56SB DSP development system for the Motorola 56001 digital signal processing is based on a stand-alone board connected by an asynchronous link to the COM1 or COM2 serial port of an IBM personal computer or clone. Prominent features of this 56SB DSP include 100 ns/instruction execution time, 8k×24 zero wait state RAM for program and data, connector for all peripheral functions and memory mapped peripherals and a serial port connection to PC. Information concerning the 56SB DSP can be found in 56SB User's Manual and DSP56000/DSP56001 User's Manual.

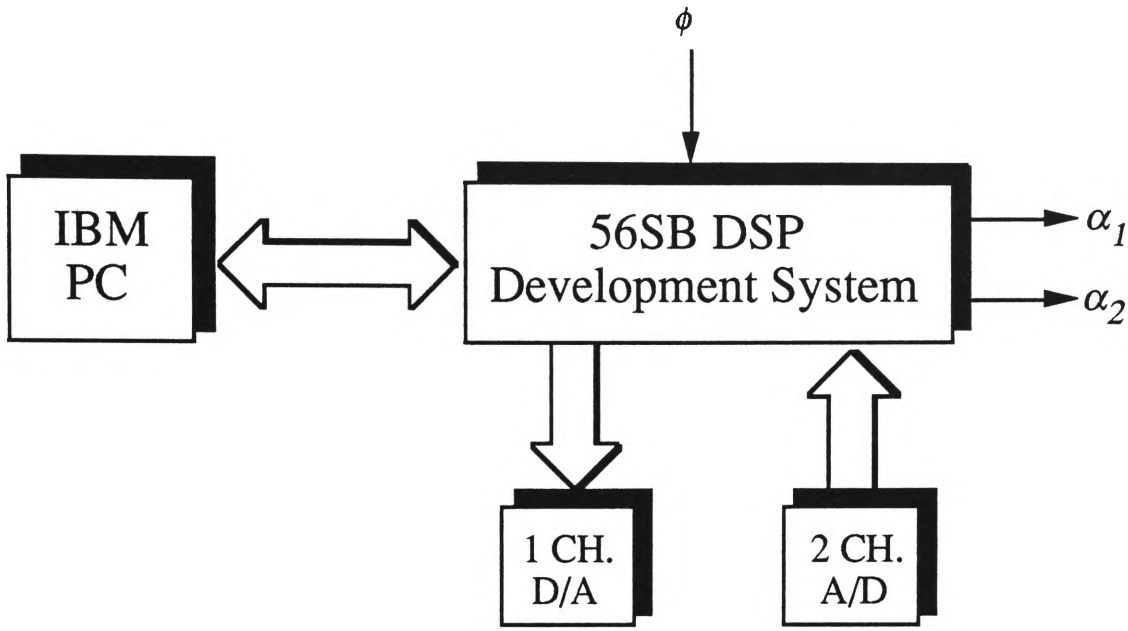

Figure 6.3 Structure of DSP based System

The major components of the DSP based system are as follows:

• One channel of digital to analog converter (D/A) is used for monitoring purposes. The D/A converter being used is a 8-bit DAC0800 interfaced to 56SB DSP through Input/Output (I/O) port B.

• Two channels of analog to digital conversion (A/D) are used for converter load current i_L and amplitude of current source I_c measurement. These A/D converters are interfaced to the 56SB system through the memory mapped peripherals connector. The A/D converters used are the 12-bit AD7870 provided by Analog Devices Inc.. The AD7870 chip is chosen because it can interface easily to 56SB DSP with a few additional gates and its conversion time is very low (about 8 μs). The circuit diagram of interfacing A/D is shown in Figure 6.4.

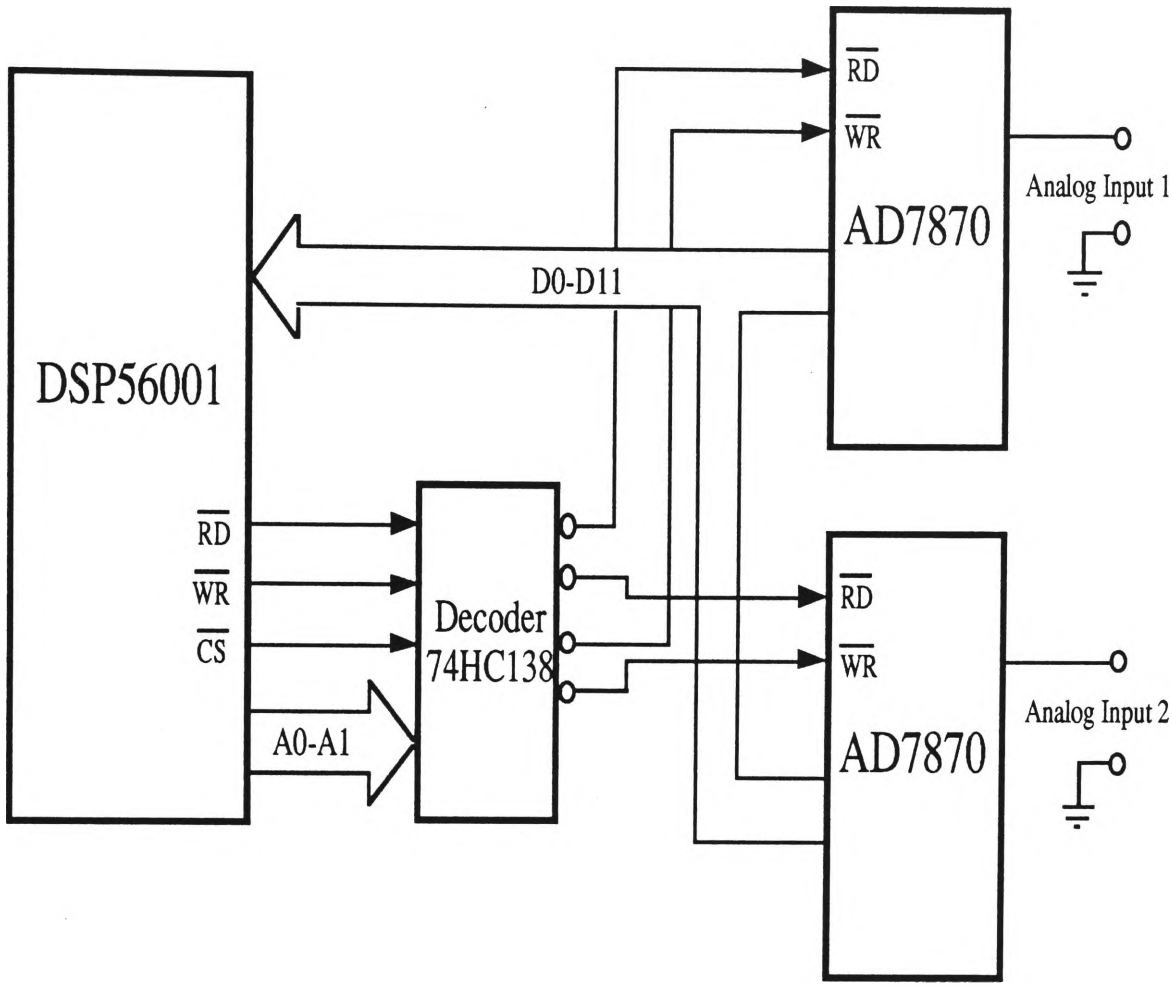

Figure 6.4 Analog to Digital Block Diagram

The decoded addresses of start conversion and reading for A/D channel 1 are $FF80 and $FF81 respectively. Identically, the start conversion address and read address for A/D channel 2 are $FF82 and $FF83 respectively. The steps of A/D conversion are shown by flowchart in Figure 6.5.

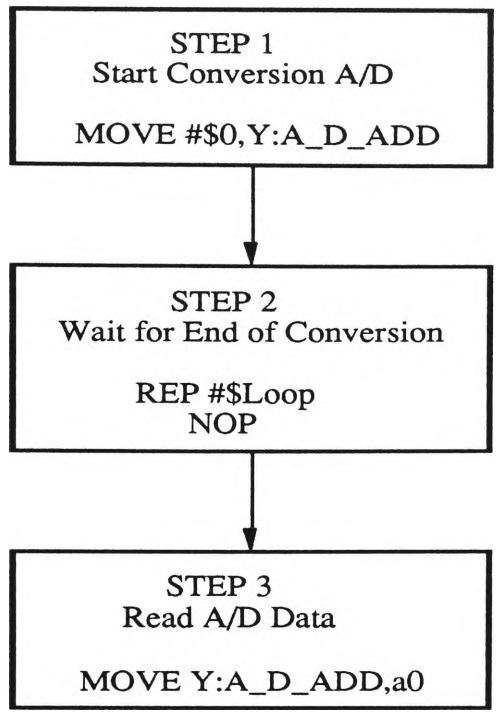

Figure 6.5 Analog to Digital Conversion Flowchart

• Clock input (ϕ) is used for synchronising the DSP based system with the system line frequency (50Hz). This clock input is used to interrupt the DSP based system every cycle of the line frequency. Therefore this signal can be generated by using zero-crossing circuit. The zero-crossing circuit being used is shown in Figure 6.6.

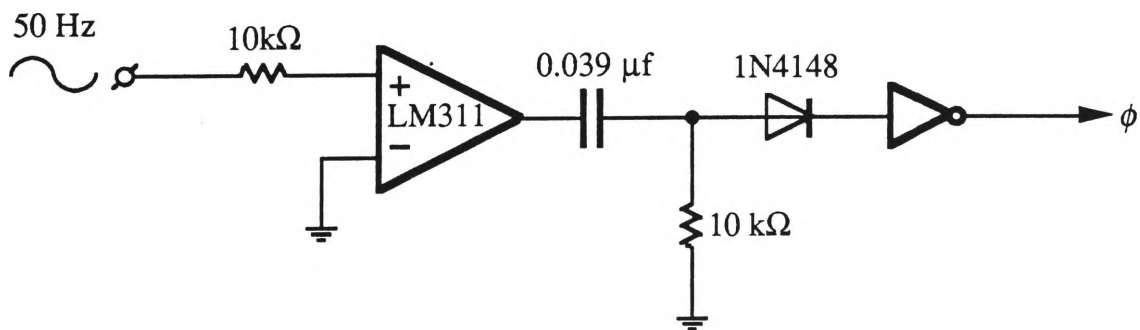

Figure 6.6 Zero-Crossing Circuit

The clock input is interfaced to interrupt request A ($\overline{\text{IRQA}}$) pin of 56SB DSP. The $\overline{\text{IRQA}}$ is configured with the interrupt priority level 2 (maskable) and level sensitive triggered. Whenever the program interrupt controller (PIC) in DSP56001 receives the interrupt request signal, it will generate the interrupt vector and update the program counter to interrupt vector. The interrupt vector contains the fast interrupt service routine which will be fetched.

• Two digital outputs (α_1, α_2) are used to output the pulsewidth of switching function from the DSP based system. Outputs 1 and 2 (α_1, α_2) are used to provide the positive and negative cycle switching functions respectively. These two outputs are in the form of digital signals which can be output directly from the 56SB DSP system via a memory mapped parallel output port (I/O port B). Figure 6.7 shows a flowchart of the configuration and output data.

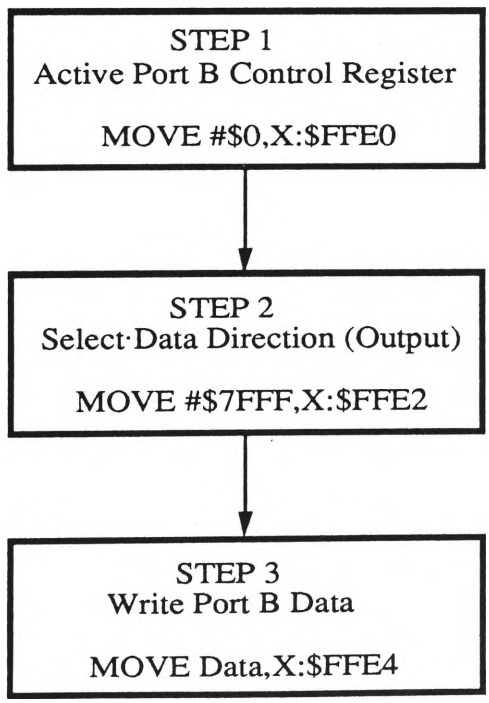

Figure 6.7 Port B Configuration Flowchart

6.4 DSP Software Development

In this section, the implementation of both modified equal-sampling technique and centroid based technique are presented. The software development of both switching strategies can be divided into three parts, namely, data input, processing of data and data output. The detailed constituent functions of software development are as follows:

- **Data Input**

  read data from A/D

  store data in input buffer
- **Processing of Data**

  read data from buffer

  calculate pulsewidth

  store output pulsewidth in output buffer
- **Data Output**

  read data from output buffer

  write data to output port

In practice, software development of each function can be broken down in turn into subroutine programs which can individually be tested out to ensure correct operation. The final stage is to combine these subroutines into the overall program using a command of jump to subroutine. By doing this we would have a convenient way of displaying or capturing the results from subroutines. Figure 6.8 depicts the flowchart of the entire software program which is to be implemented.

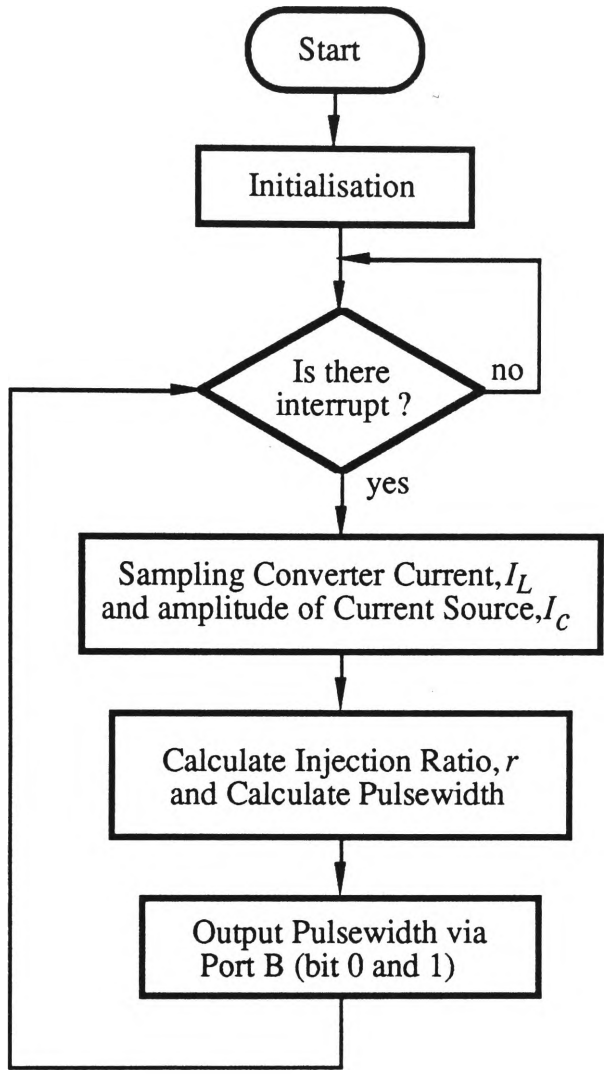

Figure 6.8 Flowchart Diagram of Software Development

Referring to Figure 6.8, the program starts with initialisation which in effect sets up the Synchronous Serial Interface (SSI) for PC communication and the I/O port for PWM output. Program initialisation also sets the address pointers of look-up table (LUT) and enables the interrupt. Next, the program will halt and wait for the interrupt signal. Whenever, the program is triggered by interrupt signal from zero-crossing circuit, it will run in loop of data input, data processing and data output until it is interrupted by the PC.

The detailed functions of data input and data output have been previously shown by flowcharts of Figures 6.5 and 6.6 respectively. At the stage of processing data (the pulsewidth calculation routine), Equation (3.10) for MEST and Equation (4.6) for CBT respectively are implemented as a process which is enabled on receiving new operating conditions from A/D converter (i.e. injection ratio r). Pulsewidths calculated are stored in a memory look-up table (LUT) until a change in injection ratio occurs, whereupon the new pulsewidths are used to overwrite the old ones.

Note that the pulsewidth calculation time can be reduced using a "symmetrisation" routine which assumes the quarter-wave symmetry inherent in the harmonic current waveform as considered earlier. When this symmetrisation routine is used, only the pulsewidths in the first one-quarter cycle need to be calculated and using appropriate reflection and negation operations, the complete cycle of pulsewidths can be quickly reproduced (Bowes and Clare, 1985). The assembly language software listings for the MEST and CBT are included in Appendices 3 and 4 respectively.

The main difference between MEST and CBT program is the subroutine used for calculating the pulsewidths. Figure 6.9 shows the flowcharts of pulsewidth calculation subroutine for MEST and CBT.

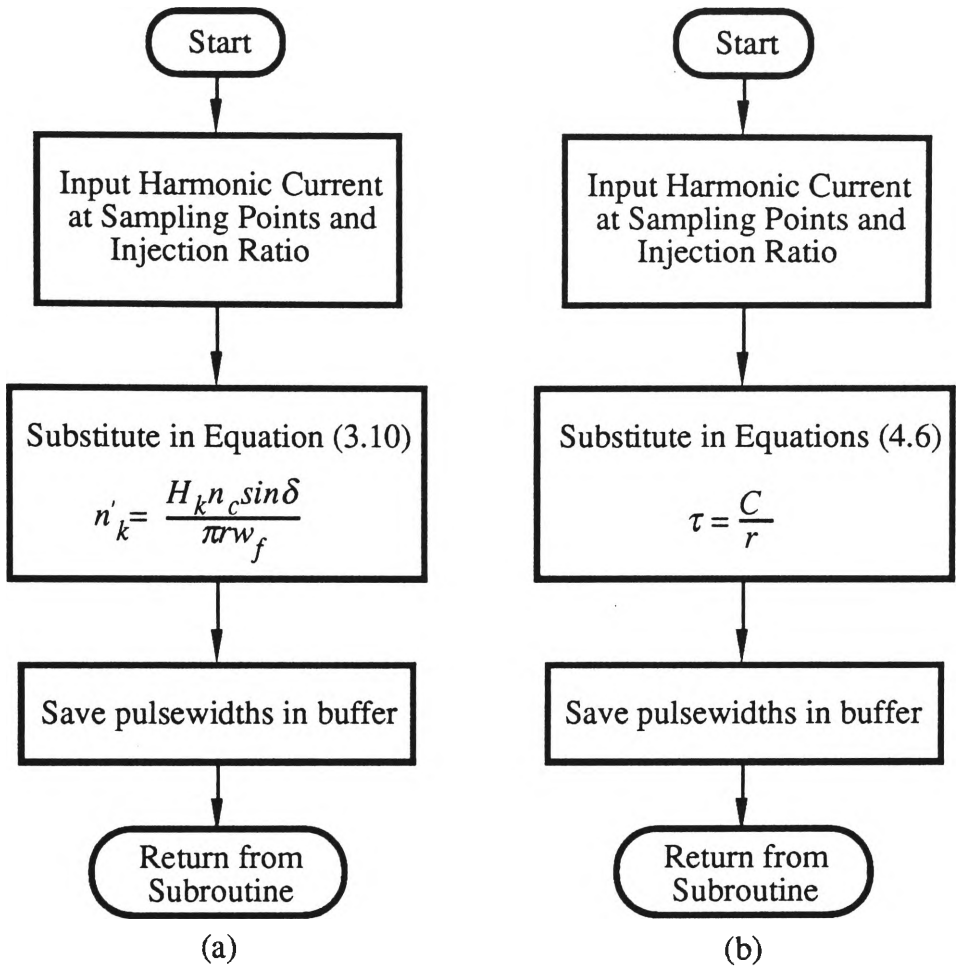

Figure 6.9 Flowchart for Calculating the Pulsewidth
(a) MEST (b) CBT

Note that, for this exercise the harmonic current is assumed to be constant. Hence, the centroid positions can be pre-programmed in memory as a look-up table and so only Equation (4.6) needs to be solved.

Figure 6.10 shows two output pulsewidths (α_1,α_2) of the switching functions based on MEST and CBT respectively. These two outputs are obtained for M = 12 and r = 0.5.

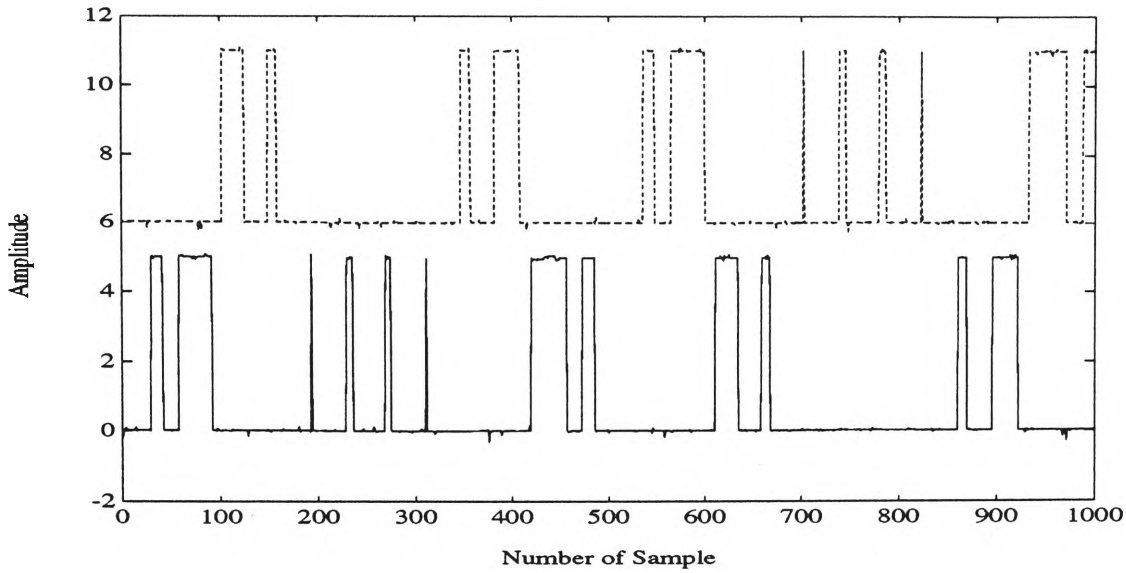

(a)

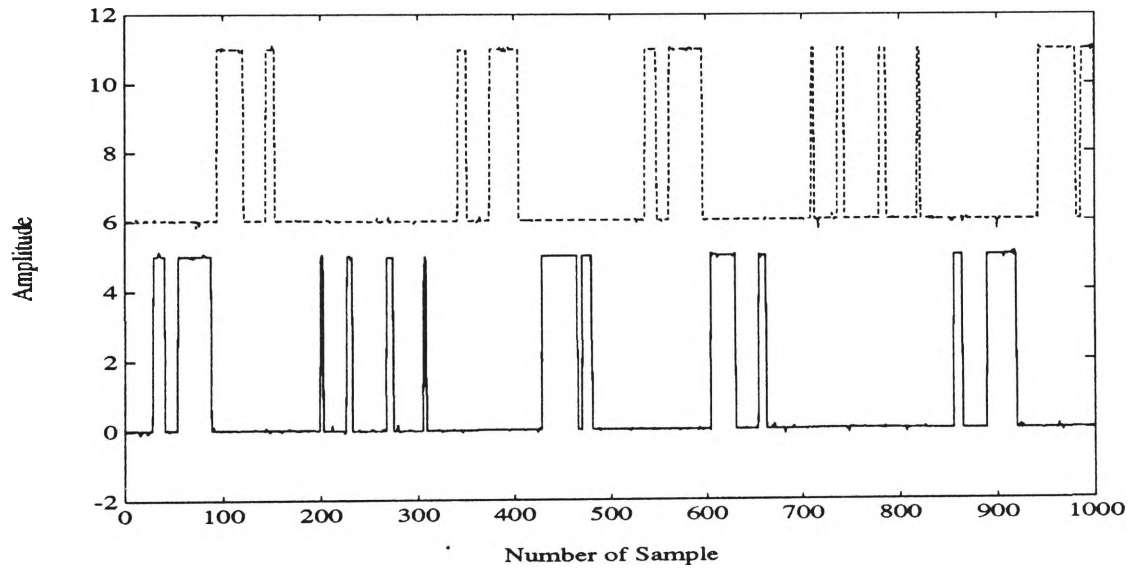

(b)

Figure 6.10 Switching Function, M=24, r=0.5

(a) Modified Equal-Sampling Technique

(b) Centroid Based Technique

6.5 Experimental Results

In this section, experimental results are presented. To obtain the compensated line current based on each switching strategy generated by the DSP, an analogue simulation circuit is used. However, it is easier to simulate the above based on a voltage signal rather than a current signal. The analogue simulation circuit being used is shown in Figure 6.11.

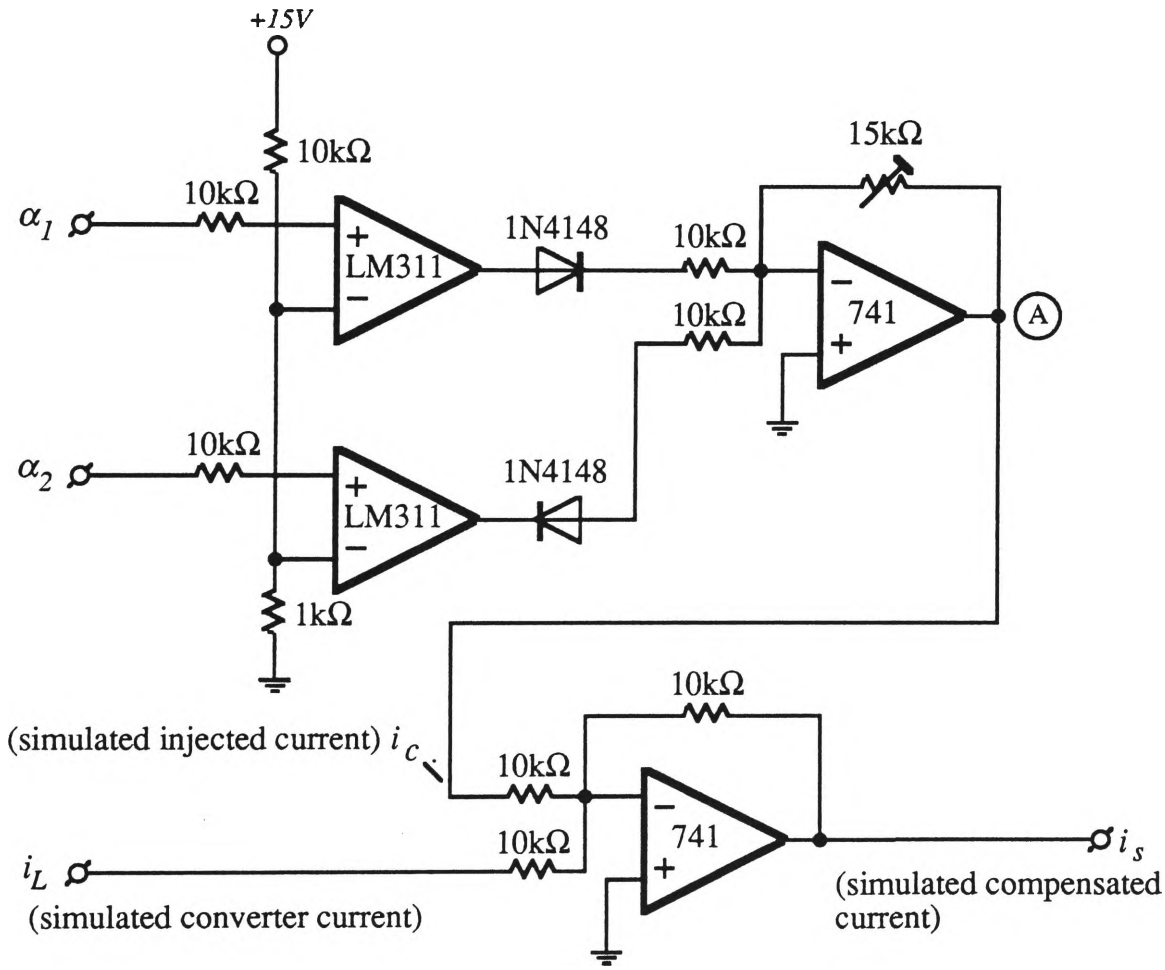

Figure 6.11 Analogue Simulation Circuit

Two PWM output signals (α_1,α_2) from DSP based system are connected to the comparator Op-Amps (LM311). The output of comparators are blocked by diode (1N4148) to make the positive and negative pulses. These signals are added using the summing circuit to make a three level signal (positive-zero-negative) of switching function. Note that the variable resistor 15kΩ is used to adjust the gain of the switching function. Figure 6.12 shows signal that represents the switching function at point A based on M=12 and r=0.5 for MEST and CBT respectively.

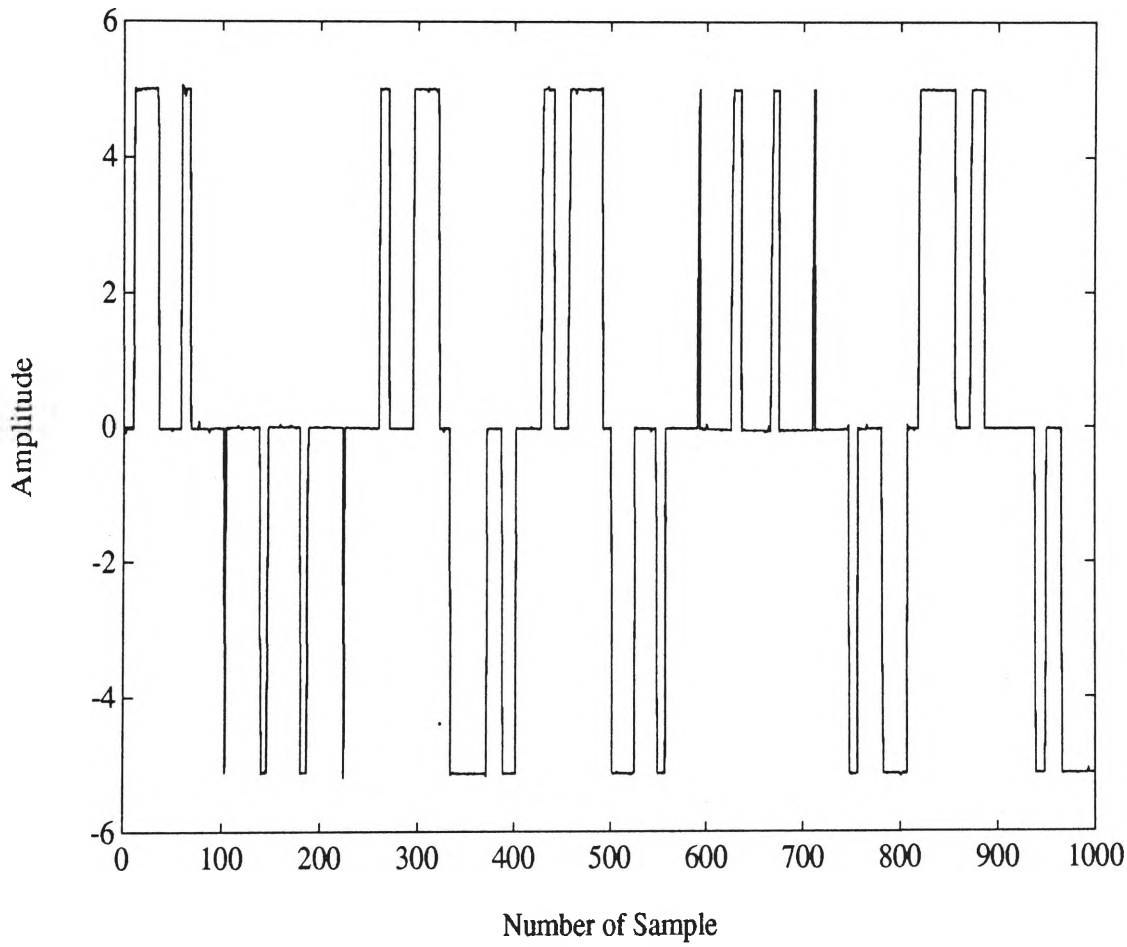

(a)

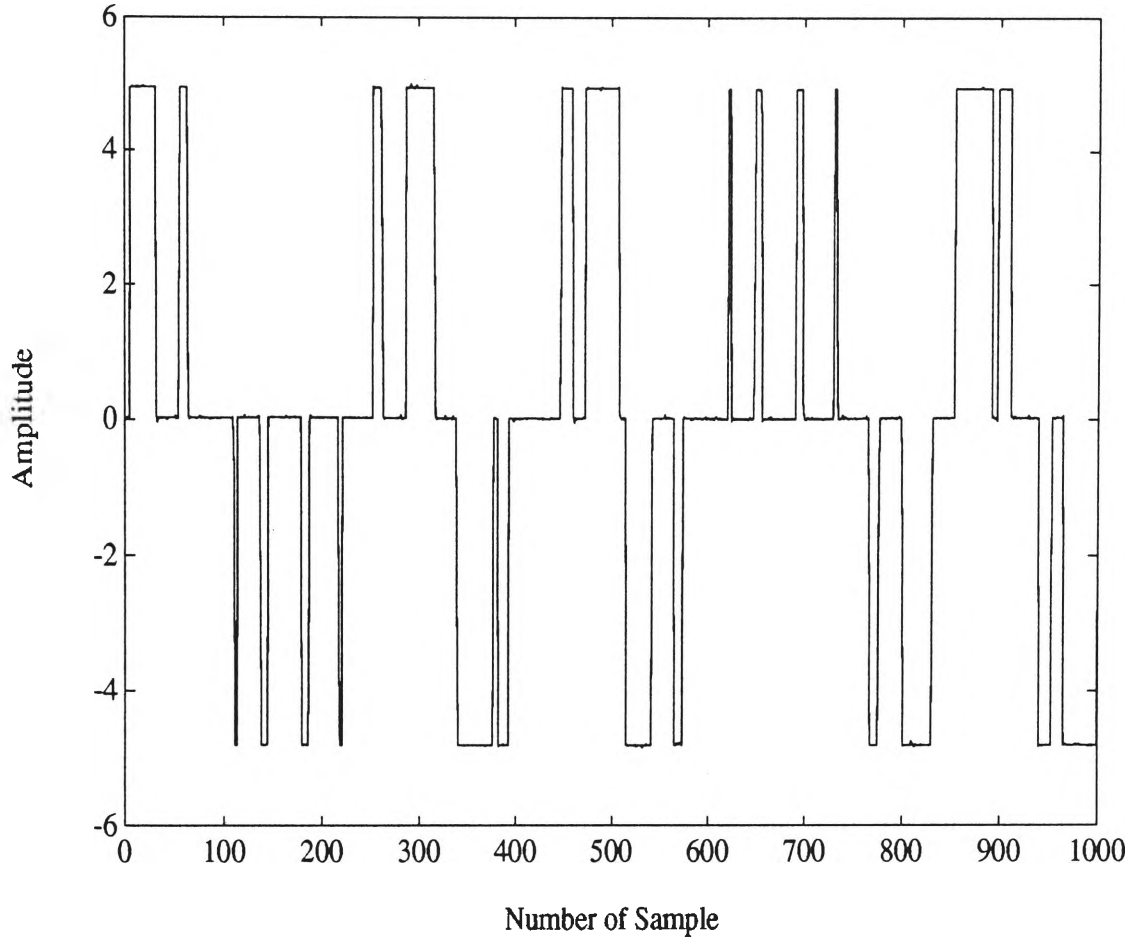

(b)

Figure 6.12 Simulated Switching Function
(a) MEST (b) CBT

Referring to Figure 6.11, the simulated switching function signal is subsequently subtracted from the simulated converter line current (i_L). Note that the converter current is obtained by employing a zero-crossing circuit. The output of the subtracting circuit will be the compensated line current (i_S). Figure 6.13 (a) and (b) show the line current after compensating as obtained from the simulation circuit for MEST and CBT respectively.

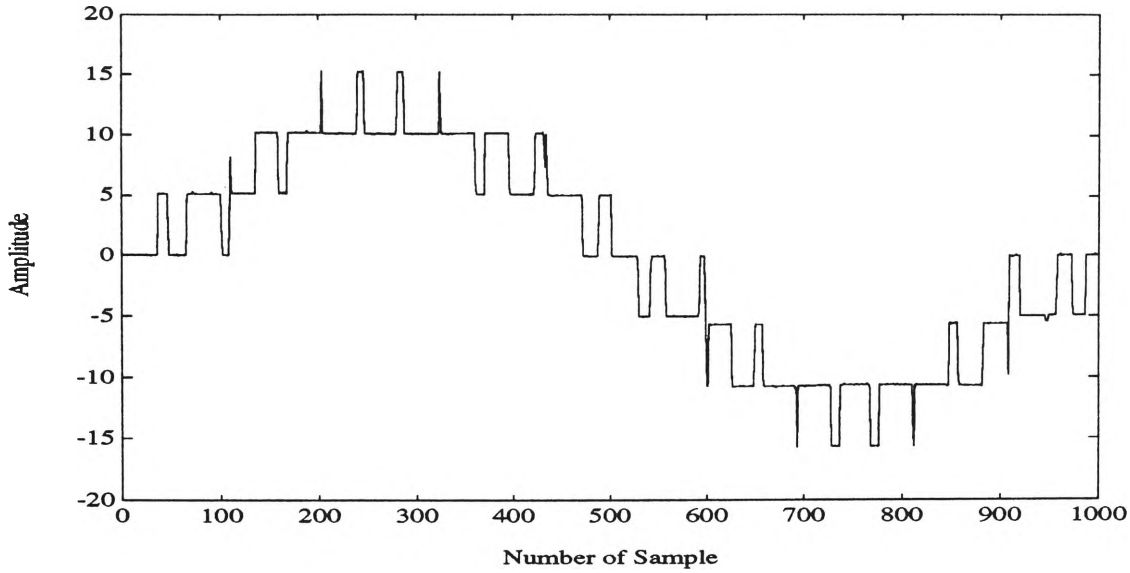

(a)

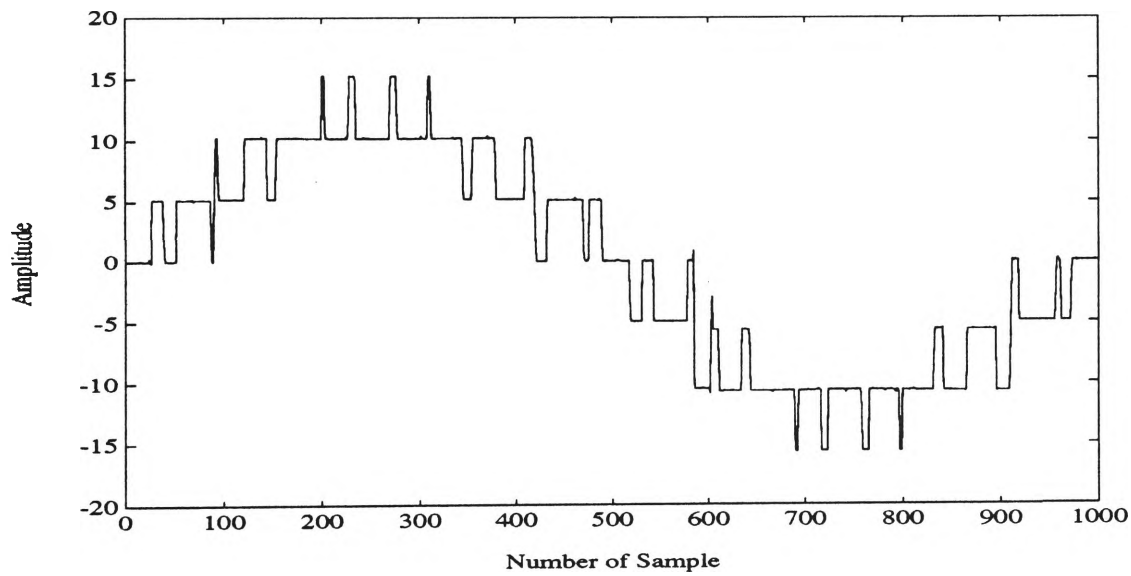

(b)

Figure 6.13 Line Current after Compensating
(a) MEST (b) CBT

Figure 6.14 (a) and (b) shows the harmonic spectrums of the line current after compensation has taken place for both the MEST and CBT.

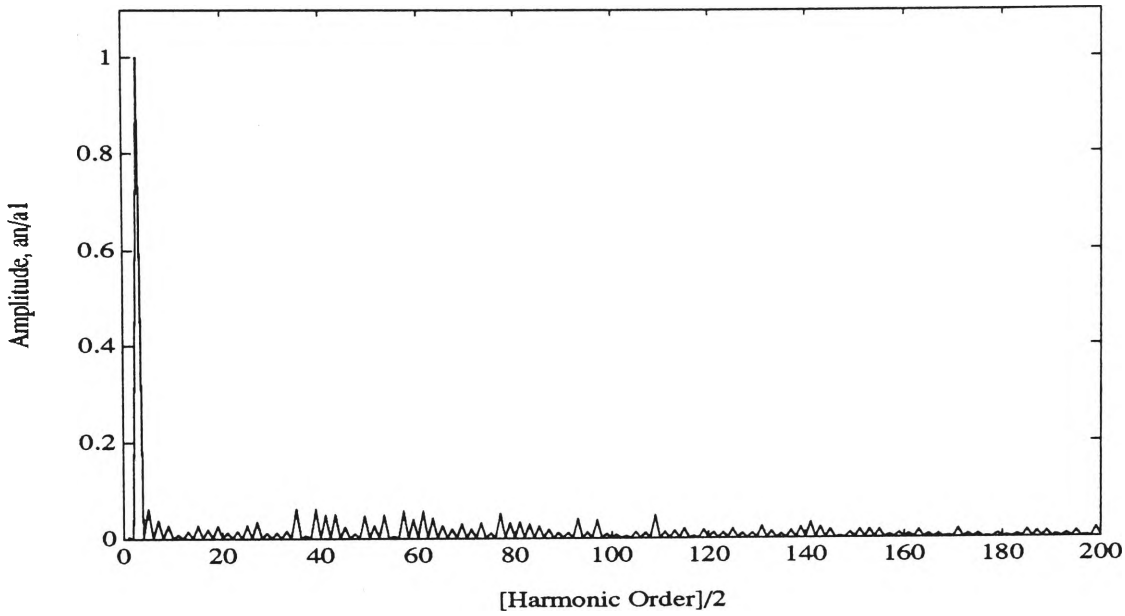

(a)

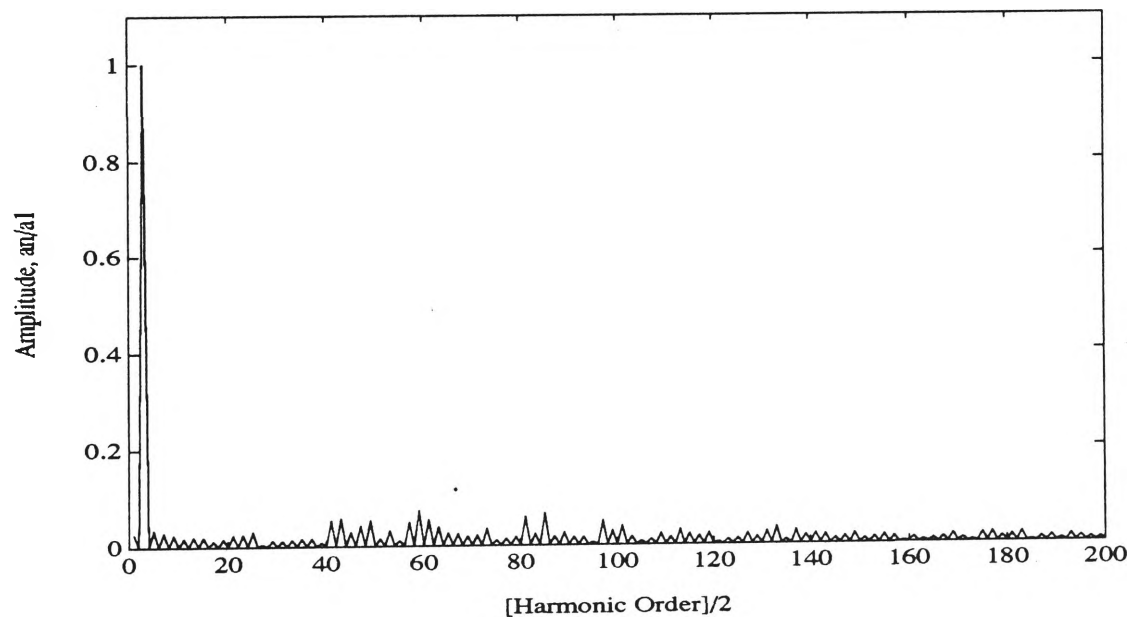

(b)

Figure 6.14 Harmonic Spectrum of Compensated Line Current

(a) MEST (b) CBT

From Figure 6.14, it can be seen that the CBT provides improved performance by more effective elimination of low order harmonics when compared to the MEST.

6.6 Conclusion

In this Chapter, the two proposed switching strategies including MEST and CBT are implemented on a Digital Signal Processor (DSP). It has been determined that the DSP has the features that are very useful in real-time implementation. In addition, the time required for the DSP chip which is used to obtain the switching function for MEST and CBT are comparatively similar (about 20 μs) assuming that the waveform of the reference harmonic current remains unchanged.

Finally, the purpose of this exercise was to show the practical feasibility of the proposed switching strategies. It can be concluded that they are indeed feasible and good performance is expected.

CHAPTER 7

CONCLUSIONS AND SUGGESTIONS FOR FURTHER RESEARCH

7.1 Conclusions

Harmonics generated by converters are one of the serious problems in power electronic engineering. In order to eliminate these harmonics, passive power filters or active power filters can be used. An active power filter was firstly presented by Sasaki and Machida in 1971, based on magnetic flux compensation but it is impractical in high power applications owing to the losses in semiconductor devices. For this reason active power filters based on injecting current pulses have been investigated and developed by many researchers such as Gyugyi and Strycula (1976), Mohan (1977), Hayafune, Ueshiba and Masada (1984), Akagi, Nabae and Atoh (1986), Choe and Park (1988), Stephen and Richard (1991). However, the switching strategies for active power filters has been received relatively little attention from researchers.

This thesis dealt with some aspects of active power filter applications, particularly, switching strategies that are suitable for active power filters. A survey of existing switching strategies was presented in Chapter 2. The switching strategies include natural sampled PWM, regular sampled PWM and programmed PWM. These techniques were developed based on the fact that the reference waveform is a single, continuous sinusoidal waveform. Therefore, they are inappropriate for active power filter applications where the reference waveform is a discontinuous waveform.

The switching strategy based on an Equal-Sampling Technique (EST) was discussed in Chapter 2. It was shown that to obtain the switching instants of the pulses, a set of non-linear equations had to be solved.

A new switching strategy based on a Modified Equal-Sampling Technique (MEST) was proposed in Chapter 3. The most significant advantage of this technique is that the switching function can be obtained by a simple algorithm. This technique is based on an energy conversion principle. Theoretical synthesis showed that the switching function can be generated by equating the area of switching function to that of the reference harmonic waveform. However, as the aim of this technique is the minimisation of computational burden (or performance criterion) the area of the reference harmonic waveform can be obtained by approximation. By doing this, the pulsewidth of the switching function can be obtained by a simple algorithm as required. In addition, it was evident that the performance based on the harmonic distortion point of view was approximately the same as the performance obtained from EST.

A more effective switching strategy based on a Centroid Based Technique (CBT) was presented in Chapter 4. The notion of the CBT is to equate the various current-time areas of the reference harmonic current to those of the switching function as in the case of MEST. Further, the centroids of the various areas are aligned. The advantage of CBT is that it offers the benefit of a reduced harmonic distortion factor (DF) as well as a reduced computational burden, compared to the EST. The theoretical synthesis of the CBT was discussed in Chapter 4.

The performance evaluation of each switching strategy was presented in Chapter 5. We have chosen two of the commonly adopted performance measures. Firstly, the harmonic distortion factor is used to evaluate the ability of eliminating harmonics. Secondly, the number of floating point operations is used to establish the computational burden associated with each switching strategy. The same conditions were maintained for all

switching strategies in order to maintain the integrity of the performance evaluation. When the overall performance was evaluated, it was found that the CBT would provide the best performance from a distortion factor point of view. Furthermore, its computational burden is less than 20% of the EST and somewhat higher than the MEST (which is about 2% of the EST).

Finally, the implementation of the switching strategies was carried out on a Digital Signal Processor (DSP) and this was presented in Chapter 6. The experimental results were used to confirm the validity of the proposed techniques. Experimental results show that the MEST and CBT software strategies can be implemented using digital signal processor with minimal complexity. In addition, the time taken to compute the pulsewidths is very low (less than 20 μs) using the stated assumptions. This means that the maximum frequency of the switching function which can be generated is 50kHz.

7.2 Suggestions for further research

The following suggestions are made for further research.

7.2.1 Reference Harmonic waveform

All work in this thesis has been based on a specific reference harmonic waveform related to an SCR phase controlled converter with a fixed delay angle. It will be of significant practical importance if suitable switching strategies are examined for a general case where the harmonic

current waveform is not pre-defined.

7.2.2 Transient mode

In this thesis, all work carried out is concerned with the operation at steady state. In the case of transient mode such as in fast load changes, the performance aspects of each switching strategy need to be evaluated carefully.

7.2.3 Three Phase Implementation and Evaluation

Ultimately, a three phase active power filter needs to be implemented and a proper evaluation undertaken. This means that the additional complexities of the three phase environment need to be considered and overcome.

7.2.4 Optimisation for Faster Running of DSP

Despite the fact that the developed software program executes efficiently, faster execution can be obtained by further optimising the software and hardware. The actions which may be taken in such an optimisation effort are as follows:

- DSP provides bus wait states to communicate with the external memory. Reducing the wait states to external memory accesses can substantially increase the speed of the system.

- DSP provides a parallel moving of X memory and Y memory and can be executed in a single instruction cycle. Use of this facility may improve the speed of execution.

- In the main software program, DSP has to spend some time to arrange and output the pulsewidth. To overcome this problem, external counter or pulse processor may be used. By using external chip supports, DSP can run freely and may improve the response of the system.

AUTHOR'S PUBLICATIONS

Dejsakulrit, D., Perera, B.S.P. and Chicharo, J.F., 'A novel equal sampling switching strategy for active power filters', *Electric Machines and Power Systems Journals.*, [Submitted for Publication].

Dejsakulrit, D., Chicharo, J.F. and Perera, B.S.P., 'A centroid based switching strategy for active power filters', *IEEE Trans. Ind. Appl.*, [Submitted for Publication].

Dejsakulrit, D., Chicharo, J.F. and Perera, B.S.P., (Oct. 1992) 'Switching strategies for current fed active power filters', *Australia Universities Power and Control Engineering Conference'92*, Queenland, Australia. pp.155-160.

REFERENCES

Akagi, H., Nabae, A. and Atoh, S., (1986) 'Control strategy of active power filters using multiple voltage source PWM converters', *IEEE Trans. Ind. Appl.*, Vol. IA-22, No. 3, pp. 460.

Akagi, H., Nabae, A. and Atoh, S., (1986) 'Compensation characteristics of active power filters using multiseries voltage source PWM converters', *Electrical Engineering in Japan.*, Vol. 106, No. 5, pp. 28-36.

Akagi, H., Tsukamoto, Y. and Nabae, A., (1990) 'Analysis and design of an active power filter using quad-series voltage source PWM converters', *IEEE Trans. Ind. Appl.*, Vol. 26, No. 1, pp. 93-98.

Arrillaga, J., Bradley, D.A. and Bodger, P.S., (1985) 'Power System Harmonics', New York, *John Wiley & Son.*

Bowes, S.R., (1975) 'New sinusoidal pulsewidth-modulated inverter', *Proc. B, Electr. Power Appl.*, Vol. 122, No. 11, pp. 1279-1285.

Bowes, S.R. and Bird, B.M., (1975) 'Novel approach to analysis and synthesis of modulation processes in power converters', *Proc. B, Electr. Power Appl.*, Vol. 128, No. 6, pp. 293-305.

Bowes, S.R. and Clement, R.R., (1982) 'Computer-aided design of PWM inverter systems', *Proc. B, Electr. Power Appl.*, Vol. 129, No. 1, pp. 1-17.

Bowes, S.R. and Midoun, A., (1985) 'Suboptimal Switching Strategies for Microprocessor-Controlled PWM Inverter Drives', *Proc. B, Electr. Power Appl.*, Vol. 132, No. 3, pp. 133-148.

Bowes, S.R. and Clare, J.C., (1985) 'Microprocessor-Based Development System for PWM Variable-Speed Drives', *Proc. B, Electr. Power Appl.*, Vol. 132, No. 1, pp. 18-45.

Buja, G.S., (1980) 'Optimal output waveforms in PWM inverters', *IEEE Trans. Ind. Appl.*, Vol. IA-16, No. 6, pp. 830-836.

Choe, G.H. and Park, M.H., (1988) 'A new injection method for ac harmonic elimination by active power filter', *IEEE Trans. Ind. Appl.*, Vol. 35, No. 1, pp. 141-147.

Choe, G.H. and Park, M.H., (1988) 'Analysis and control of active power filter with optimized injection', *IEEE Trans. Power Elec.*, Vol. 4, No. 4, pp. 427-433.

DSP56000/DSP56001 Digital Signal Processor User's Manual, Motorola Inc., 1990.

Enjeti, P.N., Ziogas, P.D. and Lindsay, J.F., (1990) 'Programmed PWM techniques to eliminate harmonics: A critical evaluation', *IEEE Trans. Ind. Appl.*, Vol. 26, No. 2, pp. 302-316.

Gyugyi, L. and Strycula, E.C., (1976) 'Active AC Power Filter.', *IEEE/IAS Ann. Meeting.*, pp. 529.

Hayafune, K., Ueshiba, T. and Masada, E., (1984) 'Microcomputer Controlled Active Power Filter', *Proc. IEEE/IECON,* pp. 1221-1226.

IEEE Guide for harmonic control and reactive compensation of static power converters, *IEEE Std 519-1981*.

Kim, Y.H. and Ehsani, M., (1990) 'An algebraic algorithm for microcomputer based (direct) inverter pulsewidth modulation', *IEEE Trans. Ind. Appl.*, Vol. IA-23, No. 4, pp. 654-660.

Mohan, N. et al., (1977) 'Active Filters for ac Harmonic suppression', *IEEE/PES Winter meeting*.

Miller, T.J.E., (1982) 'Reactive Power Control in Electrical Systems', New York, *John Wiley & Son*.

Patel, H.S. and Hoft, R.G., (1973) 'Generalized techniques of harmonic elimination and voltage control in thyristor inverter', *IEEE Trans Ind. Appl.*, Vol. IA-9, No. 3, pp. 310-317.

Sasaki, H. and Machida, T., (1971) 'A New Method to Eliminate AC Harmonic Currents by Magnetic Compensating-Considering on Basic Design.', *IEEE Trans. Power Appl. Syst.*, Vol. 90, No. 5, pp. 2009-2019.

Stephen, W., (1975) 'Circuit theory: a computational approach', New York, *John Wiley & Son*, pp. 2-3.

Stephen, M.W. and Richard, G.H., (1991) 'Adaptive frequency domain control of PWM switched power line conditioner', *IEEE Trans. Power Elec.*, Vol. 6, No. 4, pp. 665-670.

Stephen, M.W. and Richard, G.H., (1991) 'Implementation of current

source inverter for power line conditioning', *IEEE Trans. Ind. Appl.*, Vol. 27, No. 4, pp. 773-779.

Subjak, J.S. and McQuilkin, J.S., (1990) 'Harmonics-cause, effects, measurements, and analysis: an update', *IEEE Trans. Ind. Appl.*, Vol. 26, No. 6, pp. 1034-1042.

56SB DSP Development System User's Manual, Precision Design Services.

APPENDICES

APPENDIX 1 : Modified Equal-Sampling Technique (MATLAB Program)

```
echo on
clc;
% *-*-----------------------------------------------------*-*
% *   Modified Equal-Sampling Technique.MAT     *
% *-*-----------------------------------------------------*-*
echo off
clear;

 fes = input('Input equal-sampling frequency = ');
 r   = input('Input required injection ratio = ');
 wf  = input('Input required width-factor    = ');

% Change equal-sampling fre. to number of pulses/half cycle
% Note:- pulse/half cycle must be integer.
 M = (fes/50)/2;

% Change number of pulses/half cycle to number of
% pulses/quarter cycle because quarter-wave symmetry
 N = fix((M+1)/2);    % N = (M+1)/2     M:odd
                      % N = M/2         M:even

% Calculate the sampling positions or the center points of
% pulses of the switching function
 angs = 2000/(2*M):2000/M:2000-2000/(2*M);
 angs = fix(angs(1:N));

% Number of samples for cycle of the ESF [nc=fc/fes]
 nc = 200000/fes;

% Load harmonic current data from disk & normalize to 1-pu
 load dthr

% Collect the values,positions and signs of the harmonic current
% at the sampling points [Hk,pst,sgn]
   for cnt = 1:1:N
    Hk(cnt) = harc(angs(cnt));
     if Hk(cnt) >= 0
      sgn(cnt) = 1;
     else
      sgn(cnt) = -1;
     end
   end

% Calculate the half pulse-width of the switching function
   nk = abs(fix((Hk*nc)/(2*r*wf)));

% Processing of generating the switching funtion
   for cnt = 1:1:N
    Tkstr(cnt) = angs(cnt)-nk(cnt)+1;
    Tkstp(cnt) = angs(cnt)+nk(cnt)-1;
```

```
end

  swf  = zeros(1:Tkstr(1));
for cnt = 1:1:N-1
 if sgn(cnt) == 1
  swfH = ones(Tkstr(cnt)+1:Tkstp(cnt)-1);
 else
  swfH = -ones(Tkstr(cnt)+1:Tkstp(cnt)-1);
 end
  swfL = zeros(Tkstp(cnt):Tkstr(cnt+1));
  swf  = [swf swfH swfL];
end

  swfH = -ones(max(Tkstr)+1:max(Tkstp)-1);
  swfL = zeros(max(Tkstp):1000);
  swf  = [swf swfH swfL];
  swf  = [swf fliplr(swf)];
  plot(swf)
```

APPENDIX 2 : Centroid Based Technique (MATLAB Program)

```
echo on
clc;
% *-*-----------------------------------------*-*
% *     Centroid Based Technique.MAT       *
% *-*-----------------------------------------*-*
echo off
clear;

   r = input('Input injection ratio = ');
  wf = input('Input width factor = ');

% Load harmonic current data from disk & normalize to 1-pu
 load dthr

% Breaking the harmonic current into sections
  se = [166 333 528 723 861 1000];
 sgn = [-1 -1 1 1 -1 -1];

% Calculate the area by calling functions (FUNC1,FUNC2)
 for i = 1:2
  area(i) = abs(quad('func1',se(i)-165,se(i)));
 end

 for i = 1:4
  area(i+2) = abs(quad('func2',se(i+1)+1,se(i+2)));
 end

% The positions of centroid

  pos = [111 259 417 590 813 934];

% Calculate the half pulse-width of each pulses

 for i = 1:6
   nk(i) = fix(area(i)/(2*r*wf));
 end

% Generating the switching funtion
   for cnt = 1:1:6
    Tkstr(cnt) = pos(cnt)-nk(cnt)+1;
    Tkstp(cnt) = pos(cnt)+nk(cnt)-1;
   end

     swf  = zeros(1:Tkstr(1));

   for cnt = 1:1:5
    if sgn(cnt) == 1
     swfH = ones(Tkstr(cnt)+1:Tkstp(cnt)-1);
    else
     swfH = -ones(Tkstr(cnt)+1:Tkstp(cnt)-1);
    end
     swfL = zeros(Tkstp(cnt):Tkstr(cnt+1));
```

```
    swf  = [swf swfH swfL];
  end

    swfH = -ones(max(Tkstr)+1:max(Tkstp)-1);
    swfL = zeros(max(Tkstp):1000);
    swf  = [swf swfH swfL];
    swf  = [swf fliplr(swf)];

plot(swf)
load qs
si=qsq-r*swf;
si=[si -si];
q=fft(si);
w=2*abs(q)/4000;
plot(w(1:100))
end
```

APPENDIX 3 : Modified Equal-Sampling Technique (DSP56001 Assembly Language)

```
; ---------------------------------------------------------
;|  "Modified Equal-Sampling Technique.ASM"               |
;|                                                        |
;|              DSP56SB SYSTEM                            |
; ---------------------------------------------------------
        opt     mu,cre
        include         'pcp1.asm'      ;Macro of pulsewidth calculation
        include         'mdiv.asm'      ;Division macro

A_D1  equ     $F800 ;A/D[1]
A_D2  equ     $F801 ;A/D[2]
base          equ     $12
Hk            equ     x:base
Inj           equ     x:base+1
Ic            equ     x:base+2
Id            equ     x:base+3

M_BCR                 equ     $FFFE
M_IPR                 equ     $FFFF
M_PBC                 equ     $FFE0
M_PBD                 equ     $FFE4
M_PBDDR               equ     $FFE2
M_PCC                 equ     $FFE1

;Sine amplitude table at sampling points

        org     x:$0

        dc      $154
        dc      $3E5
        dc      $632
        dc      $813
        dc      $968
        dc      $A18
        dc      $A18
        dc      $968
        dc      $813
        dc      $632
        dc      $3E5
        dc      $154

;Sampling positions table

        org     y:$0

        dc      $215
        dc      $240
        dc      $26A
        dc      $295
        dc      $2C0
```

```
        dc      $2EA
        dc      $315
        dc      $340
        dc      $36A
        dc      $395
        dc      $3C0
        dc      $3EA
        dc      $415
        dc      $440
        dc      $46A
        dc      $495
        dc      $4C0
        dc      $4EA
        dc      $515
        dc      $540
        dc      $56A
        dc      $595
        dc      $5C0
        dc      $5EA

; --------------------------------
; | Start main program address |
; --------------------------------

        org     p:$40

; -------------------------------
; | Initialization Subrountine |
; -------------------------------

;Set up port B and C

        move  #$0001f8,x0               ;Set SSI for PC communication
        movep         x:M_PCC,a1
        or      x0,a
        movep         a1,x:M_PCC

        movep         #$0000,x:M_PBC    ;Setup port B as general I/O port
        movep         #$7fff,x:M_PBDDR  ;O/P data direction

;Set up address pointers

        move  #$200,r0          ;Set sampling data LUT's pointer
                                ;and pulsewidth LUT
        move  #$0,r1            ;Set sine LUT's pointer
        move  #$B,m1            ;modulo 11

        move  #$20,r2           ;Set width of pulses pointer
        move  #$17,m2           ;modulo 23

        move  #$40,r3           ;Set pulsewidth edge pointer
        move  #$2F,m3           ;modulo 47

        move  #$0,r4            ;Set sampling position pointer
        move  #$17,m4           ;modulo 23

        move  #$40,r5           ;Set positive pulsewidth edge pointer
        move  #$2F,m5           ;modulo 47
```

```
        move  #$2,n5                ;offset 2

        move  #$41,r6               ;Set negative pulsewidth edge pointer
        move  #$2F,m6               ;modulo 47
        move  #$2,n6                ;offset 2

        move  #$111F,y0             ;One wait state
        move  y0,x:M_BCR

;Initialize Inj,Hk

        move  #$37f,x0
        move  x0,x:base+1
        move  #$7ff000,x0
        move  x0,x:base

;Set up interrupt and enable

        move  #$3007,x0             ;Enable NIRQA(Edge Trig,IPL2)
        move  x:M_IPR,a1            ;Enable SSI interrupt
        or    x0,a
        move  a1,x:M_IPR
        andi  #$fc,MR               ;Unmask interrupts

; ------------------------------------------------------------
; | Read A/D, Synchronization, Calculate Pulse-Width |
; | and Output Pulsewidth                            |
; ------------------------------------------------------------

;Infinite loop, waiting for PC interrupt

self    wait                        ;Wait for zero crossing 50Hz

;Sampling data in 1 cycle and ouput pulsewidth from LUT pointed by [r0]


        .repeat
        move  b1,y:A_D1             ;Start conversion A/D[1], Hk
        move  b1,y:A_D2             ;Start conversion A/D[2], Ic

        rep   #$A                   ;Wait for end of conversion
        nop

;Output pulsewidth from Y memory LUT to bit 0,1 port B

;Check output bit (bit 0 or bit1)

        move  y:(r0),b0
        .if   r0 <lt> #$400
              .if     r0 <gt> #$27f and r0 <lt> #$37F
                      asl     b
                      move    b0,x:M_PBD
              .else
                      move    b0,x:M_PBD
              .endi
        .else
              .if     r0 <gt> #$47F and r0 <lt> #$57F
                      move    b0,x:M_PBD
```

```
            .else
                    asl     b
                    move    b0,x:M_PBD
            .endi
        .endi

;Arranging pulses

        .if     r0 <ge> x:(r5) and r0 <le> x:(r6)
                move    #>1,a0
                move    a0,y:(r0)
        .else
                move    #>0,a0
                move    a0,y:(r0)
        .endi
        .if     r0 <gt> x:(r6)
                move    x:(r5)+n5,x0
                move    x:(r6)+n6,x0
        .endi

;Harmonic current generating

        move    x:(r1)+,x1              ;Read sine LUT
        move    x:base+3,a1             ;Read converter current input
        sub     x1,a    #$1000,x1
        abs     a
        move    a1,y1
        mpy     x1,y1,a
        asr     a
        move    a0,x:base               ;Save harmonic current

;Solving injection ratio

        mdiv    Id,Ic                   ;Call macro division for solving
        move    a0,x:base+1             ;injection ratio

;Solving pulsewidth

        pcp     Hk,Inj                  ;Call macro of pulsewidth calculation (10us)
        move    a0,x:(r2)+              ;Save width of pulses
        move    a0,x0
        move    y:(r4),b1
        sub     x0,b
        move    b1,x:(r3)+              ;Save positive pulsewidth edge
        move    y:(r4)+,b1
        add     x0,b                    ;Load PW vector to a0 for o/p port B
        move    b1,x:(r3)+              ;Save negative pulsewidth edge

        move    y:A_D2,b1               ;Read data from A/D[2]
        move    #$000FFF,x0             ;Eliminate 3 MSB of data
        and     x0,b
        move    b1,x:base+2             ;Save data A/D[2] (Ic) in x:base+2
        move    y:A_D1,b1               ;Read data from A/D[1] (Hk)
        and     x0,b

        .if     r0 <eq> #$500
        move    b1,x:base+3
        move    b1,x:(r0)+              ;Save A/D[1] data & increases address pointer
```

```
;       move  b1,x:M_PBD          ;O/P to D/A for monitor purpose
        .else
        move  b1,x:(r0)+
;       move  b1,x:M_PBD
        .endi

        .until  r0 <eq> #$600     ;Do 1024 loops
        move  #$200,r0
        jmp   self

; ---------------------------------
; | Interrupt A service routine  |
; | start conversion A/D 1,2     |
; ---------------------------------

        org   p:$0008             ;NIRQA interrupt vector
        move  y0,x:A_D1

        end                   ;end program
```

APPENDIX 4: Centroid Based Technique (DSP56001 Assembly Language)

```
; ---------------------------------------------------
;|  "Centroid Based Technique.ASM"                   |
;|                                                   |
;|          DSP56SB SYSTEM                           |
; ---------------------------------------------------
        opt     mu,cre
        include         'mdiv1.asm'     ;Division macro1
        include         'mdiv2.asm'     ;Division macro2

A_D1    equ     $F800   ;A/D[1]
A_D2    equ     $F801   ;A/D[2]
base            equ     $12
Hk              equ     x:base
Inj             equ     x:base+1
Ic              equ     x:base+2
Id              equ     x:base+3
Coeff           equ     x:base+4

M_BCR                   equ     $FFFE
M_IPR                   equ     $FFFF
M_PBC                   equ     $FFE0
M_PBD                   equ     $FFE4
M_PBDDR                 equ     $FFE2
M_PCC                   equ     $FFE1


;Sine amplitude table at centroid's position

        org     x:$0

        dc      $15E
        dc      $42F
        dc      $682
        dc      $8CC
        dc      $9A1
        dc      $A1F
        dc      $A1F
        dc      $9A1
        dc      $8CC
        dc      $682
        dc      $42F
        dc      $15E

;Centroid position table

        org     y:$0

        dc      $216
        dc      $245
        dc      $271
```

```
        dc      $2AA
        dc      $2CA
        dc      $2EE
        dc      $316
        dc      $345
        dc      $371
        dc      $3AA
        dc      $3CA
        dc      $3EE
        dc      $416
        dc      $445
        dc      $471
        dc      $4AA
        dc      $4CA
        dc      $4EE
        dc      $516
        dc      $545
        dc      $571
        dc      $5AA
        dc      $5CA
        dc      $5EE

;Centroid coefficient table [C]

        org     y:$20

        dc      $64
        dc      $37
        dc      $F
        dc      $5
        dc      $F
        dc      $14
        dc      $14
        dc      $F
        dc      $5
        dc      $F
        dc      $37
        dc      $64
; --------------------------------
; | Start main program address |
; --------------------------------

        org     p:$40

; ------------------------------
; | Initialization Subrountine |
; ------------------------------

;Set up port B and C

        move  #$0001f8,x0               ;Set SSI for PC communication
        movep         x:M_PCC,a1
        or      x0,a
        movep         a1,x:M_PCC

        movep         #$0000,x:M_PBC    ;Setup port B as general I/O port
        movep         #$7fff,x:M_PBDDR  ;O/P data direction
```

```
;Set up address pointers

        move  #$200,r0          ;Set sampling data LUT's pointer
                                ;and pulsewidth LUT
        move  #$0,r1            ;Set sine LUT's pointer
        move  #$B,m1            ;modulo 11

        move  #$20,r2           ;Set width of pulses pointer
        move  #$17,m2           ;modulo 23

        move  #$40,r3           ;Set pulsewidth edge pointer
        move  #$2F,m3           ;modulo 23

        move  #$0,r4            ;Set sampling position pointer
        move  #$17,m4           ;modulo 23

        move  #$40,r5           ;Set positive pulsewidth edge pointer
        move  #$2F,m5           ;modulo 47
        move  #$2,n5            ;offset 2

        move  #$41,r6           ;Set negative pulsewidth edge pointer
        move  #$2F,m6           ;modulo 47
        move  #$2,n6            ;offset 2

        move  #$20,r7           ;Set centroid coefficient pointer
        move  #$B,m7            ;modulo 11

        move  #$111F,y0         ;One wait state
        move  y0,x:M_BCR

;Initialize Inj,Hk

        move  #$37f,x0
        move  x0,x:base+1
        move  #$7ff000,x0
        move  x0,x:base

;Set up interrupt and enable

        move  #$3007,x0         ;Enable NIRQA(Edge Trig,IPL2)
        move  x:M_IPR,a1        ;Enable SSI interrupt
        or    x0,a
        move  a1,x:M_IPR
        andi  #$fc,MR           ;Unmask interrupts

; ------------------------------------------------------------
; | Read A/D, Synchronization, Calculate Pulse-Width |
; | and Output Pulsewidth                            |
; ------------------------------------------------------------

;Infinite loop, waiting for PC interrupt

self    wait                    ;Wait for zero crossing 50Hz

;Sampling data in 1 cycle and ouput pulsewidth from LUT pointed by [r0]

        .repeat
```

```
        move  b1,y:A_D1     ;Start conversion A/D[1], Hk
        move  b1,y:A_D2     ;Start conversion A/D[2], Ic

        rep   #$9           ;Wait for end of conversion
        nop

;Output pulsewidth from Y memory LUT to bit 0,1 port B

;Check output bit (bit 0 or bit1)

        move  y:(r0),b0
        .if   r0 <lt> #$400
              .if   r0 <gt> #$27f and r0 <lt> #$37F
                    asl   b
                    move  b0,x:M_PBD
              .else
                    move  b0,x:M_PBD
              .endi
        .else
              .if   r0 <gt> #$47F and r0 <lt> #$57F
                    move  b0,x:M_PBD
              .else
                    asl   b
                    move  b0,x:M_PBD
              .endi
        .endi

;Arranging pulses

        .if   r0 <ge> x:(r5) and r0 <le> x:(r6)
              move  #>1,a0
              move  a0,y:(r0)
        .else
              move  #>0,a0
              move  a0,y:(r0)
        .endi
        .if   r0 <gt> x:(r6)
              move  x:(r5)+n5,x0
              move  x:(r6)+n6,x0
        .endi

        move  x:(r1)+,x1          ;Read sine LUT
        move  x:base+3,a1         ;Read converter current input
        sub   x1,a    #$1000,x1
        abs   a
        move  a1,y1
        mpy   x1,y1,a
        asr   a
        move  a0,x:base           ;Save harmonic current
        mdiv_a      Id,Ic         ;Call macro division for solving-
        move  a0,x:base+1         ;-injection ratio
        move  y:(r7)+,x0
        move  x0,x:base+4
        mdiv_b      Coeff,Inj     ;Call macro division for solving pulsewidth
        move  a0,x:(r2)+          ;Save width of pulses
        move  a0,x0
        move  y:(r4),b1
        sub   x0,b
```

```
        move    b1,x:(r3)+          ;Save positive pulsewidth edge
        move    y:(r4)+,b1
        add     x0,b                ;Load PW vector to a0 for o/p port B
        move    b1,x:(r3)+          ;Save negative pulsewidth edge

        move    y:A_D2,b1           ;Read data from A/D[2]
        move    #$000FFF,x0         ;Eliminate 3 MSB of data
        and     x0,b
        move    b1,x:base+2         ;Save data A/D[2] (Ic) in x:base+2
        move    y:A_D1,b1           ;Read data from A/D[1] (Hk)
        and     x0,b

        .if     r0 <eq> #$500
        move    b1,x:base+3
        move    b1,x:(r0)+          ;Save A/D[1] data & increases address pointer
;       move    b1,x:M_PBD          ;O/P to D/A for monitor purpose
        .else
        move    b1,x:(r0)+
;       move    b1,x:M_PBD
        .endi

        .until  r0 <eq> #$600       ;Do 1024 loops
        move    #$200,r0
        jmp     self

; --------------------------------
; | Interrupt A service routine  |
; | start conversion A/D 1,2     |
; --------------------------------

        org     p:$0008             ;NIRQA interrupt vector
        move    y0,x:A_D1

        end                 ;end program
```